

**Supplementary Information:**

**Electrochemically Modulated Separation of Olefin-Paraffin Gas Mixtures  
in Membrane Electrode Assemblies**

**Table of Contents – Supplementary Information**

***Section S0: Introduction on How to Interpret the Experimental Data***..... 4

***Section S1: Variable Nickel Dithiolene Loading onto GDL*** ..... 8

**Figure S1-A: 0 mg/cm<sup>2</sup> [N[Et]<sub>4</sub>]<sub>2</sub>[Ni(mnt)<sub>2</sub>]**. .... 9

**Figure S1-B: 2 mg/cm<sup>2</sup> [N[Et]<sub>4</sub>]<sub>2</sub>[Ni(mnt)<sub>2</sub>]**. .... 11

**Figure S1-C: 3 mg/cm<sup>2</sup> [N[Et]<sub>4</sub>]<sub>2</sub>[Ni(mnt)<sub>2</sub>]**. .... 13

**Figure S1-D: 4 mg/cm<sup>2</sup> [N[Et]<sub>4</sub>]<sub>2</sub>[Ni(mnt)<sub>2</sub>]**. .... 15

**Figure S1-E: 8 mg/cm<sup>2</sup> [N[Et]<sub>4</sub>]<sub>2</sub>[Ni(mnt)<sub>2</sub>]**..... 17

**Figure S1-F: [Ni(mnt)<sub>2</sub>] Utilization Fraction**..... 18

***Section S2: Variable Ionic Liquid Loading onto GDL***..... 19

**Figure S2-A: 0 mg/cm<sup>2</sup> IL**..... 21

**Figure S2-B: 2 mg/cm<sup>2</sup> IL**..... 23

**Figure S2-C: 4 mg/cm<sup>2</sup> IL**..... 25

**Figure S2-D: 8 mg/cm<sup>2</sup> IL**..... 27

**Figure S2-E: 16 mg/cm<sup>2</sup> IL**. .... 29

***Section S3: Variable Feed Composition*** ..... 30

**Figure S3-A: 0:100 Propylene-Propane Feed**..... 32

**Figure S3-B: 25:75 Propylene-Propane Feed**..... 34

**Figure S3-C: 50:50 Propylene-Propane Feed**..... 36

**Figure S3-D: 100:0 Propylene-Propane Feed**. .... 38

***Section S4: Variable Oxidative Potential (while using constant reductive potential of -2V)*** ..... 39

**Figure S4-A: 0V Oxidative Potential**..... 40

**Figure S4-B: +0.5V Oxidative Potential**. .... 41

**Figure S4-C: +1.0V Oxidative Potential**. .... 43

**Figure S4-D: +1.5V Oxidative Potential**..... 45

**Figure S4-E: +2.0V Oxidative Potential**..... 47

**Figure S4-F: +2.5V Oxidative Potential**..... 49

**Figure S4-G: +3.0V Oxidative Potential**. .... 51

***Section S5: Variable Reductive Potential (while using constant oxidative potential of +1.5V)*** ..... 52

**Figure S5-A: 0V Reductive Potential**. .... 53

**Figure S5-B: -0.5V Reductive Potential**..... 54

**Figure S5-C: -1.0V Reductive Potential**..... 55

**Figure S5-D: -2.0V Reductive Potential**..... 57

**Figure S5-E: -3.0V Reductive Potential**..... 58

***Section S6: Variable Feed Exposure Time*** ..... 59

**Figure S6-A: 5-minute Feed Exposure**..... 61

**Figure S6-B: 10-minute Feed Exposure**..... 63

**Figure S6-C: 20-minute Feed Exposure**. .... 65

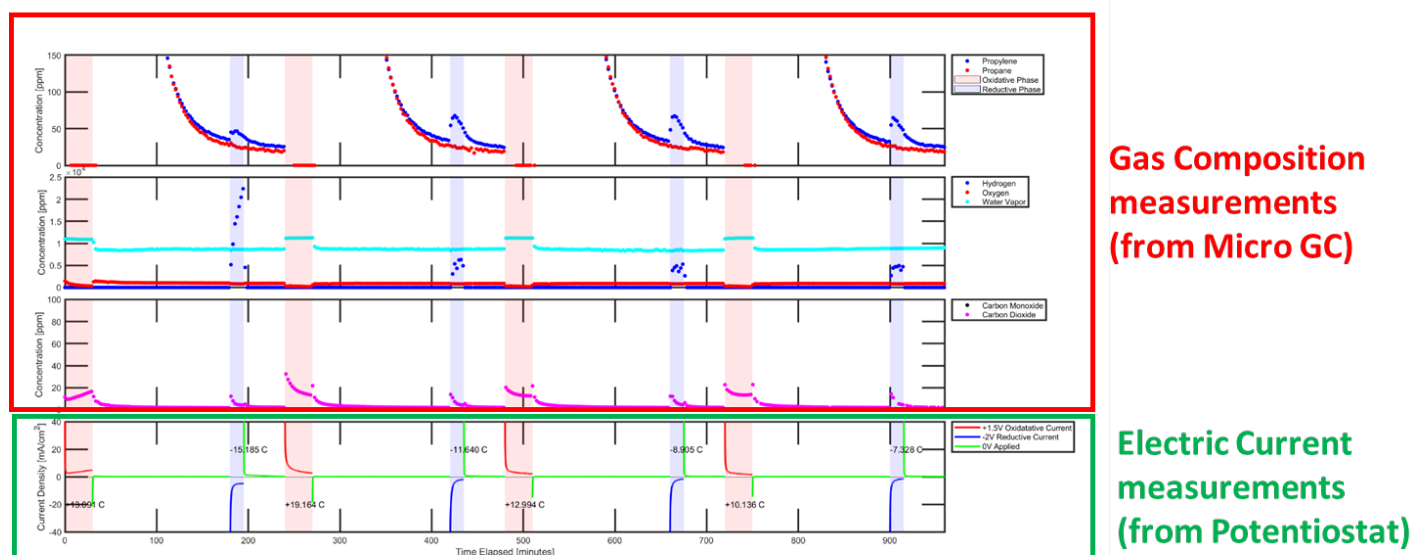
**Figure S6-D: 30-minute Feed Exposure**..... 67

<b>Figure S6-E: 45-minute Feed Exposure.</b> .....	69
<b>Figure S6-F: 60-minute Feed Exposure.</b> .....	71
<b><i>Section S7: Spin-Coating of Varying Nickel Dithiolene, IL, and Nafion solution</i></b> .....	72
<b><i>Section S8: Preparation Method of Nickel Dimercaptomaleonitrile complex as a Tetraethylammonium salt</i></b> .....	73
<b><i>Section S9: Characterizations of Synthesized Tetraethylammonium Nickel Dimercaptomaleonitrile</i></b> .....	75
<b><i>Section S10: Cyclic Voltammetry of Nickel Dithiolene in Organic Solvent Medium</i></b> .....	77
<b>Figure S10: Liquid Solution CV with Propane/Propylene.</b> .....	77
<b><i>Section S11: Cyclic Voltammetry of Nickel Dithiolene containing MEA system</i></b> .....	78
<b>Figure S11. Cyclic Voltammogram of MEA sample.</b> .....	78
<b><i>Section S12: Spray Deposition System</i></b> .....	79
<b><i>Section S13: Physisorption and Chemisorption of Propylene Gas</i></b> .....	80
<b><i>Section S14: Thermodynamic Minimum Potentials for Electrochemical Modulation in MEA</i></b> .....	81

## Section S0: Introduction on How to Interpret the Experimental Data

The supplementary information packet at first glance can seem overwhelming in abundance of data. To help readers understand how to interpret the graphs, this section is dedicated to explaining how the graphs in the *Figures* of the Supplementary Information are organized. A sample *Figure* (Figure S1-E) will be used in this introductory guide.

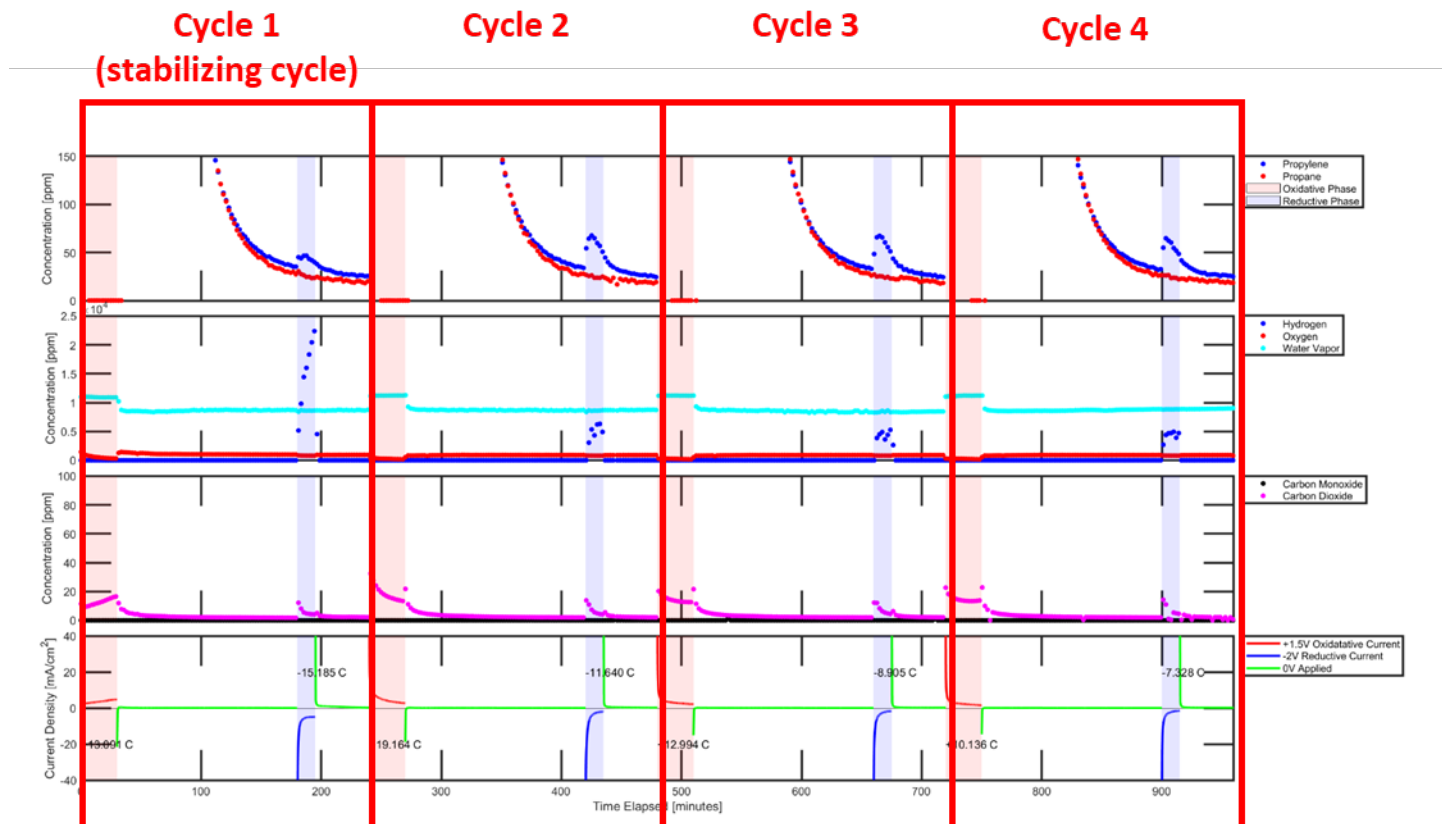
First, each *Figure* will have an appropriate caption detailing the loading compositions (*i.e.* mass of carbon nanoparticle electrodes, Nickel Dithiolene salt, Nafion, and IL per area) as well as relevant experimental conditions. There will also be a summary description at the beginning of each *Section* regarding the most notable findings observed from that series of experiments conducted in that *Section*. The summary will also describe how each *Section* is related to the content of the main manuscript. Each *Figure* will have gas composition measurements from the Micro GC and electrical current measurements from the Potentiostat. Since data from the Micro GC and the Potentiostat are experimentally accessible variables or quantities, they are typically grouped together in the first half of the *Figure's* space (which is shown below). The remaining half of the *Figure*, depending on the nature of the data observed, will consist of data analysis plots (using the data from the first half). The data analysis plots can include deconvoluted propylene gas concentration plots (to help quantify the amount of propylene gas captured and released) as well as Faradaic efficiency calculations based on the charge applied by the Potentiostat onto the MEA flow cell reactor.



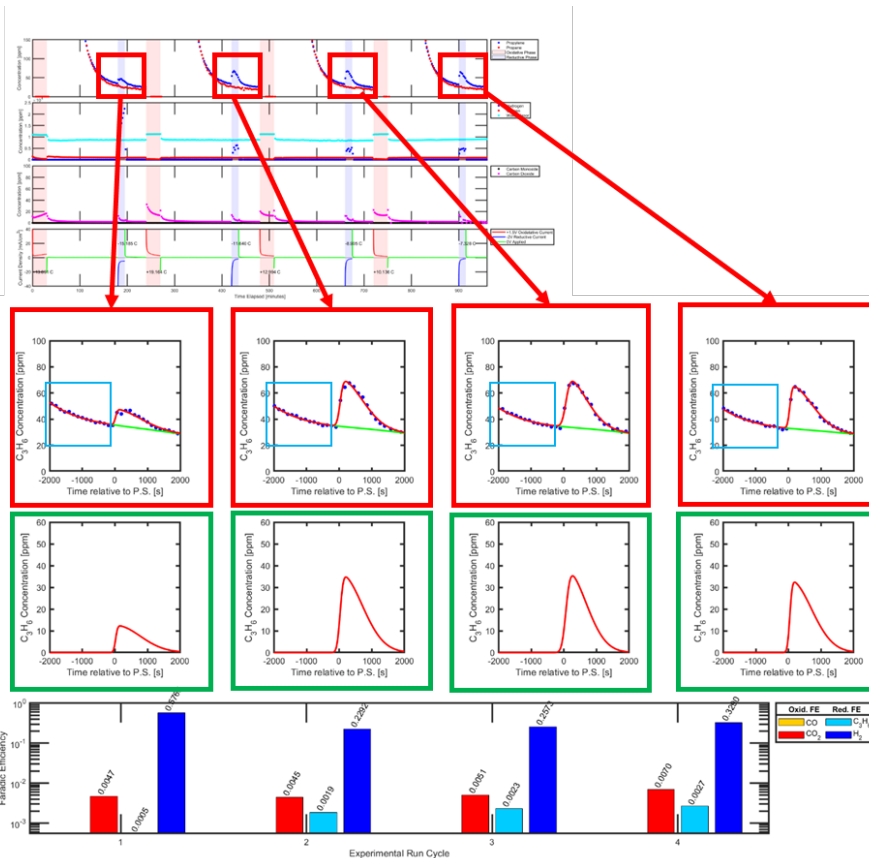
Many different experimentally accessible variables (EAV's) are being observed while an experiment is being run. Showing all these EAV's on a single graph would prove to be too congested. Therefore, only a few EAV's are plotted on each individual graph to make them more visually readable. The top 3 plots represent gas composition measurements (ppm) of the outlet stream coming out of the MEA flow cell reactor vs. time. The bottom plot represents electrical current (mA) applied to the MEA flow cell reactor over time. Columbic charge (C) derived from the integral area of the chronoamperometric plot is labeled at each oxidative and reductive potential segment. All 4 plots are vertically aligned on the time-axis as shown above.

The most important EAV plots pertaining to the main manuscript's propylene/propane separation work are the top plot showing the propylene and propane concentration and the bottom plot showing the electrical current measurements. The middle two plots are used primarily to keep track of possible parasitic reactions. The middle two plots showing hydrogen, oxygen, water vapor, carbon monoxide, and carbon dioxide gas concentrations are not the main gases of interest for this work, but they are important to be included in the supplementary information so that Faradaic efficiency relationship can be shown in subsequent analysis. It should be noted that the propylene and propane concentrations are cut off at earlier time intervals per cycle because the concentration of propylene

and propane were approximately 3 orders of magnitude greater during the oxidative capture phase. The concentration profile during the reductive phase would have appeared flat (no peaks) should the entire concentration range have been scaled to be visible when graphing the plots.



For each individual MEA experiment, commonly 4 cycles are employed consecutively. The first cycle usually exhibits propylene/propane concentration changes that seem different from the subsequent 3 cycles. Therefore, the first cycle, which is suspected of being a stabilizing event, is excluded from plots shown in Figures 3 and 4 in the main manuscript (*i.e.* only the last 3 cycles' average and standard deviation bars are shown in the main manuscript's figures).



Use local data points prior to polarity switch to fit decreasing propylene concentration trend

Deconvolute propylene graph and fit deconvoluted points with skewed Gaussian Distribution Curve

After the oxidative phase in each cycle, nitrogen flush was used to clear the system of excess propylene/propane gas. It should be noted that there was an obvious downward trend in the propylene concentration over time in any given cycle (at least until right before the polarity switch) because of the nitrogen flush actively “cleaning” the system of residual free propylene and propane gas. In an ideal scenario, nitrogen flush should be continued until both propylene and propane concentration reaches zero. However, that ideal scenario was not feasible because propylene and propane proved to be difficult to completely rid of from the system even after flushing it for several weeks. Since the MEA reactor’s active surface area was approximately 2 cm<sup>2</sup>, only a relatively small amount of propylene can be captured and released, and therefore the Micro GC must be able to detect propylene concentration changes at below 300 ppm. The experimental procedure outlined in the main manuscript was designed in a way that “just enough” flush can be achieved to allow the Micro GC to detect subtle concentration changes below 300 ppm without spending excessive time in waiting for the propylene and propane concentration to decrease to low enough ppm ranges. In order to isolate the general downward concentration trend of propylene from the electrochemically induced propylene release, the graph was deconvoluted by subtracting a local polynomial fit of data points prior to polarity switch (i.e. before reductive phase begins).

The deconvoluted points were then fitted to a skewed Gaussian distribution curve for each individual cycle. The mathematical product of the integral area under this fitted Gaussian curve and the flow rate of the nitrogen flush was calculated as the amount of propylene captured and released via electrochemical modulation. Appropriate unit conversions assuming ideal gas law conditions were applied in this calculation, resulting in moles of propylene captured and released. It should be noted that only the number of moles of propylene “released” was able to be calculated through the gas stream outlet composition measurements. The number of moles of propylene “captured” was unable to be calculated via this method.

Although not shown in the *Figures*, other gas components including hydrogen, carbon monoxide, and carbon dioxide, were quantified through a similar method. However, no deconvolution was conducted for those gases’ graph because the concentration changes of the said gases due to electrochemically induced effect were at least 2 orders of magnitude greater compared to propylene’s concentration change during polarity switch, making deconvolution effect negligible for those other gases. Hydrogen gas was quantified in the time of the reductive

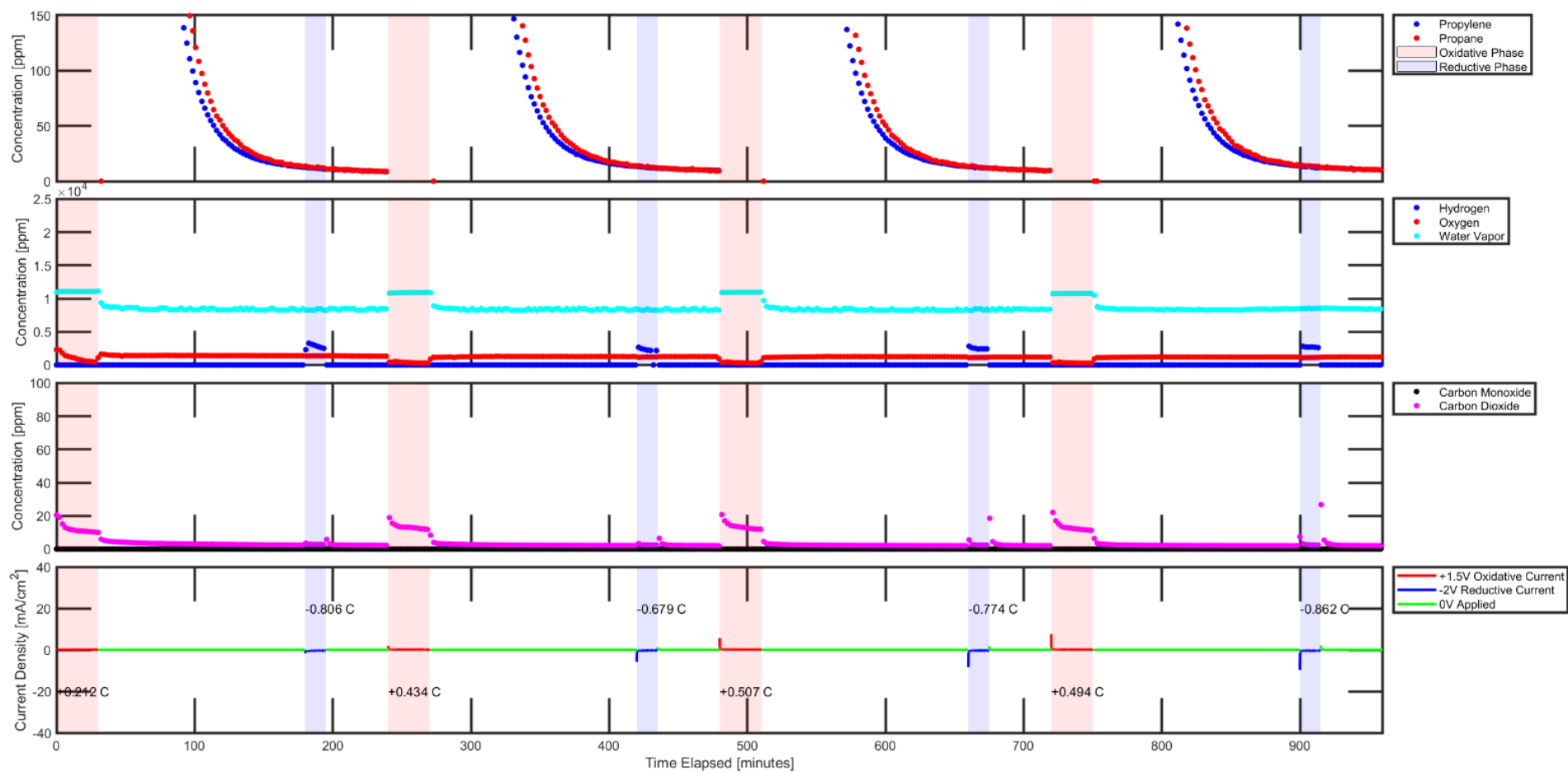
phase only, like that of propylene. Carbon monoxide and carbon dioxide moles were calculated only within the oxidative phase period. Also, simple area integration via trapezoidal rule between the actual data points was used instead of integrating under a fitted Gaussian curve.

The Faradaic efficiency (FE) bar graph at the bottom of the *Figure* shows two different groups of FE: oxidative FE and reductive FE. The oxidative FE is calculated with respect to the total charge applied during the oxidative phase of its corresponding cycle. Carbon dioxide and carbon monoxide oxidative FE's are shown as yellow and red-colored bars, respectively. The reductive FE is calculated with respect to the total charge applied during the reductive phase of its corresponding cycle. Propylene and hydrogen reductive FE's are shown as cyan and navy blue-colored bars, respectively. It should be noted that hydrogen F.E.'s was sometimes  $>1$  because GC standard calibrations with hydrogen gas were not as accurate like the ones used for propylene/propane quantification and because hydrogen was not a prioritized factor during observation of the experiments. In most cases, the reductive FE of propylene was  $>2$  orders of magnitude smaller than the reductive FE of hydrogen. In order to make the bar plot visually convenient to compare the FE's between propylene and hydrogen, the vertical axis is scaled logarithmically.

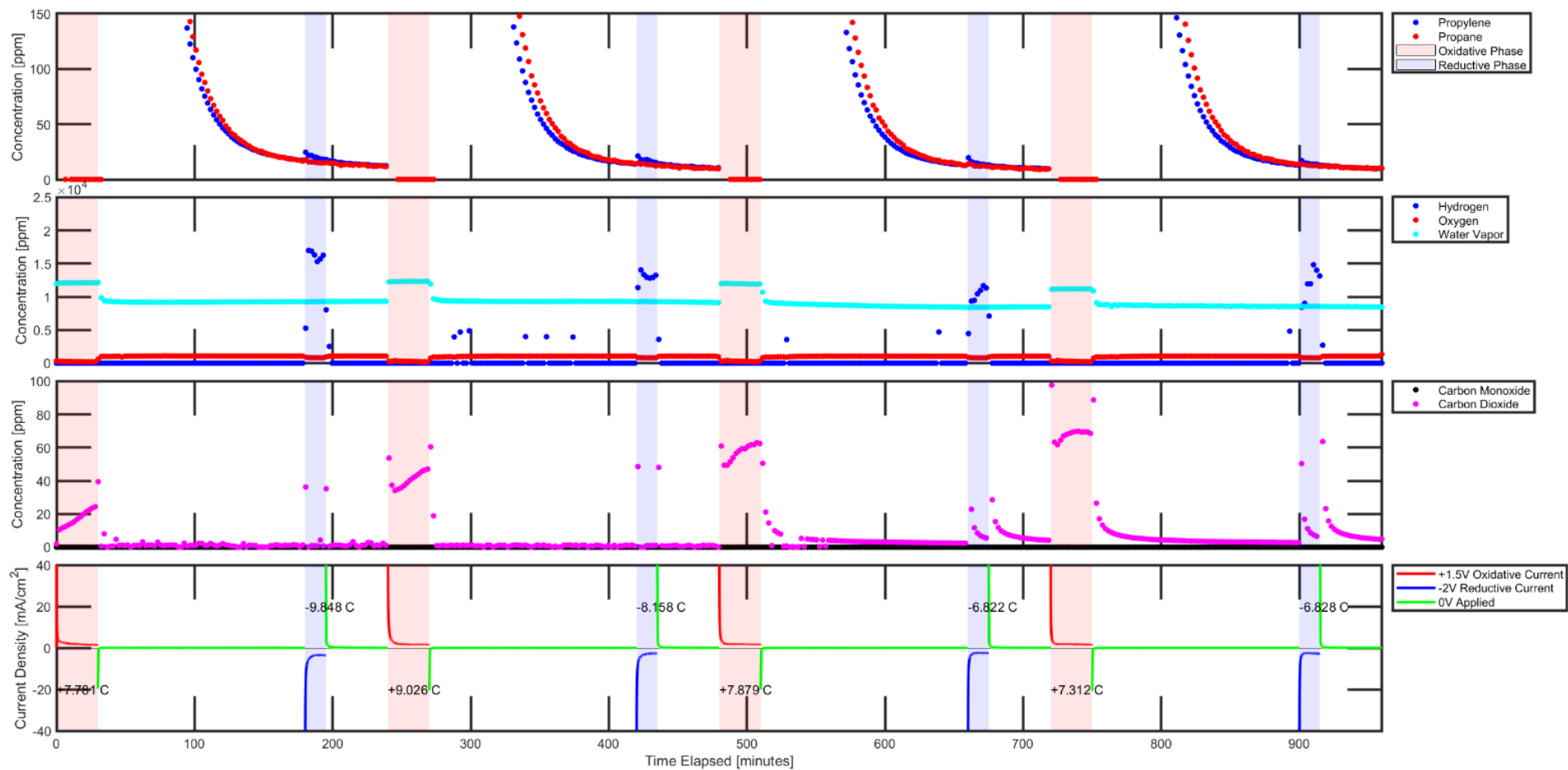
**Section Summary:**

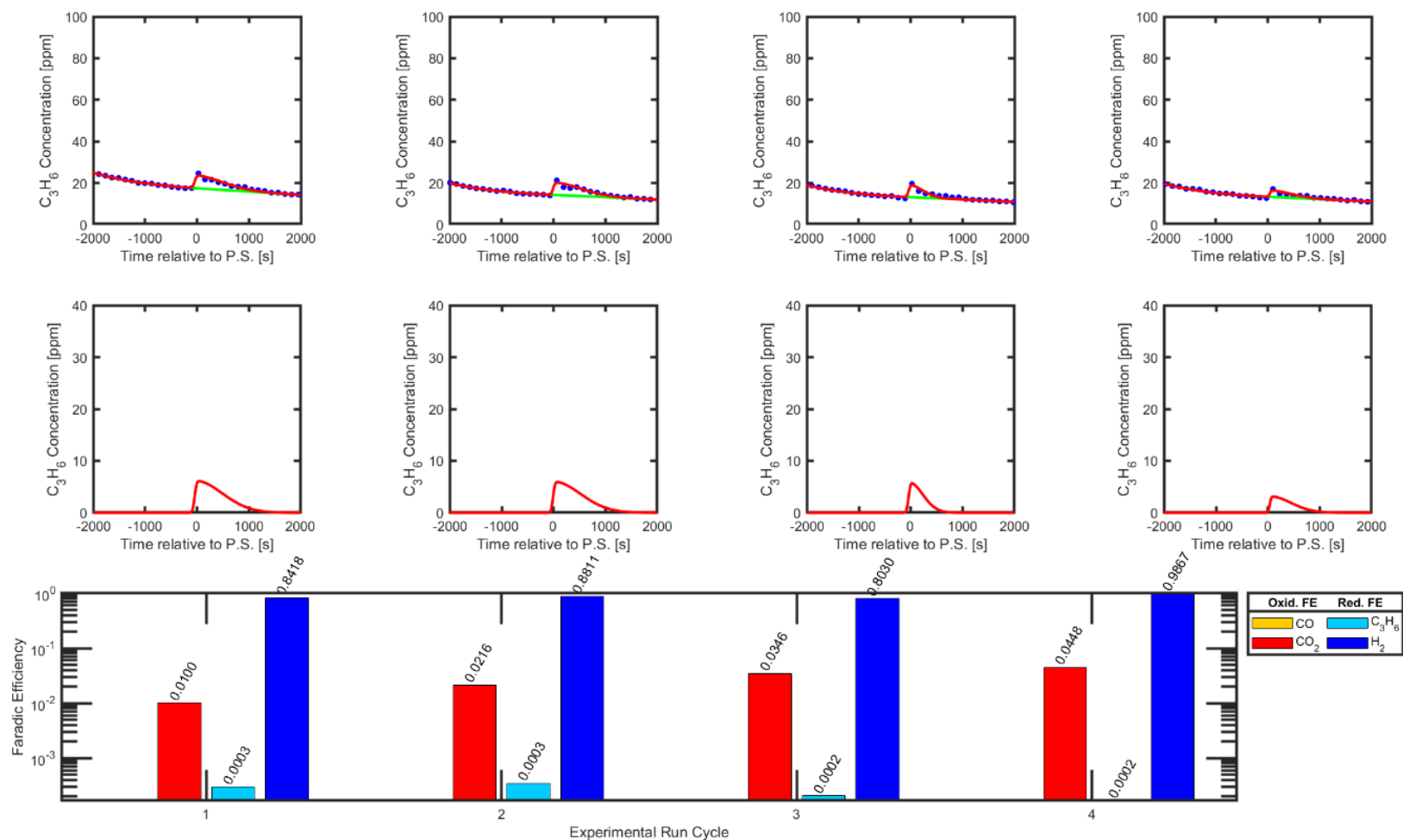
5 MEA samples of varying tetraethylammonium nickel dithiolene salts were tested in this series of experiments. Therefore, this section consists of 5 *Figures* each with its own corresponding loading for the tetraethylammonium nickel dithiolene salt (i.e., 0, 2, 3, 4, and 8 mg/cm<sup>2</sup>). This series of experiments contributed to the data shown in **Figure 3-A1** and **3-A2** of the main manuscript. All other parameters, including IL, Nafion, and Carbon loadings were kept constant for the purpose of observing the effect of nickel dithiolene loading on propylene separation performance. All 5 MEA samples utilized the same oxidative and reductive potentials of +1.5V and -2V, respectively. A 50:50 molar ratio propylene-propane feed was introduced to the MEA during the oxidative phase as well. It was found that the at loadings between 2-4 mg/cm<sup>2</sup> (**Figures S1-B** thru **S1-D**) the propylene separation performance is a strong function of the complex loading, but eventually approaches a plateau as the loading approaches >4 mg/cm<sup>2</sup> (**Figures S1-D** thru **S1-E**). This asymptotic behavior suggests that at high complex loadings, the separation is hindered due to transport limitations that limit the access of [Ni(mnt)<sub>2</sub>]<sup>n</sup> to the electrode surface, or the ability for propylene to reach all reaction sites. In subsequent experiments, the loading was kept constant at 8 mg/cm<sup>2</sup> since it exhibited a sufficiently high throughput of purified propylene.

S1-A

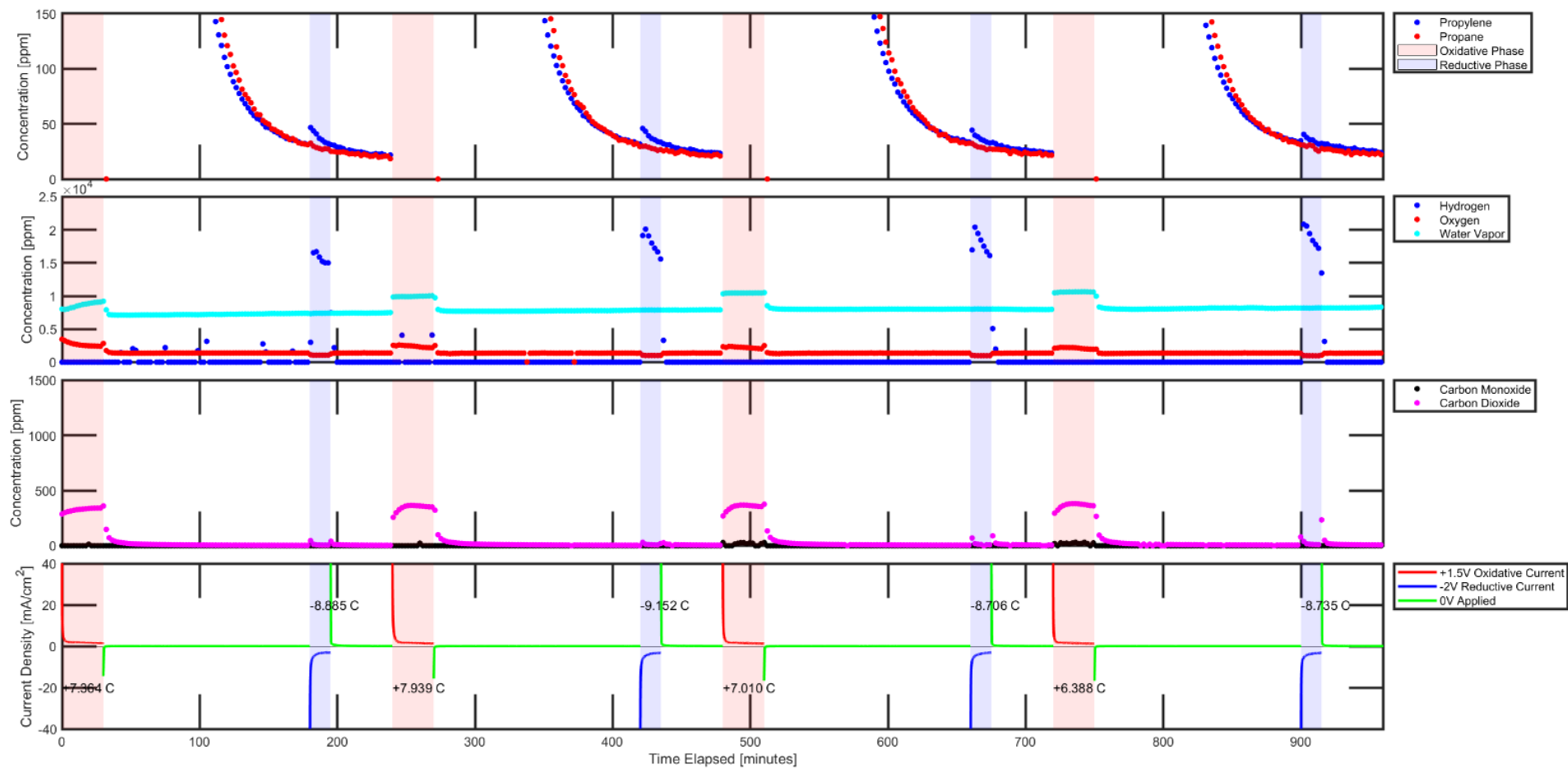


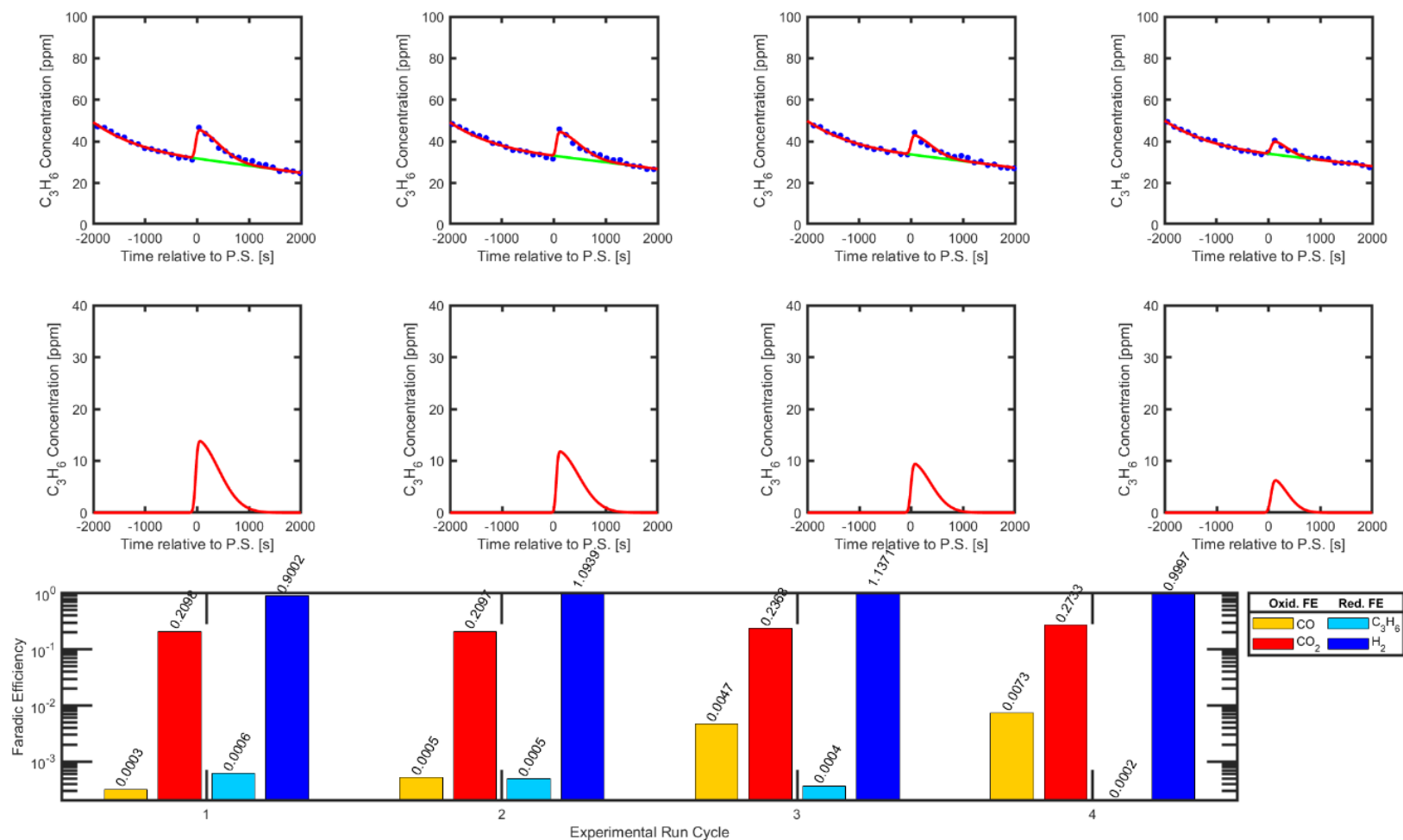
**Figure S1-A:  $0 \text{ mg}/\text{cm}^2$   $[\text{N}(\text{Et})_4]_2[\text{Ni}(\text{mnt})_2]$ .** Gas concentration measurements via Agilent Micro GC 990 and Chronoamperometry via Potentiostat. This was a control experiment with no Nickel Dithiolene deposited onto GDL.



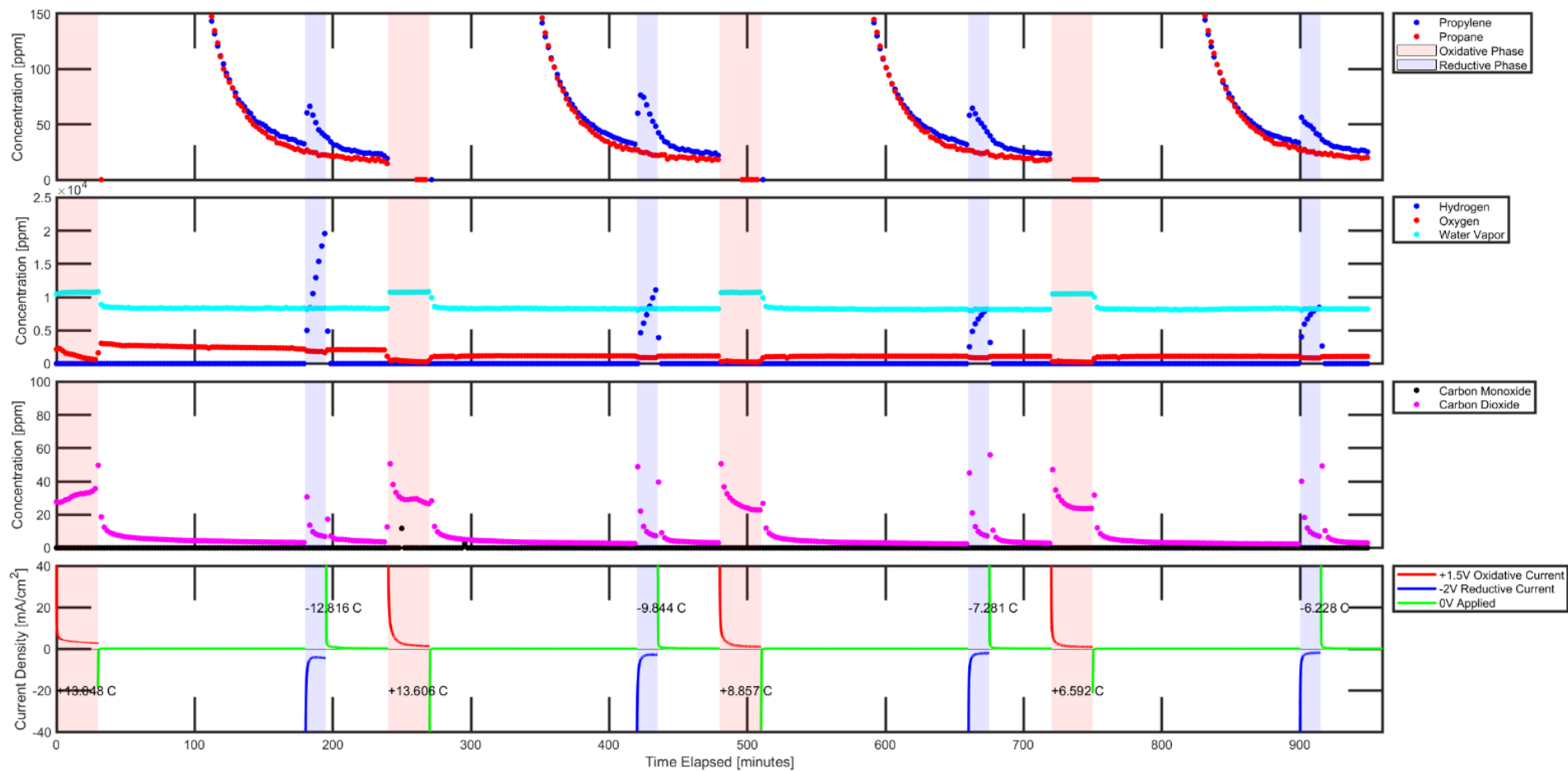


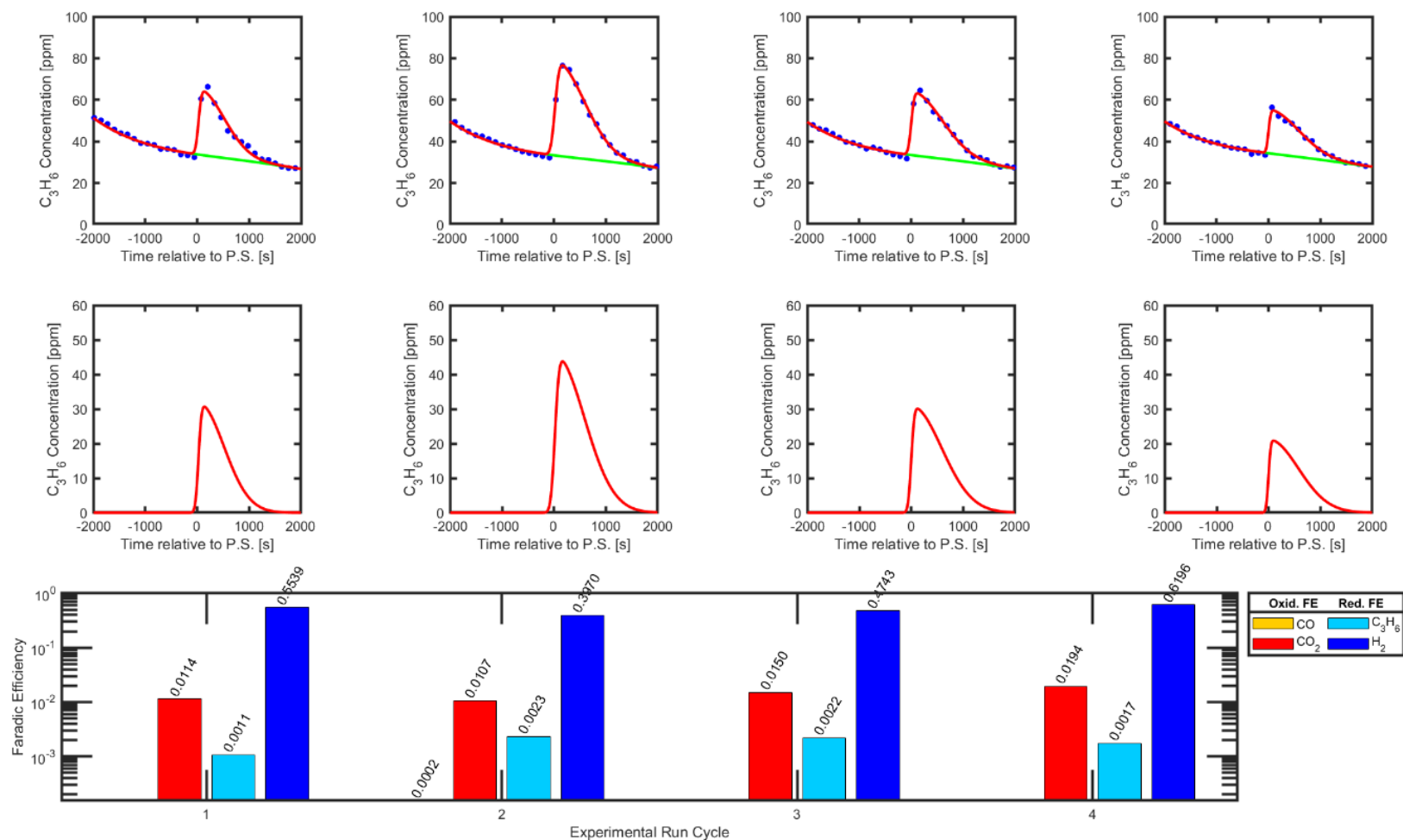
**Figure S1-B: 2 mg/cm<sup>2</sup> [N[Et]<sub>4</sub>]<sub>2</sub>[Ni(mnt)<sub>2</sub>].** Gas concentration measurements via Agilent Micro GC 990, Chronoamperometry via Potentiostat, graphical analysis of propylene captured and released via Electrochemical Modulation, and Faradic efficiency of secondary gas products and propylene separated via electrochemical capture-and-release mechanism. Second row of graphical analysis depicts deconvoluted graphs of propylene concentration separated by electrochemically modulated complexation mechanism. Spray-deposited layer consisted of 5 mg/cm<sup>2</sup> Carbon Nanoparticles, 4 mg/cm<sup>2</sup> Nafion ionomer, 4 mg/cm<sup>2</sup> [BMIM][PF<sub>6</sub>] ionic liquid, and 2 mg/cm<sup>2</sup> [N[Et]<sub>4</sub>]<sub>2</sub>[Ni(mnt)<sub>2</sub>] salt onto Sigracet 39 BB Carbon GDL.



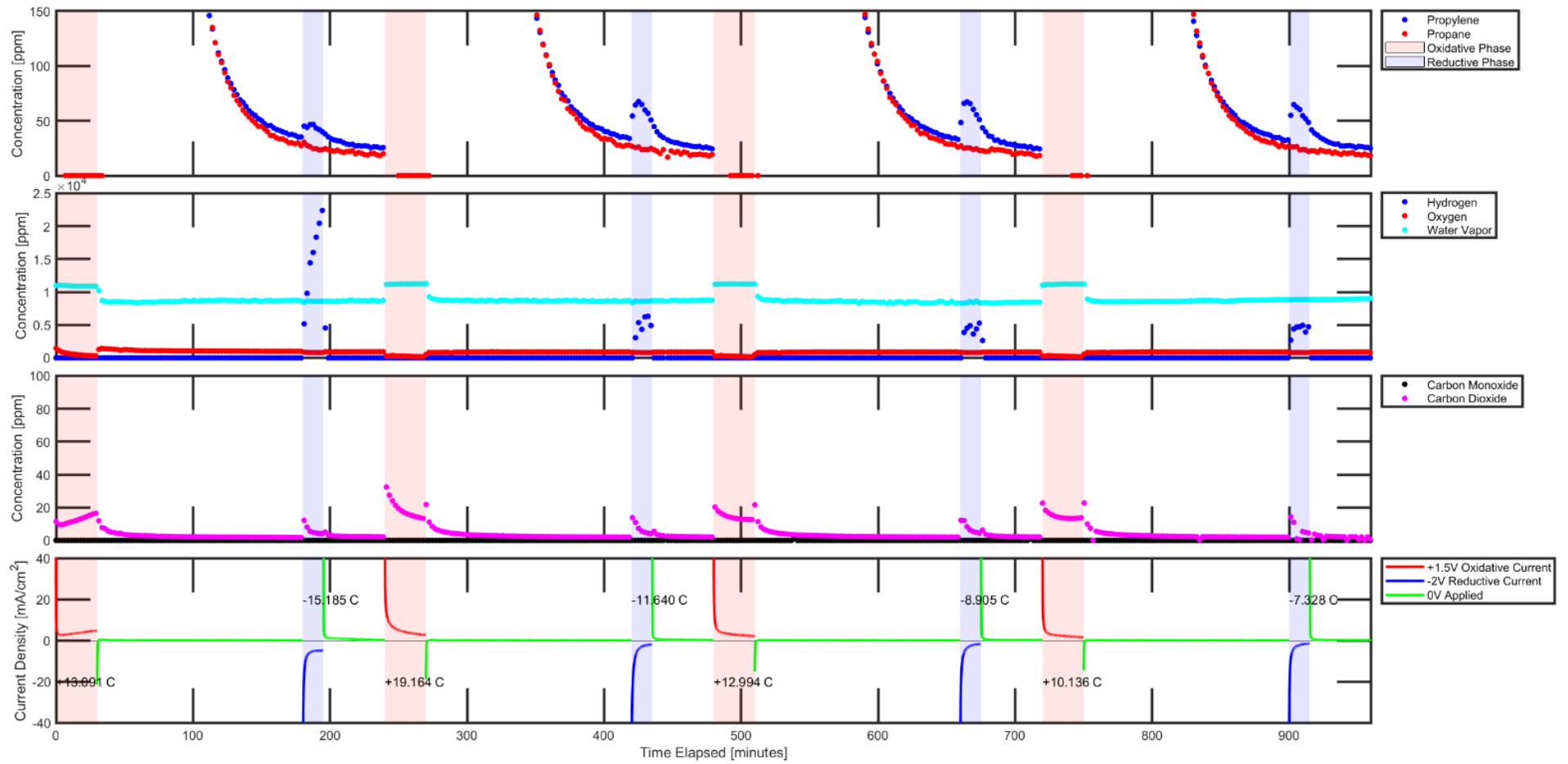


**Figure S1-C: 3 mg/cm<sup>2</sup> [N(Et)<sub>4</sub>]<sub>2</sub>[Ni(mnt)<sub>2</sub>].** Gas concentration measurements via Agilent Micro GC 990, Chronoamperometry via Potentiostat, graphical analysis of propylene captured and released via Electrochemical Modulation, and Faradic efficiency of secondary gas products and propylene separated via electrochemical capture-and-release mechanism. Second row of graphical analysis depicts deconvoluted graphs of propylene concentration separated by electrochemically modulated complexation mechanism. Spray-deposited layer consisted of 5 mg/cm<sup>2</sup> Carbon Nanoparticles, 4 mg/cm<sup>2</sup> Nafion ionomer, 4 mg/cm<sup>2</sup> [BMIM][PF<sub>6</sub>] ionic liquid, and 3 mg/cm<sup>2</sup> [N(Et)<sub>4</sub>]<sub>2</sub>[Ni(mnt)<sub>2</sub>] salt onto Sigracet 39 BB Carbon GDL. Please note that hydrogen F.E.'s were sometimes >1 because GC standard calibrations with hydrogen gas were not as accurate like the ones used for propylene/propane quantification and because hydr





**Figure S1-D: 4 mg/cm<sup>2</sup> [N(Et)<sub>4</sub>]<sub>2</sub>[Ni(mnt)<sub>2</sub>].** Gas concentration measurements via Agilent Micro GC 990, Chronoamperometry via Potentiostat, graphical analysis of propylene captured and released via Electrochemical Modulation, and Faradic efficiency of secondary gas products and propylene separated via electrochemical capture-and-release mechanism. Second row of graphical analysis depicts deconvoluted graphs of propylene concentration separated by electrochemical modulated complexation mechanism. Spray-deposited layer consisted of 5 mg/cm<sup>2</sup> Carbon Nanoparticles, 4 mg/cm<sup>2</sup> Nafion ionomer, 4 mg/cm<sup>2</sup> [BMIM][PF<sub>6</sub>] ionic liquid, and 4 mg/cm<sup>2</sup> [N(Et)<sub>4</sub>]<sub>2</sub>[Ni(mnt)<sub>2</sub>] salt onto Sigracet 39 BB Carbon GDL.



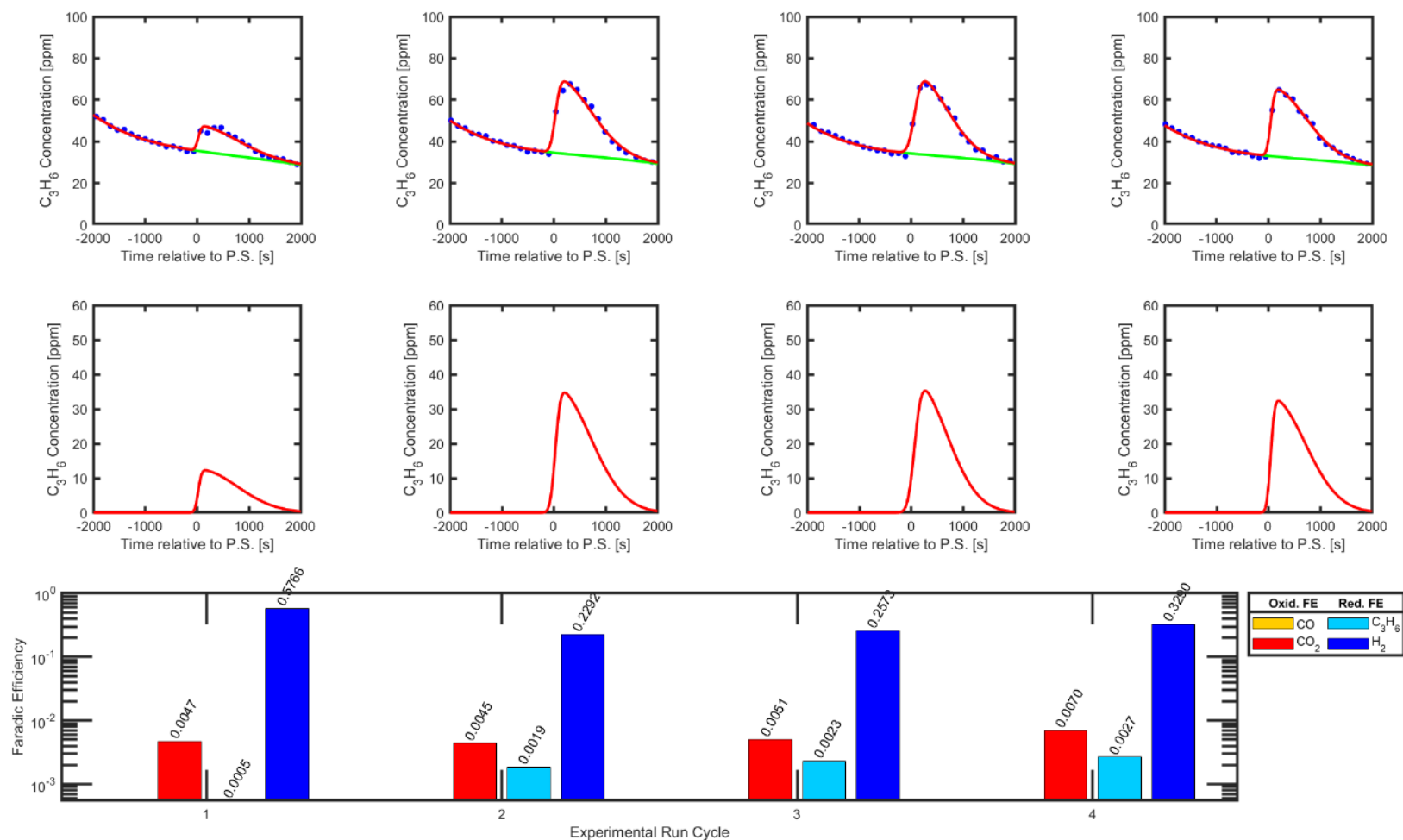


**Figure S1-E:  $8 \text{ mg/cm}^2$   $[N(\text{Et})_4]_2[\text{Ni}(\text{mnt})_2]$ .** Gas concentration measurements via Agilent Micro GC 990, Chronoamperometry via Potentiostat, graphical analysis of propylene captured and released via Electrochemical Modulation, and Faradic efficiency of secondary gas products and propylene separated via electrochemical capture-and-release mechanism. Second row of graphical analysis depicts deconvoluted graphs of propylene concentration separated by electrochemical modulated complexation mechanism. Spray-deposited layer consisted of  $5 \text{ mg/cm}^2$  Carbon Nanoparticles,  $4 \text{ mg/cm}^2$  Nafion ionomer,  $4 \text{ mg/cm}^2$   $[\text{BMIM}][\text{PF}_6]$  ionic liquid, and  $8 \text{ mg/cm}^2$   $[N(\text{Et})_4]_2[\text{Ni}(\text{mnt})_2]$  salt onto Sigracet 39 BB Carbon GDL.

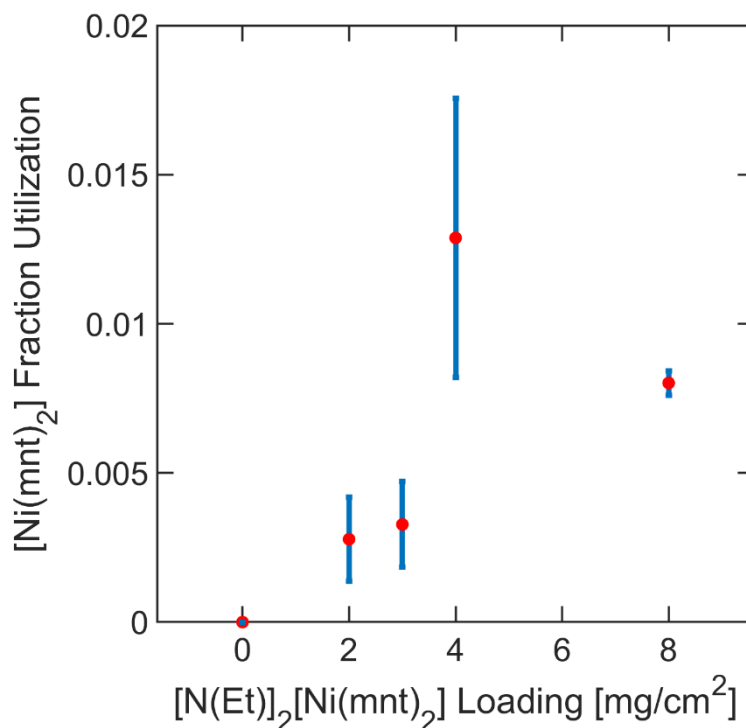


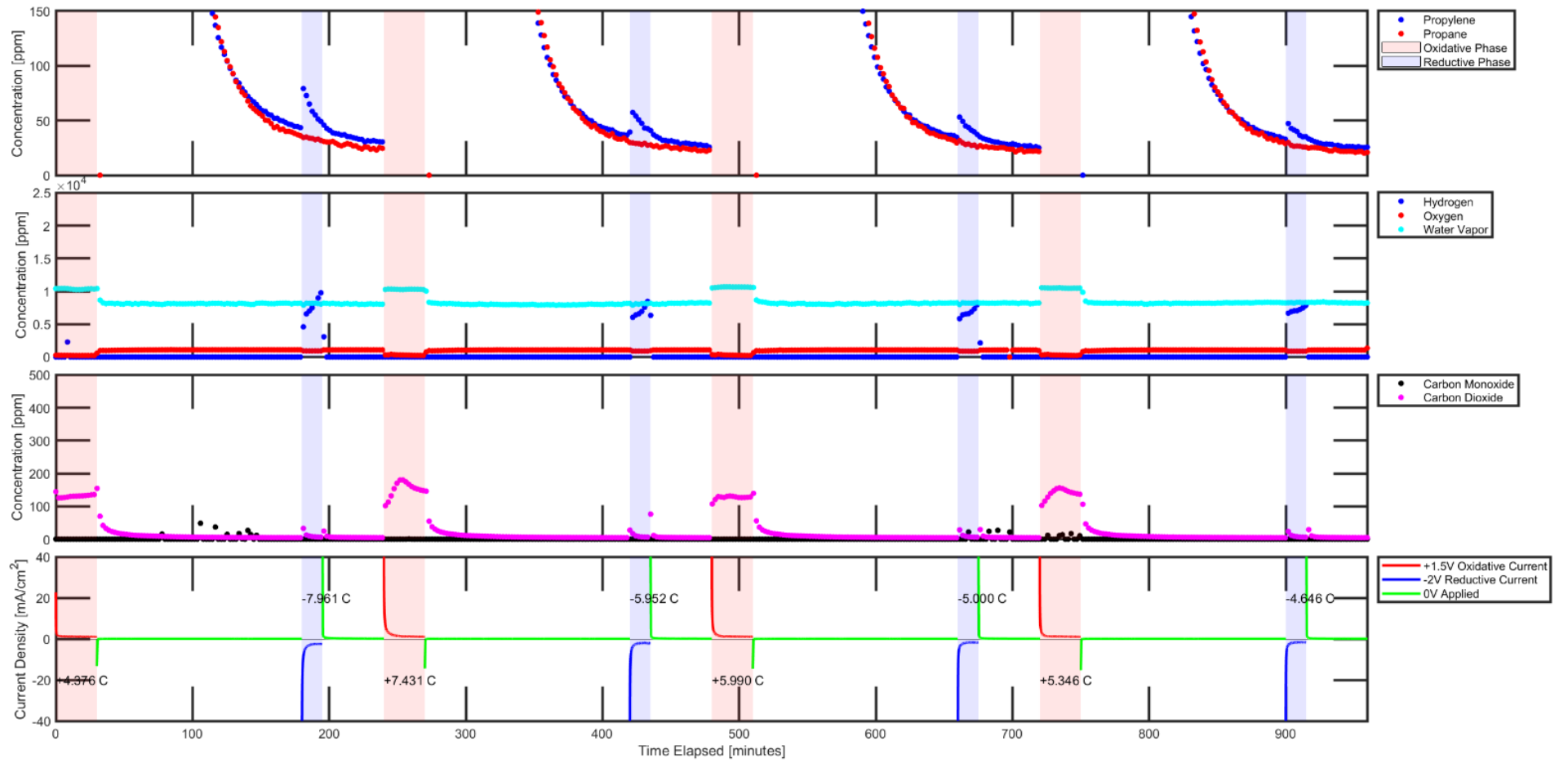
**Figure S1-F: [Ni(mnt)<sub>2</sub>] Utilization Fraction.** Based on the amount of propylene captured and released per MEA sample of varying [N(Et)<sub>4</sub>]<sub>2</sub>[Ni(mnt)<sub>2</sub>] loadings, the material utilization fraction of the [Ni(mnt)<sub>2</sub>] species that facilitated the propylene separation is shown in the above graph. The material utilization generally did not exceed 2% utilization, which means that most of the [Ni(mnt)<sub>2</sub>] species present on the MEA system were not fully committed to the capture-and-release of propylene. The utilization fraction seems to have reached a local maxima at approximately 4 mg/cm<sup>2</sup> because it is very likely that the ionogel was saturated with the species at that loading, and therefore could not access any additional amount of [N(Et)<sub>4</sub>]<sub>2</sub>[Ni(mnt)<sub>2</sub>] beyond that point. Phase separation of the [N(Et)<sub>4</sub>]<sub>2</sub>[Ni(mnt)<sub>2</sub>] crystals (refer to section S7) seems to indicate saturation of the [Ni(mnt)<sub>2</sub>] species at approximately 4 mg/cm<sup>2</sup>. Error bars represent standard deviations of the last 3 cycles per MEA sample.

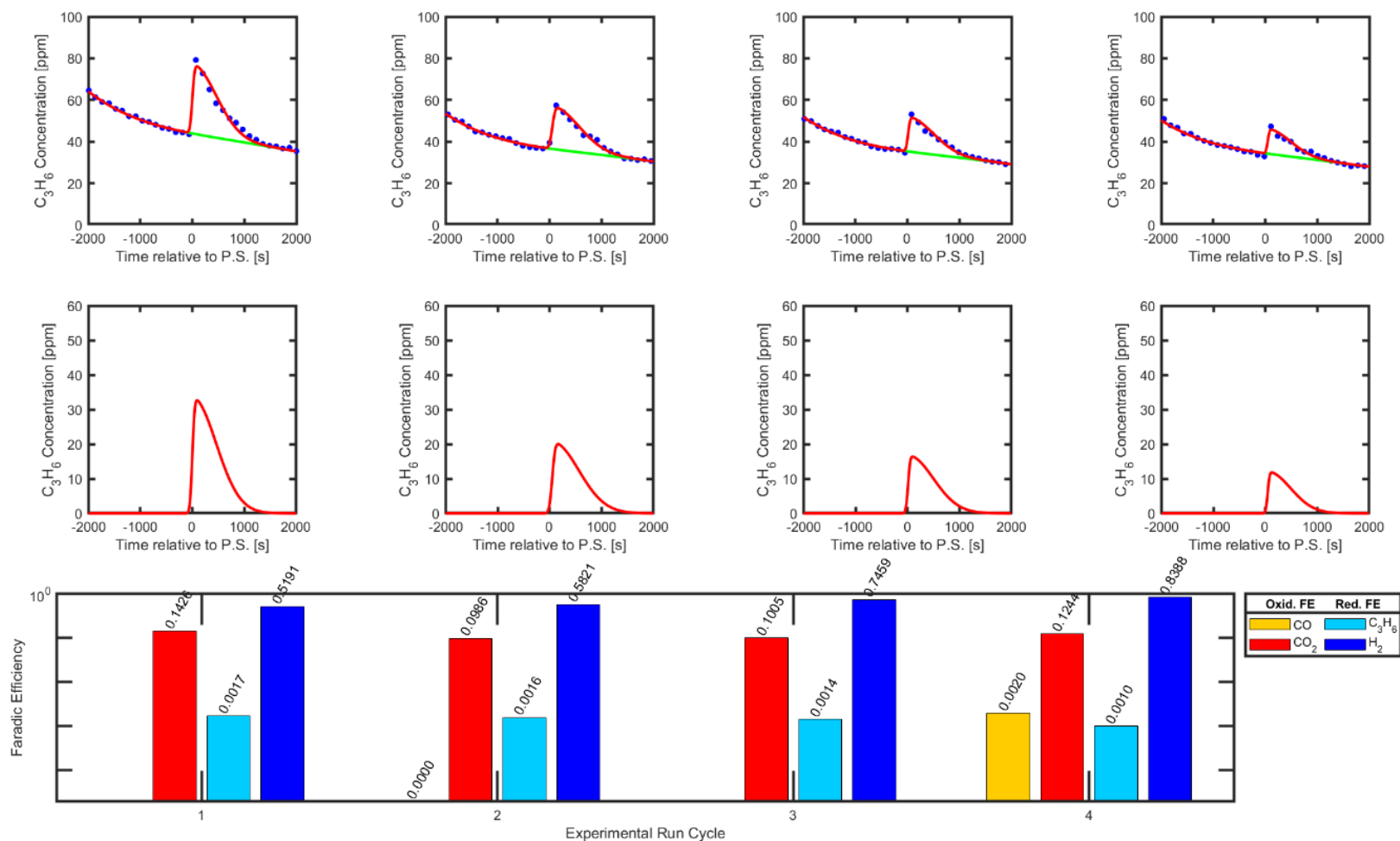
**Section Summary:**

5 MEA samples of varying ionic liquid loadings were tested in this series of experiments. Therefore, this section consists of 5 *Figures* each with its own corresponding loading for the tetraethylammonium nickel dithiolene salt (i.e., 0, 2, 4, 8, and 16 mg/cm<sup>2</sup>). This series of experiments contributed to the data shown in **Figure 3-B** of the main manuscript. All other parameters, including tetraethylammonium nickel dithiolene salt, Nafion, and Carbon loadings were kept constant for the purpose of observing the effect of IL loading on propylene separation performance. All 5 MEA samples utilized the same oxidative and reductive potentials of +1.5V and -2V, respectively. A 50:50 molar ratio propylene-propane feed was introduced to the MEA during the oxidative phase as well.

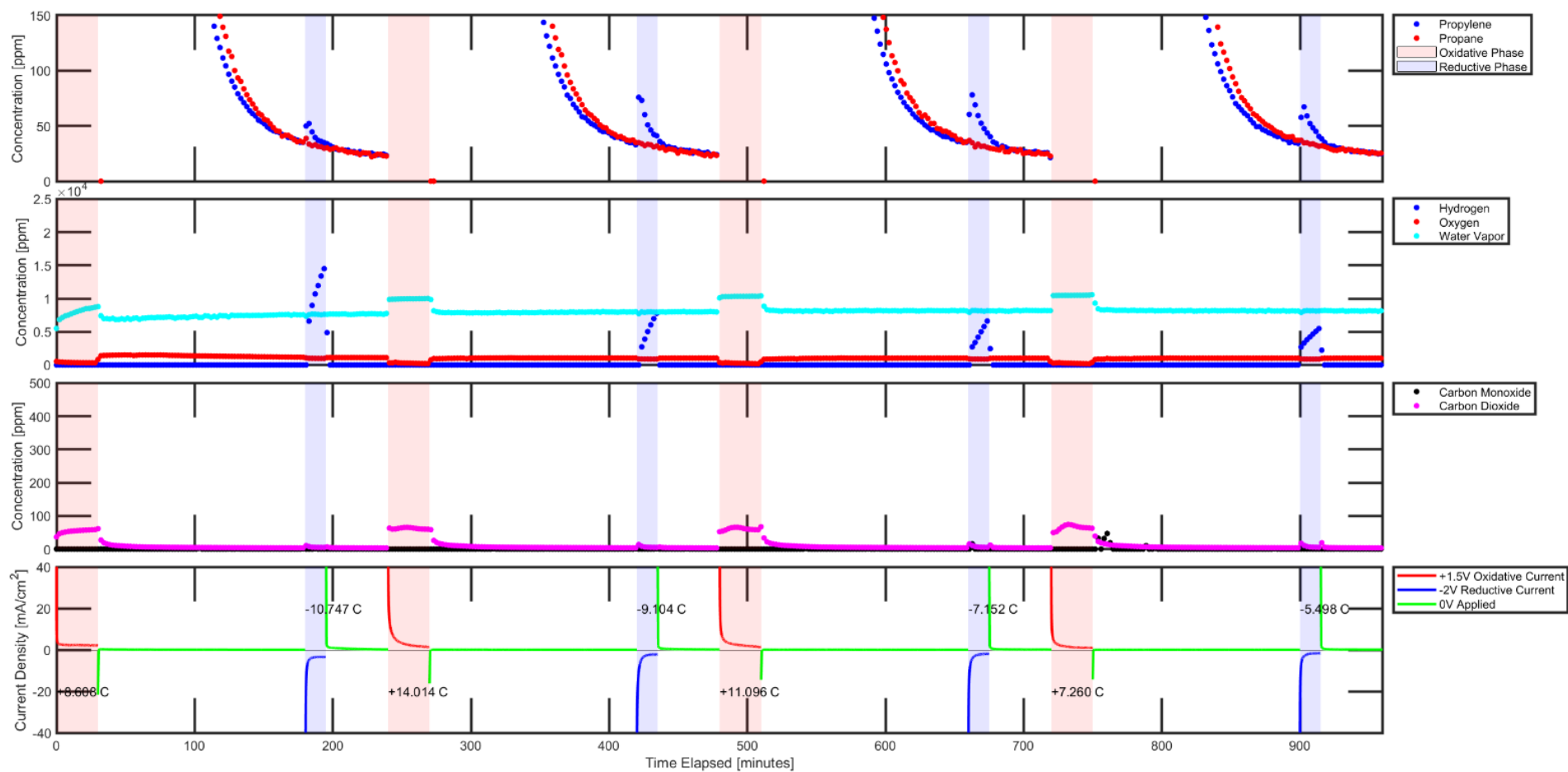
It was determined that the presence of the ionic liquid can improve the separation performance of the MEA. In MEAs where no IL was used (**Figure S2-A**), only modest separation performance was observed, likely due to lack of mobility of [Ni(mnt)<sub>2</sub>]<sup>n</sup> through the neat Nafion polymer matrix. By introducing IL into the Nafion medium, the separation performance increased by as much as 2.5 times at an IL loading of 4 mg/cm<sup>2</sup> (**Figure S2-C**).

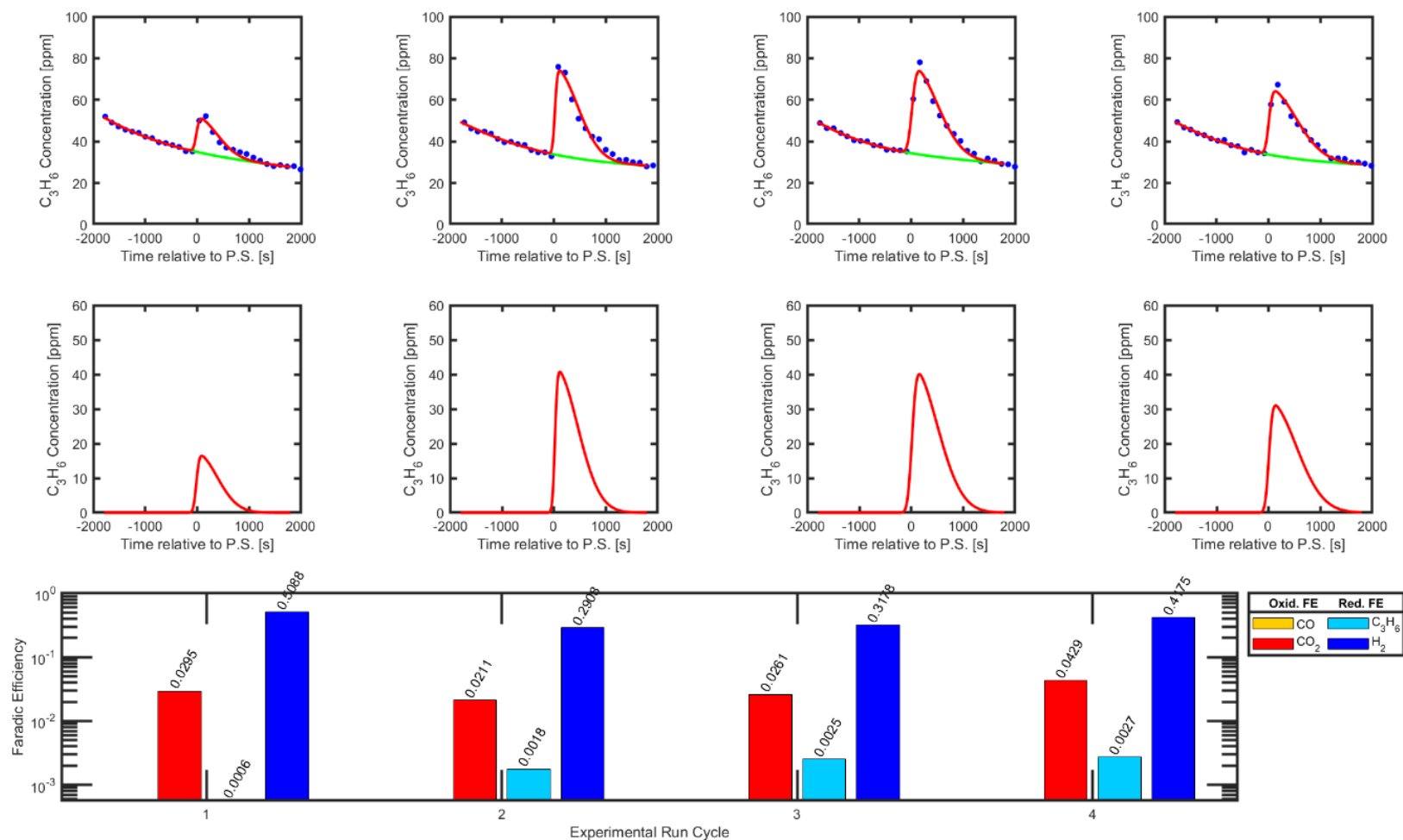
Furthermore, a local maximum was discovered in the relationship between IL loading and separation performance because of transport limitations induced by increased concentration of IL in the MEA. The separation performance decreased progressively after reaching an IL loading of 4 mg/cm<sup>2</sup> (**Figures S2-C** thru **S2-E**). It is possible that excessive IL in the ionogel can inadvertently lower the gas/ionogel interfacial area, consequentially restricting the amount of propylene that can be absorbed into the MEA. Furthermore, the ionogel can easily be swelled with increased IL ratio, which can then increase the overall physical distance between the carbon electrode surface and the gas interface increase the mass transport resistance. Since an IL loading of 4 mg/cm<sup>2</sup> demonstrated optimal functionality with 8 mg/cm<sup>2</sup> of [N(Et)<sub>4</sub>]<sub>2</sub>[Ni(mnt)<sub>2</sub>] in terms of propylene separation performance, these parameters were kept constant on subsequent studies.



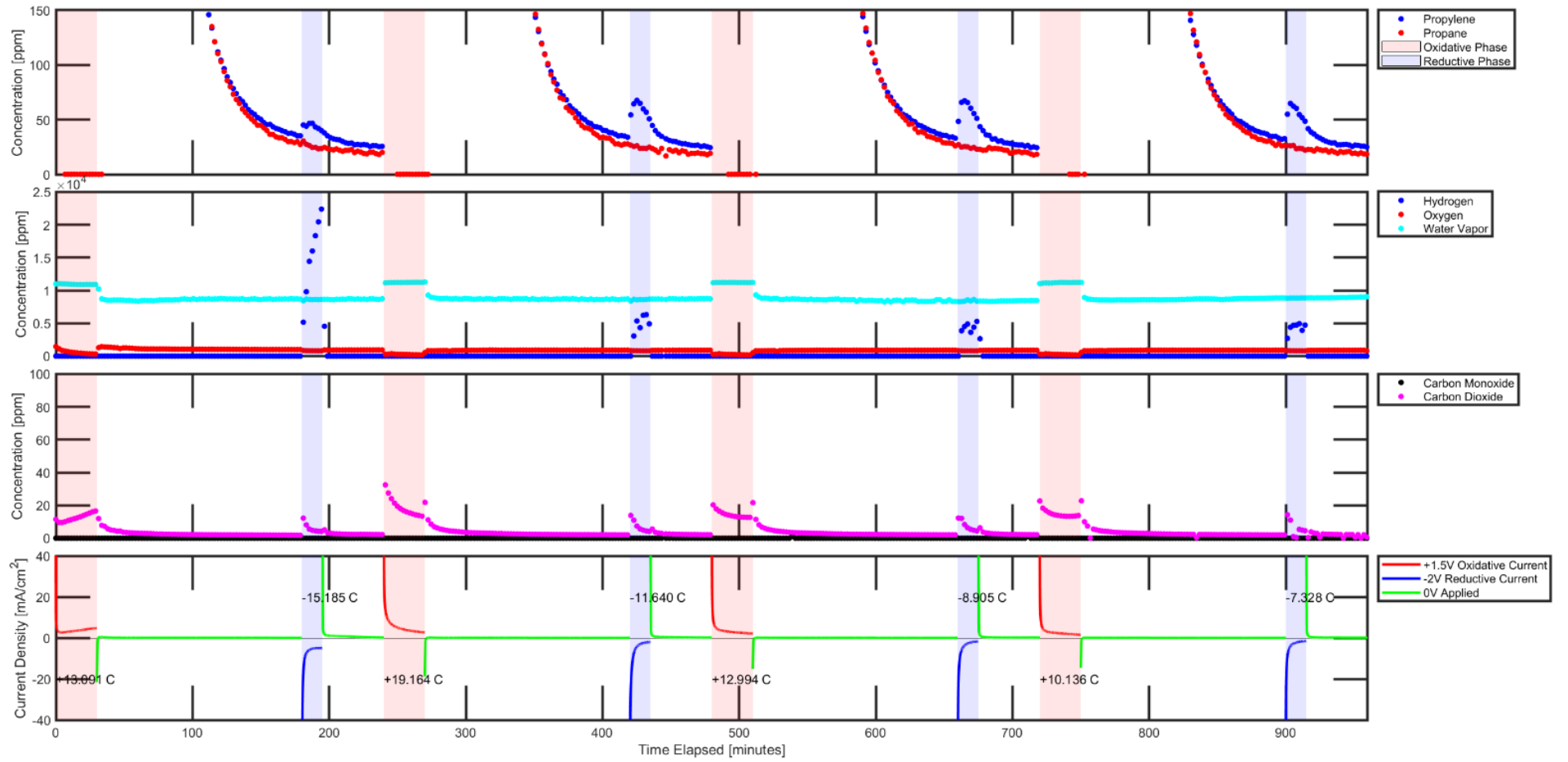


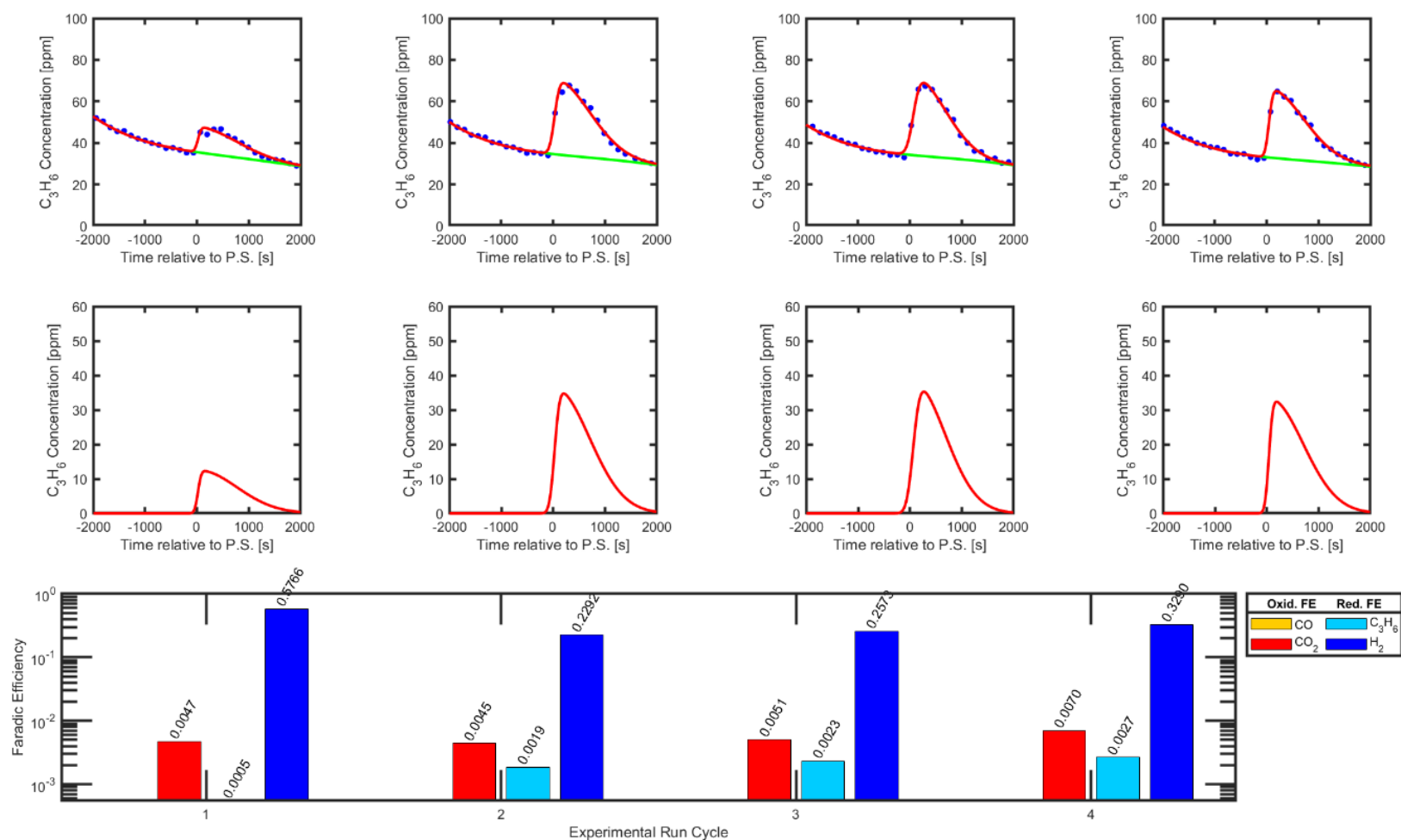
**Figure S2-A: 0 mg/cm<sup>2</sup> IL.** Gas concentration measurements via Agilent Micro GC 990, Chronoamperometry via Potentiostat, graphical analysis of propylene captured and released via Electrochemical Modulation, and Faradic efficiency of secondary gas products and propylene separated via electrochemical capture-and-release mechanism. Second row of graphical analysis depicts deconvoluted graphs of propylene concentration separated by electrochemical modulated complexation mechanism. Spray-deposited layer consisted of 5 mg/cm<sup>2</sup> Carbon Nanoparticles, 4 mg/cm<sup>2</sup> Nafion ionomer, 0 mg/cm<sup>2</sup> [BMIM][PF<sub>6</sub>] ionic liquid, and 8 mg/cm<sup>2</sup> [N(Et)<sub>4</sub>]<sub>2</sub>[Ni(mnt)<sub>2</sub>] salt onto Sigracet 39 BB Carbon GDL.



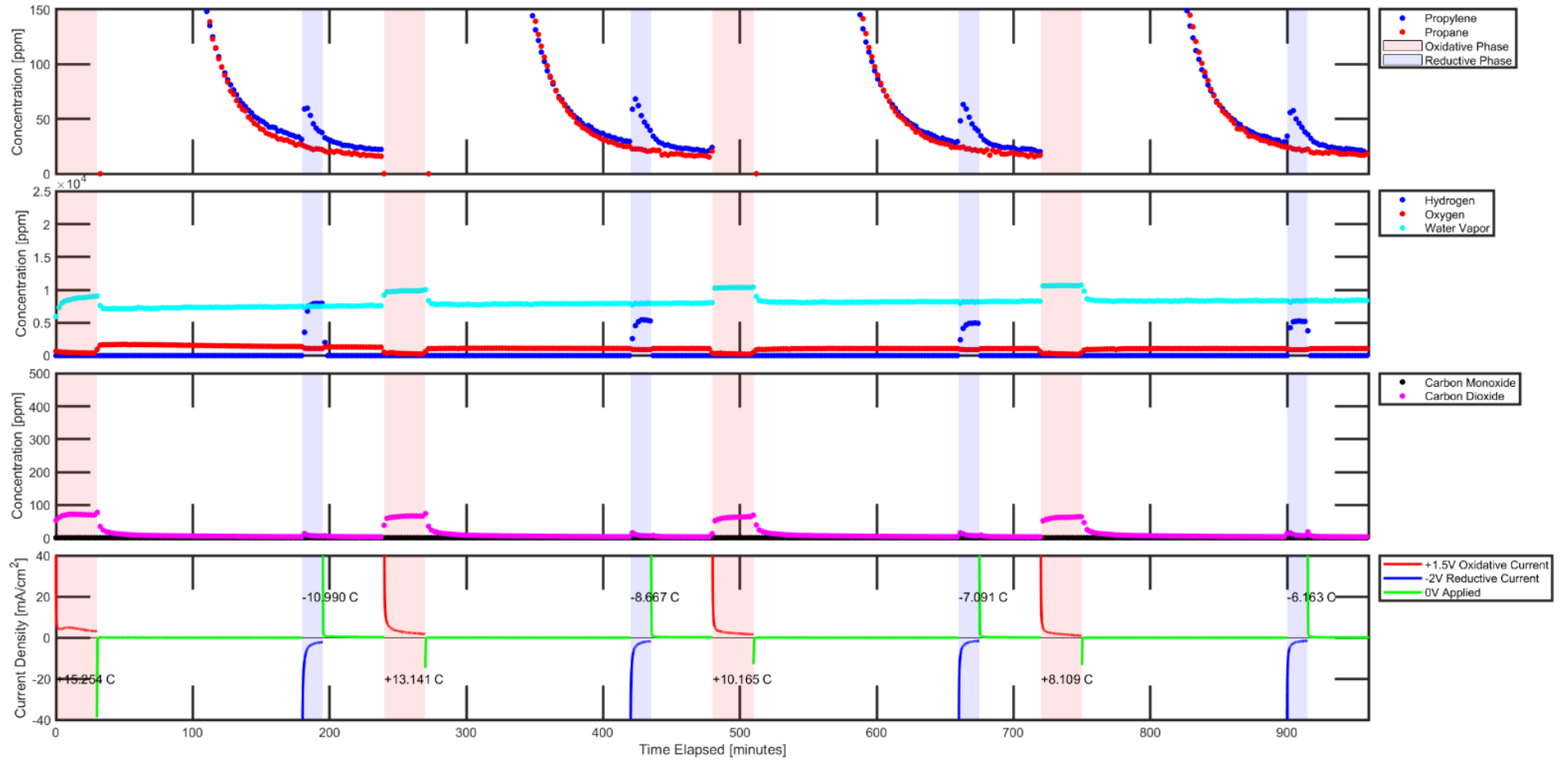


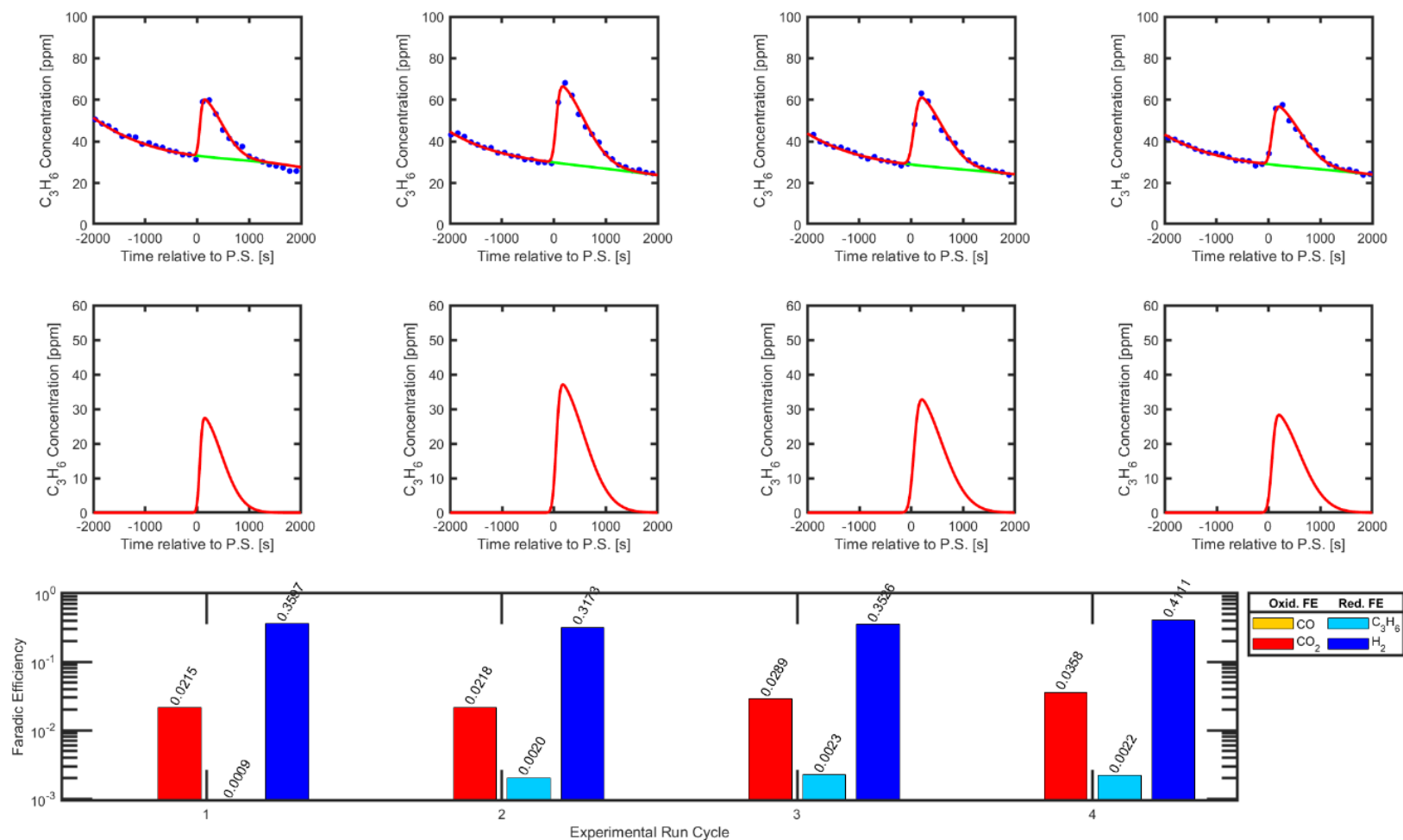
**Figure S2-B: 2 mg/cm<sup>2</sup> IL.** Gas concentration measurements via Agilent Micro GC 990, Chronoamperometry via Potentiostat, graphical analysis of propylene captured and released via Electrochemical Modulation, and Faradic efficiency of secondary gas products and propylene separated via electrochemical capture-and-release mechanism. Second row of graphical analysis depicts deconvoluted graphs of propylene concentration separated by electrochemical modulated complexation mechanism. Spray-deposited layer consisted of 5 mg/cm<sup>2</sup> Carbon Nanoparticles, 4 mg/cm<sup>2</sup> Nafion ionomer, 2 mg/cm<sup>2</sup> [BMIM][PF<sub>6</sub>] ionic liquid, and 8 mg/cm<sup>2</sup> [N(Et)<sub>4</sub>]<sub>2</sub>[Ni(mnt)<sub>2</sub>] salt onto Sigracet 39 BB Carbon GDL.



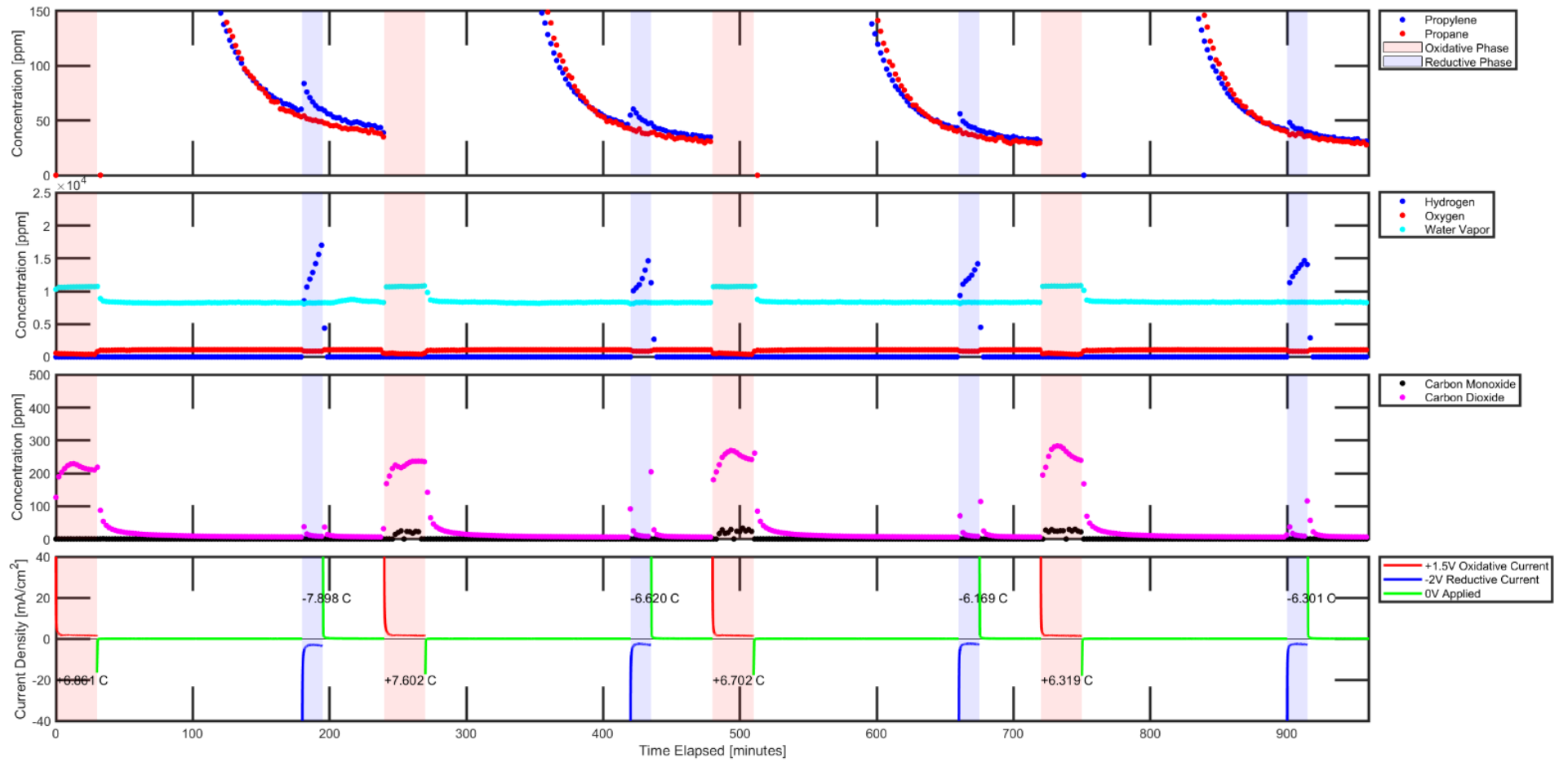


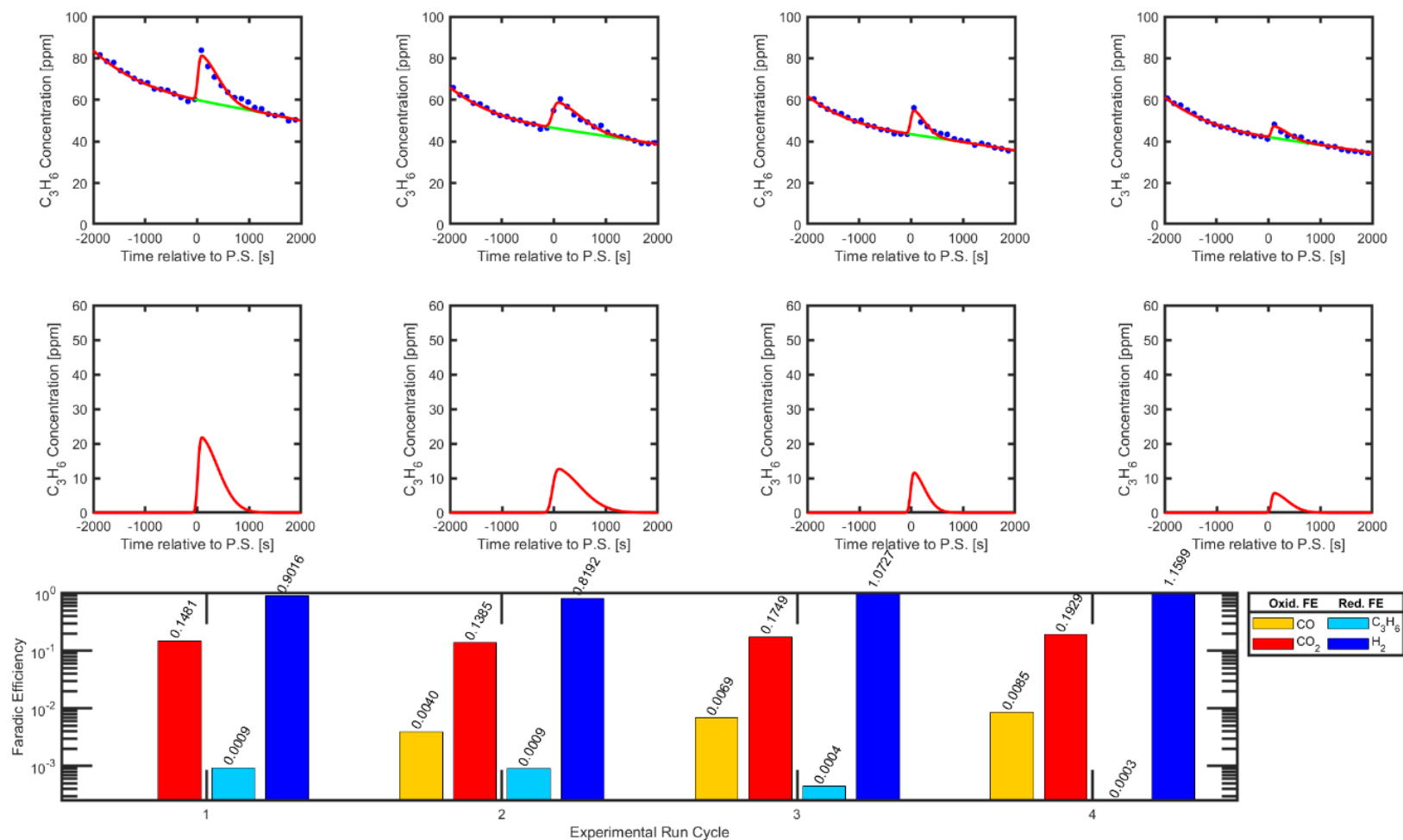
**Figure S2-C: 4 mg/cm<sup>2</sup> IL.** Gas concentration measurements via Agilent Micro GC 990, Chronoamperometry via Potentiostat, graphical analysis of propylene captured and released via Electrochemical Modulation, and Faradic efficiency of secondary gas products and propylene separated via electrochemical capture-and-release mechanism. Second row of graphical analysis depicts deconvoluted graphs of propylene concentration separated by electrochemical modulated complexation mechanism. Spray-deposited layer consisted of 5 mg/cm<sup>2</sup> Carbon Nanoparticles, 4 mg/cm<sup>2</sup> Nafion ionomer, 4 mg/cm<sup>2</sup> [BMIM][PF<sub>6</sub>] ionic liquid, and 8 mg/cm<sup>2</sup> [N(Et)<sub>4</sub>]<sub>2</sub>[Ni(mnt)<sub>2</sub>] salt onto Sigracet 39 BB Carbon GDL. (Note: Duplicate of **Figure S1-E** posted here for reading convenience)





**Figure S2-D: 8 mg/cm<sup>2</sup> IL.** Gas concentration measurements via Agilent Micro GC 990, Chronoamperometry via Potentiostat, graphical analysis of propylene captured and released via Electrochemical Modulation, and Faradic efficiency of secondary gas products and propylene separated via electrochemical capture-and-release mechanism. Second row of graphical analysis depicts deconvoluted graphs of propylene concentration separated by electrochemical modulated complexation mechanism. Spray-deposited layer consisted of 5 mg/cm<sup>2</sup> Carbon Nanoparticles, 4 mg/cm<sup>2</sup> Nafion ionomer, 8 mg/cm<sup>2</sup> [BMIM][PF<sub>6</sub>] ionic liquid, and 8 mg/cm<sup>2</sup> [N(Et)<sub>4</sub>]<sub>2</sub>[Ni(mnt)<sub>2</sub>] salt onto Sigracet 39 BB Carbon GDL.

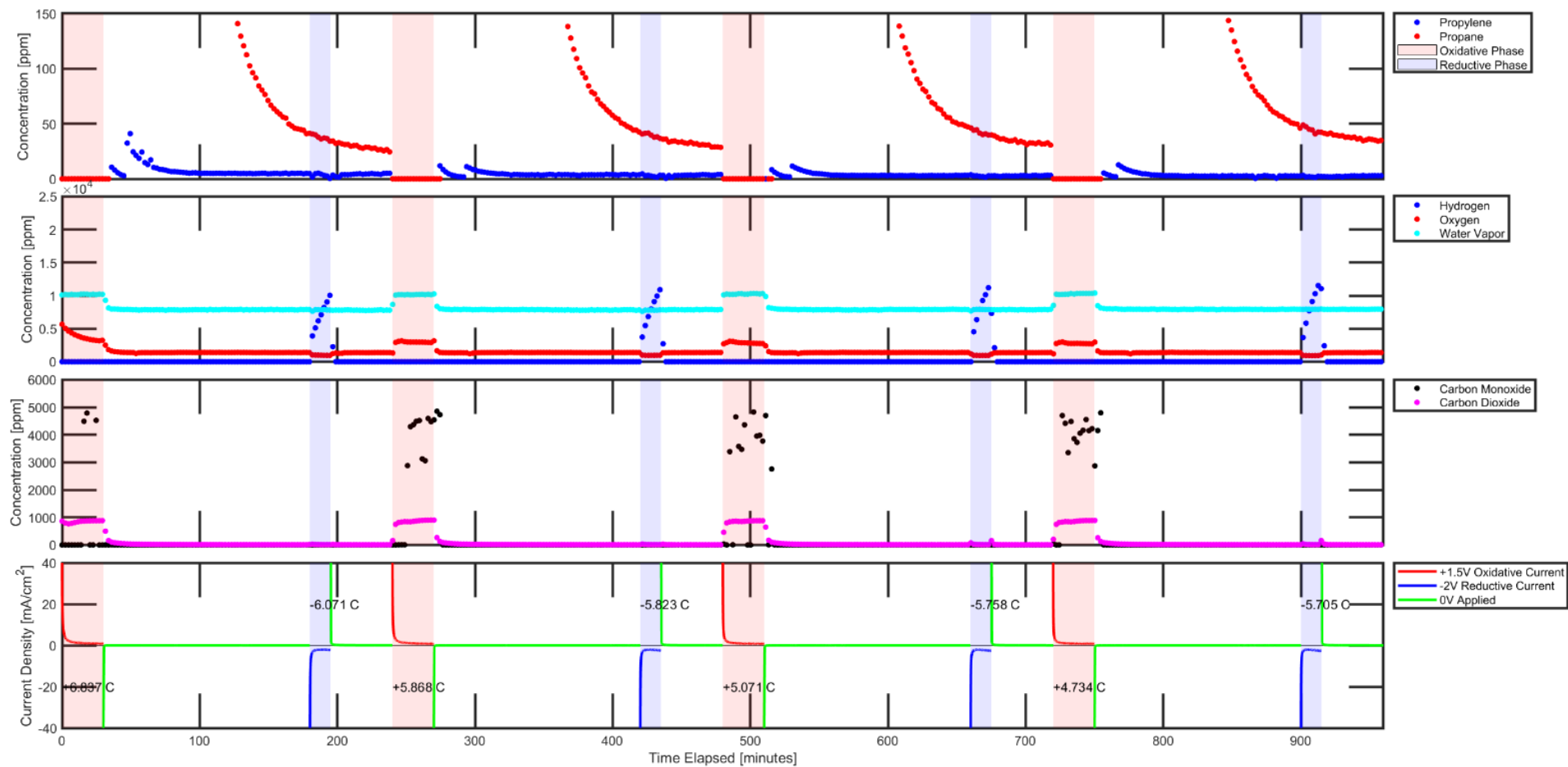


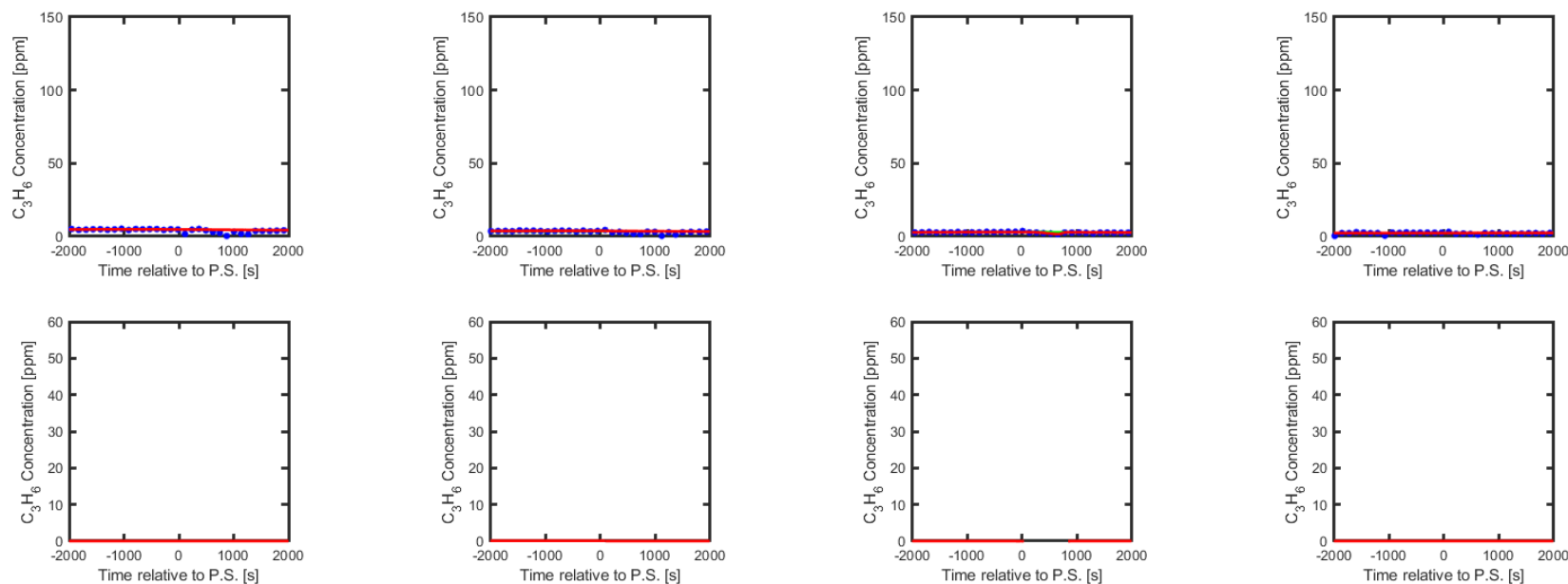


**Figure S2-E: 16 mg/cm<sup>2</sup> IL.** Gas concentration measurements via Agilent Micro GC 990, Chronoamperometry via Potentiostat, graphical analysis of propylene captured and released via Electrochemical Modulation, and Faradic efficiency of secondary gas products and propylene separated via electrochemical capture-and-release mechanism. Second row of graphical analysis depicts deconvoluted graphs of propylene concentration separated by electrochemical modulated complexation mechanism. Spray-deposited layer consisted of 5 mg/cm<sup>2</sup> Carbon Nanoparticles, 4 mg/cm<sup>2</sup> Nafion ionomer, 16 mg/cm<sup>2</sup> [BMIM][PF<sub>6</sub>] ionic liquid, and 8 mg/cm<sup>2</sup> [N(Et)<sub>4</sub>]<sub>2</sub>[Ni(mnt)<sub>2</sub>] salt onto Sigracet 39 BB Carbon GDL. Please note that hydrogen F.E.'s were sometimes >1 because GC standard calibrations with hydrogen gas were not as accurate like the ones used for propylene/propane quantification and because hydrogen was not a prioritized factor during observation of the experiments.

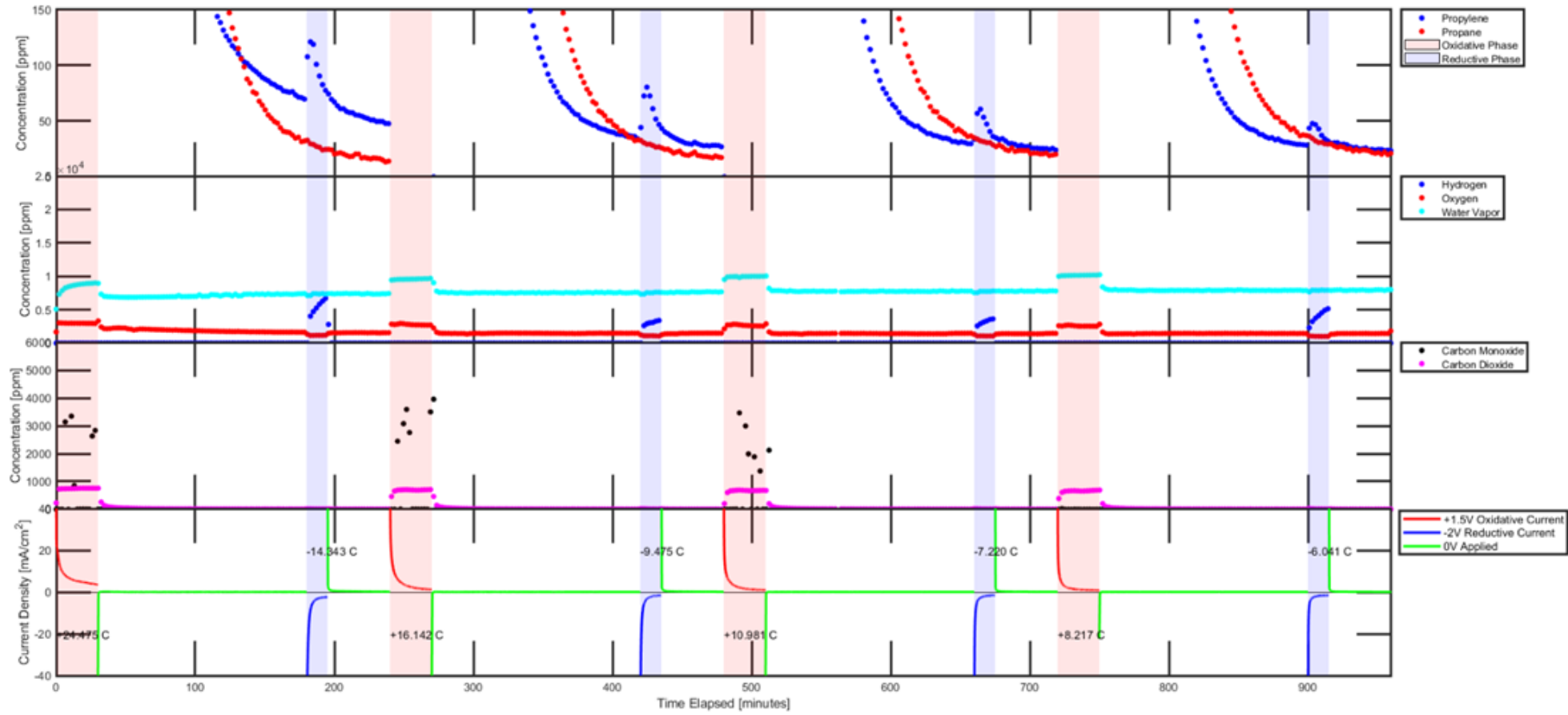
#### **Section Summary:**

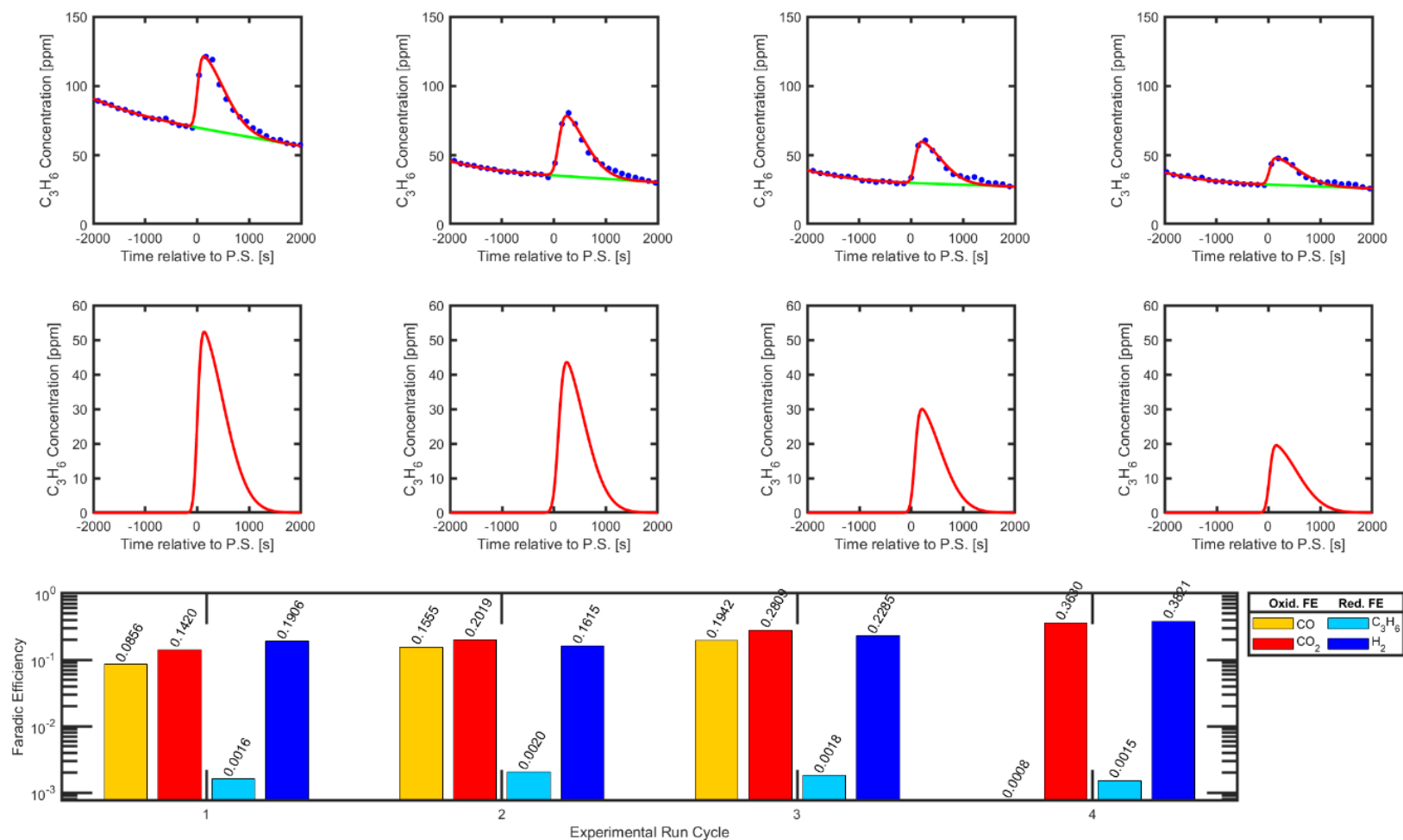
4 MEA samples of varying propylene-propane feed compositions were tested in this series of experiments. Therefore, this section consists of 4 *Figures* each with its own corresponding feed composition introduced to the MEA during the oxidative phase of each cycle (i.e., 0:100, 25:75, 50:50, and 100:0 propylene vs. propane mole ratio). This series of experiments contributed to the data shown in **Figure 3-C** of the main manuscript. All other parameters, including tetraethylammonium nickel dithiolene salt, IL Nafion, and Carbon loadings were kept constant for the purpose of observing the effect of propylene-propane feed composition on propylene separation performance. All 4 MEA samples utilized the same oxidative and reductive potentials of +1.5V and -2V, respectively. No separation performance or any propylene activity was observed when no propylene was introduced to the system (**Figure S3-A**). Separation performance was observed initially at 0.25 propylene fraction (**Figure S3-B**), followed by gentler linear increase at higher propylene fraction (**Figure S3-C and 3S-D**), which may be due to finite saturation of propylene molecules complexing in the MEA after approximately 0.25 propylene fraction. The slight linear slope at higher fractions may be due to the increased concentration gradient that can increase the transport rate of propylene into the ionogel.



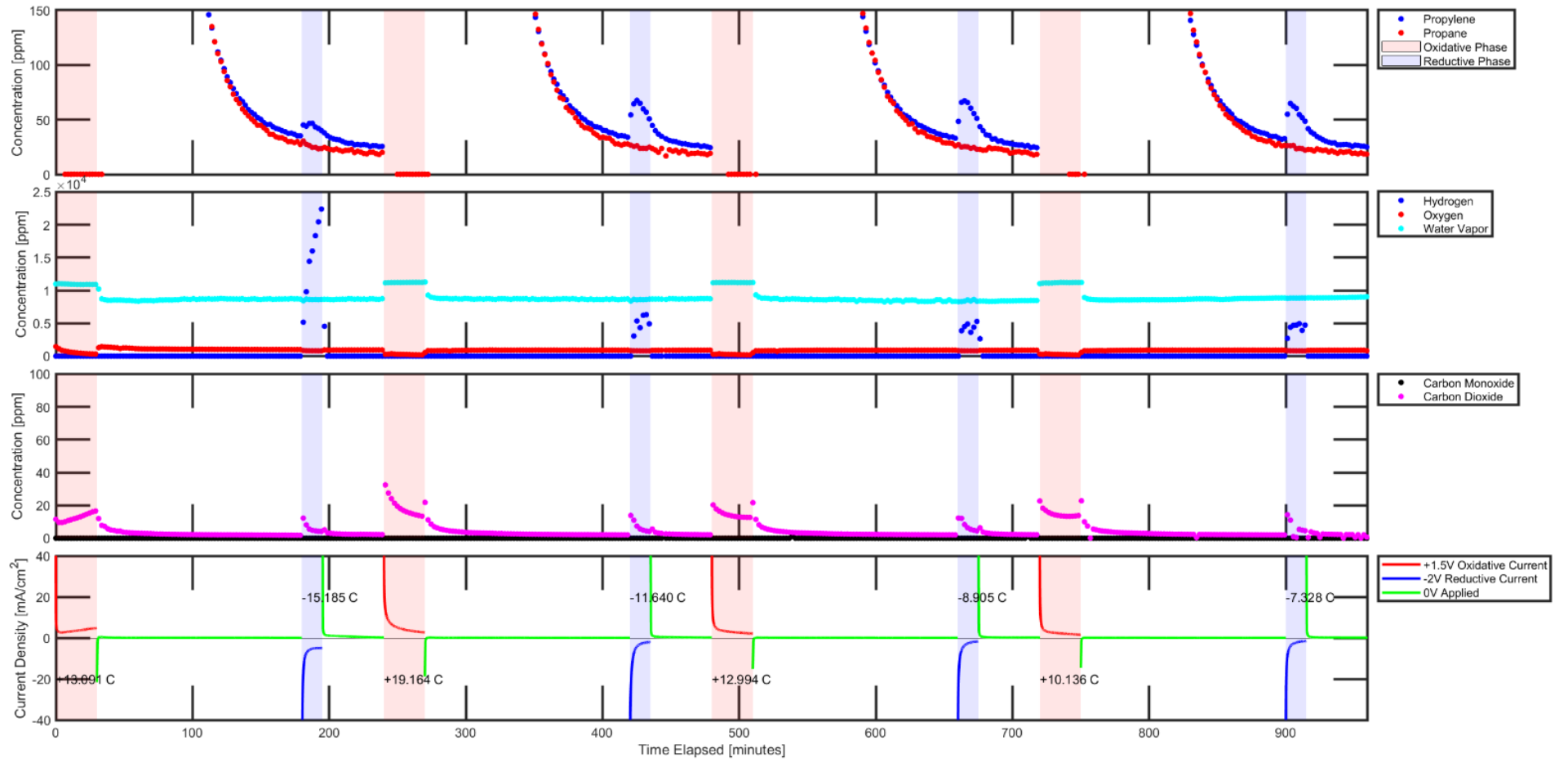


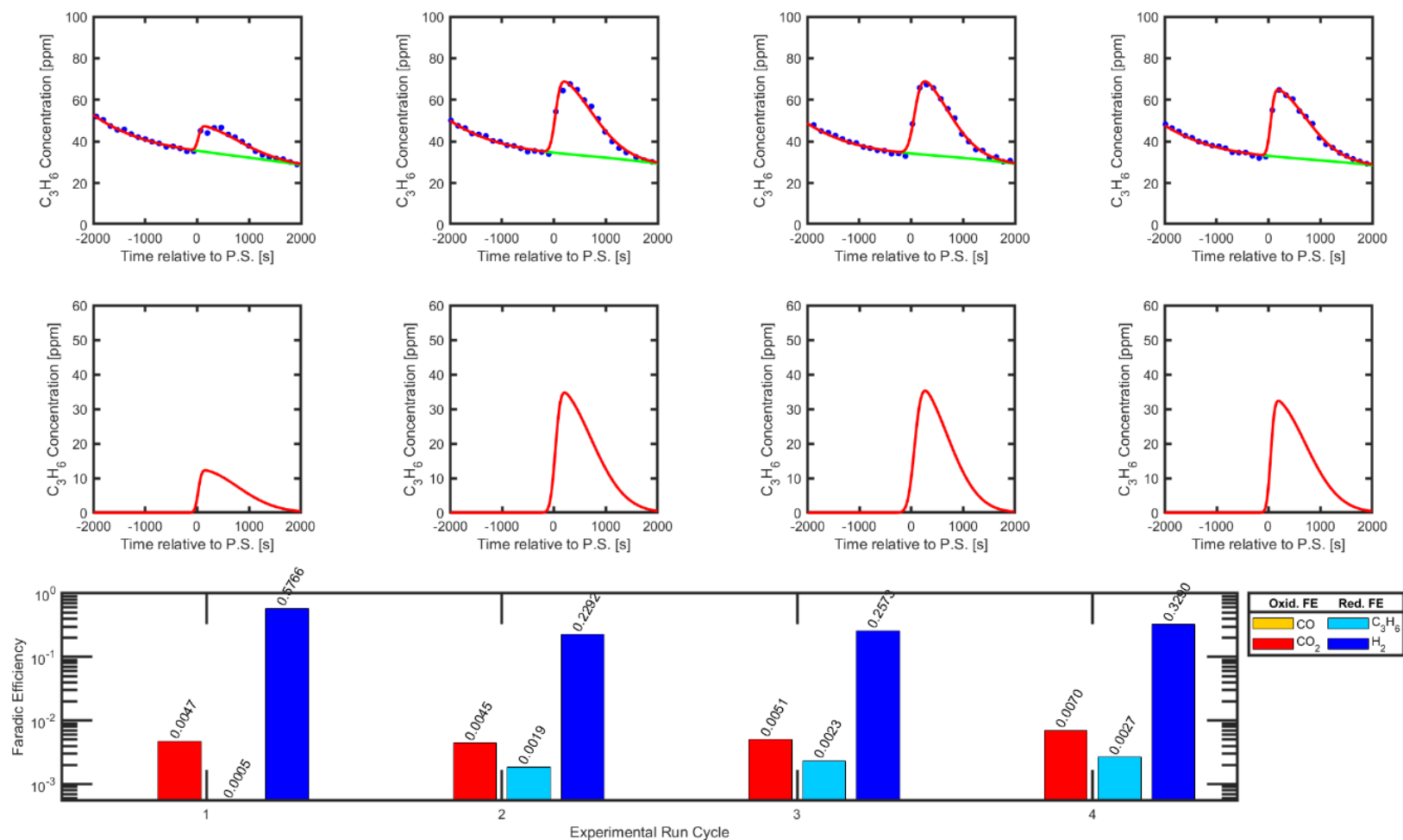
**Figure S3-A: 0:100 Propylene-Propane Feed.** Gas concentration measurements via Agilent Micro GC 990, Chronoamperometry via Potentiostat, and graphical analysis of propylene captured and released via Electrochemical Modulation. Second row of graphical analysis depicts deconvoluted graphs of propylene concentration separated by electrochemically modulated complexation mechanism. Spray-deposited layer consisted of 5 mg/cm<sup>2</sup> Carbon Nanoparticles, 4 mg/cm<sup>2</sup> Nafion ionomer, 4 mg/cm<sup>2</sup> [BMIM][PF<sub>6</sub>] ionic liquid, and 8 mg/cm<sup>2</sup> [N(Et)<sub>4</sub>]<sub>2</sub>[Ni(mnt)<sub>2</sub>] salt onto Sigracet 39 BB Carbon GDL. Feed composition of pure propane feed by volume at 10 sccm total flow rate. Small trace amount of propylene impurity has been detected in the pure propane reserve stock which is 99.5% pure.



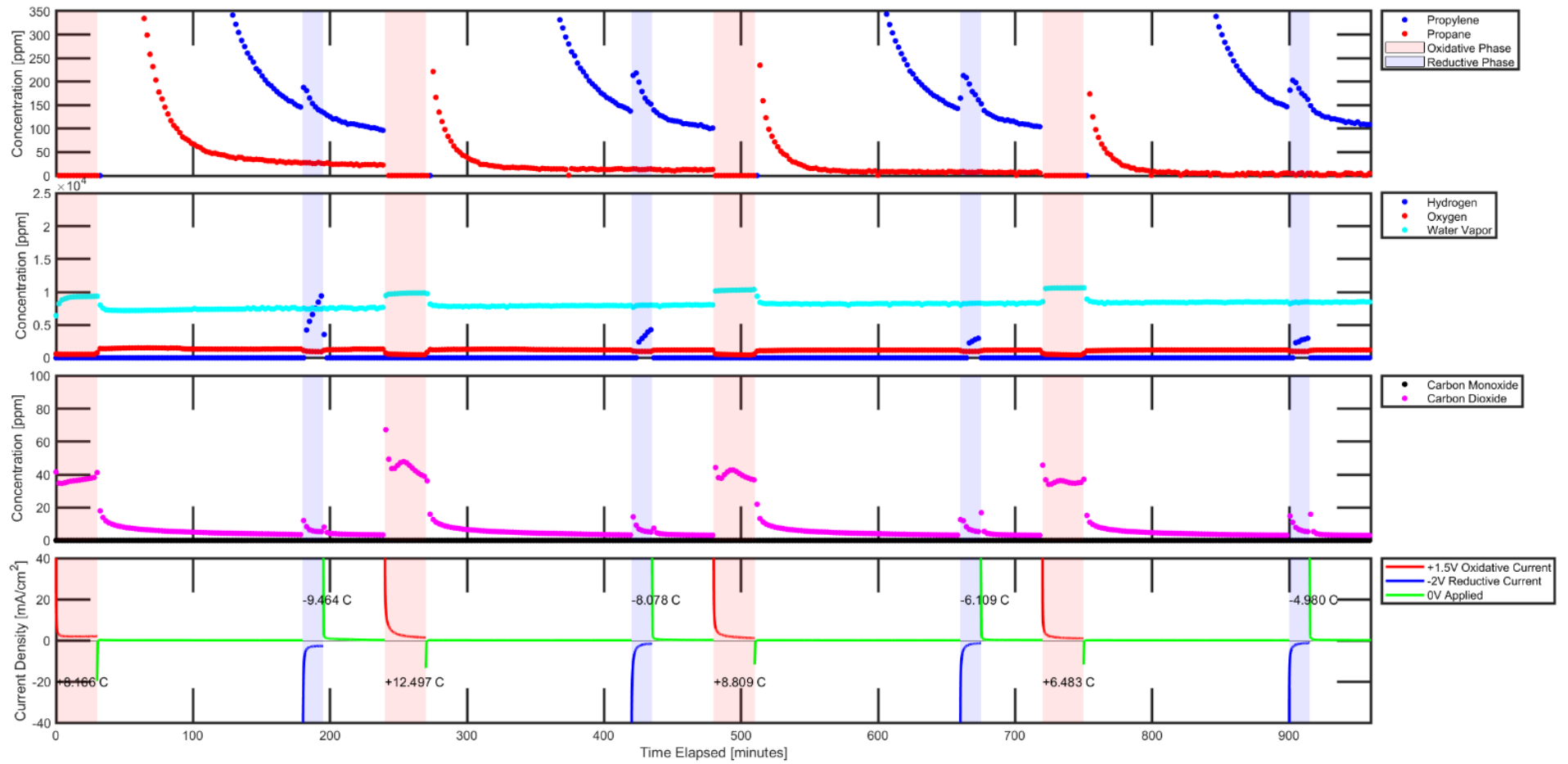


**Figure S3-B: 25:75 Propylene-Propane Feed.** Gas concentration measurements via Agilent Micro GC 990, Chronoamperometry via Potentiostat, and graphical analysis of propylene captured and released via Electrochemical Modulation. Second row of graphical analysis depicts deconvoluted graphs of propylene concentration separated by electrochemically modulated complexation mechanism. Spray-deposited layer consisted of 5 mg/cm<sup>2</sup> Carbon Nanoparticles, 4 mg/cm<sup>2</sup> Nafion ionomer, 4 mg/cm<sup>2</sup> [BMIM][PF<sub>6</sub>] ionic liquid, and 8 mg/cm<sup>2</sup> [N(Et)<sub>4</sub>]<sub>2</sub>[Ni(mnt)<sub>2</sub>] salt onto Sigracet 39 BB Carbon GDL. Feed composition of propane/propylene mixture was 25% by volume at 10 sccm total flow rate.





**Figure S3-C: 50:50 Propylene-Propane Feed.** Gas concentration measurements via Agilent Micro GC 990, Chronoamperometry via Potentiostat, and graphical analysis of propylene captured and released via Electrochemical Modulation. Second row of graphical analysis depicts deconvoluted graphs of propylene concentration separated by electrochemically modulated complexation mechanism. Spray-deposited layer consisted of 5 mg/cm<sup>2</sup> Carbon Nanoparticles, 4 mg/cm<sup>2</sup> Nafion ionomer, 4 mg/cm<sup>2</sup> [BMIM][PF<sub>6</sub>] ionic liquid, and 8 mg/cm<sup>2</sup> [N(Et)<sub>4</sub>]<sub>2</sub>[Ni(mnt)<sub>2</sub>] salt onto Sigracet 39 BB Carbon GDL. Feed composition of propane/propylene mixture was 50% by volume at 20 sccm total flow rate. (Note: Duplicate of **Figure S1-E** posted here for reading convenience)



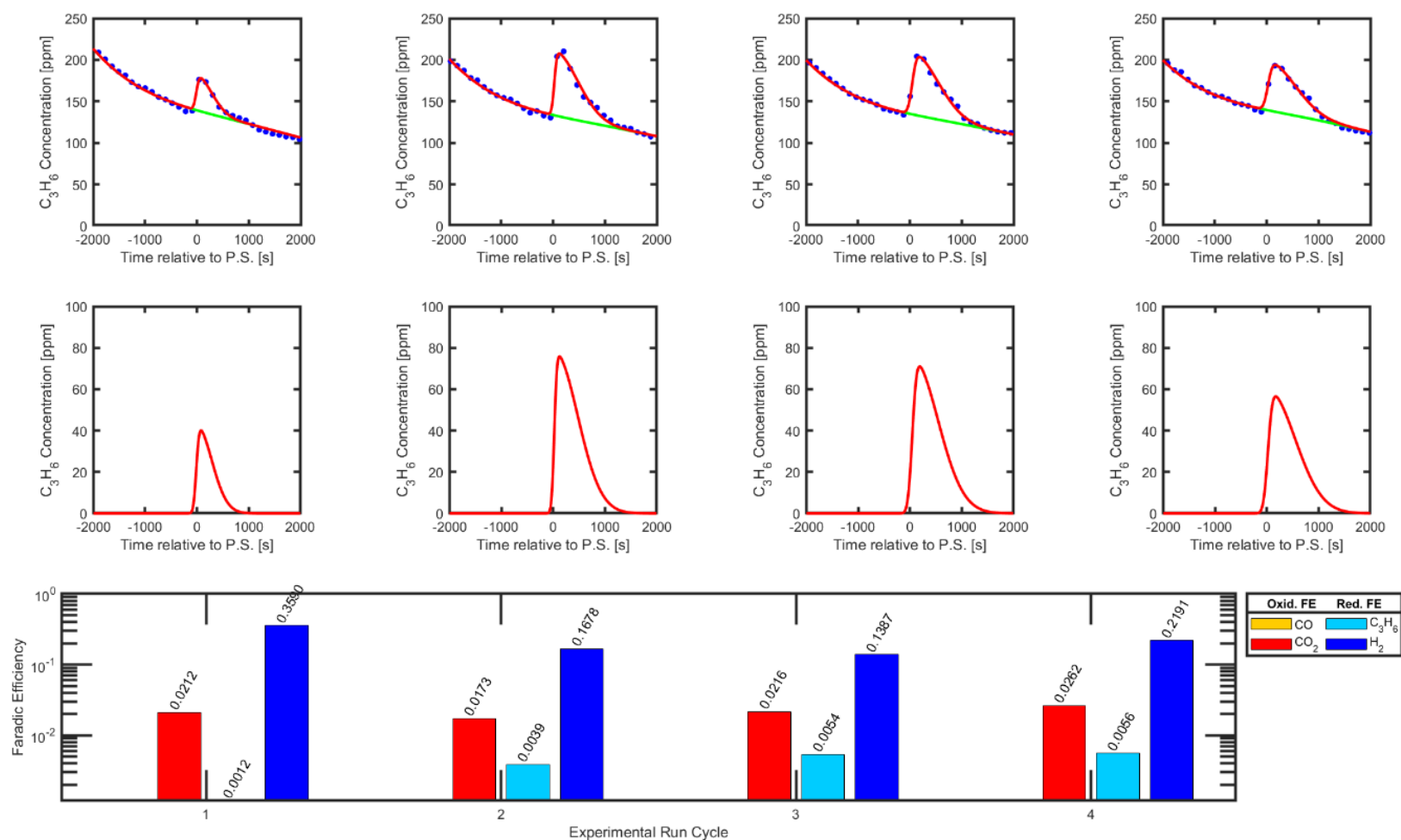


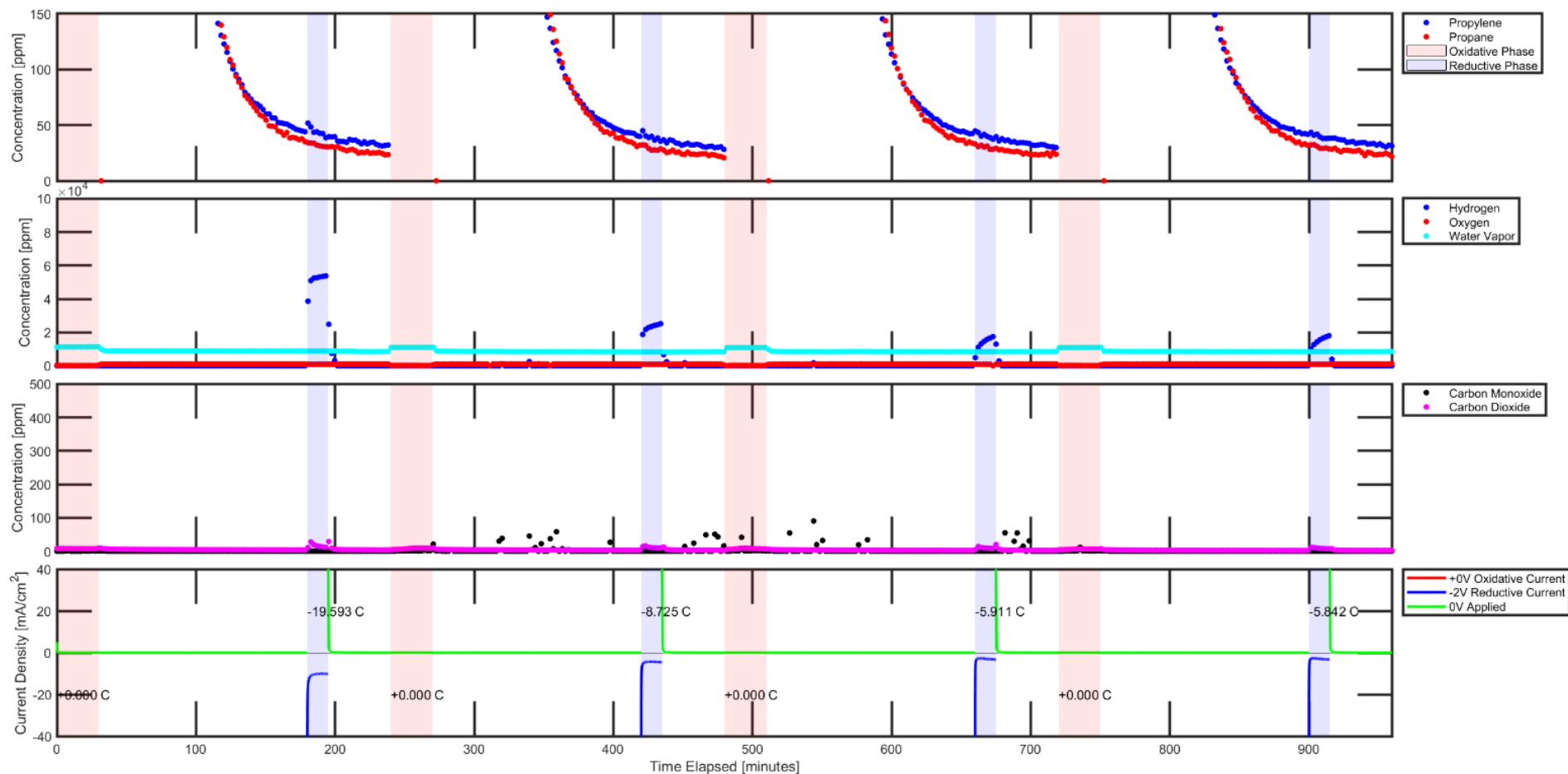
**Figure S3-D: 100:0 Propylene-Propane Feed.** Gas concentration measurements via Agilent Micro GC 990, Chronoamperometry via Potentiostat, and graphical analysis of propylene captured and released via Electrochemical Modulation. Second row of graphical analysis depicts deconvoluted graphs of propylene concentration separated by electrochemically modulated complexation mechanism. Spray-deposited layer consisted of 5 mg/cm<sup>2</sup> Carbon Nanoparticles, 4 mg/cm<sup>2</sup> Nafion ionomer, 4 mg/cm<sup>2</sup> [BMIM][PF<sub>6</sub>] ionic liquid, and 8 mg/cm<sup>2</sup> [N(Et)<sub>4</sub>]<sub>2</sub>[Ni(mnt)<sub>2</sub>] salt onto Sigracet 39 BB Carbon GDL. Feed composition of pure propylene feed by volume at 10 sccm total flow rate. Small trace amount of propane impurity has been detected in the pure propylene reserve stock which is 99.5% pure.

**Section Summary:**

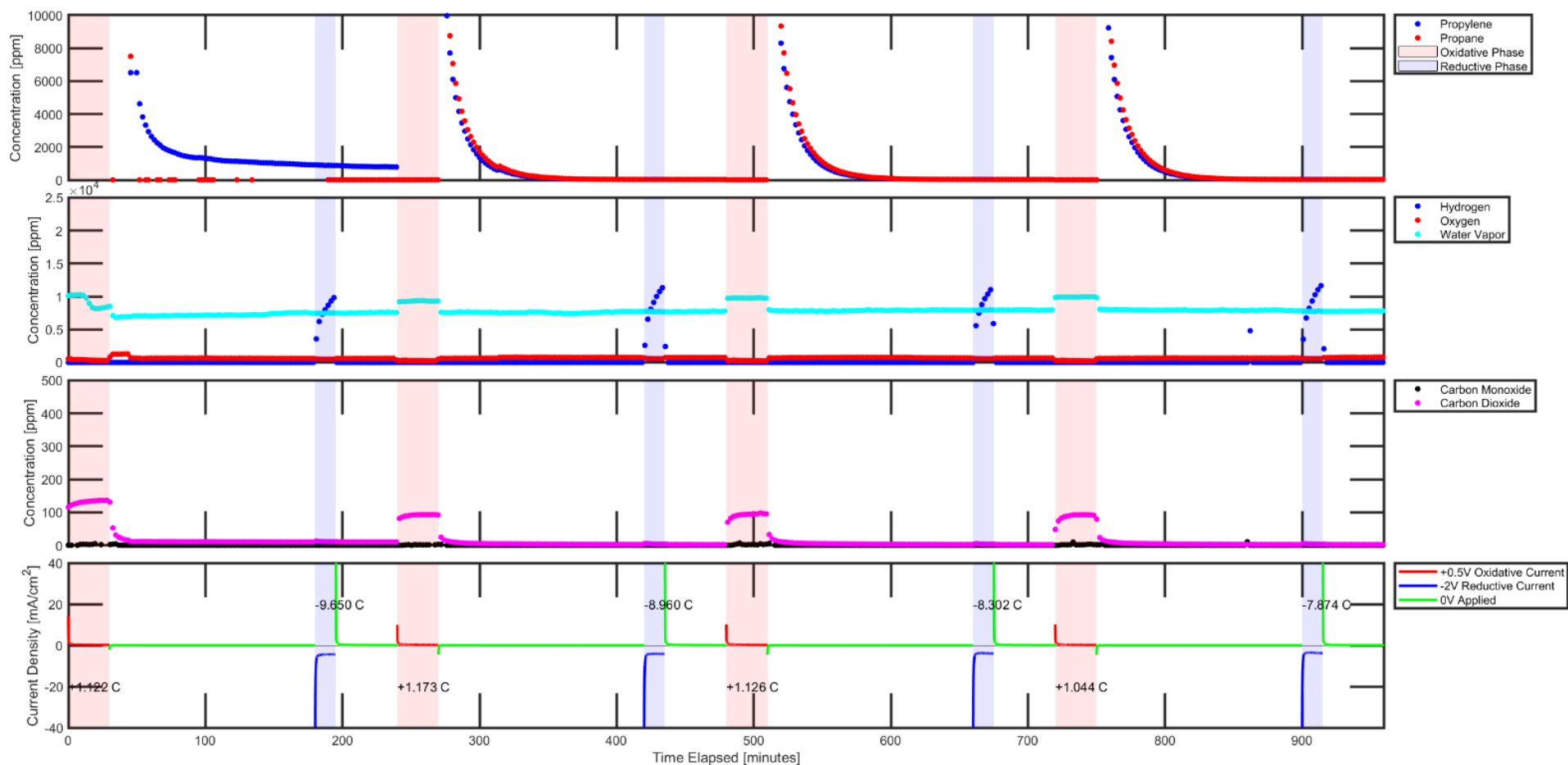
7 MEA samples of identical loading compositions were tested at varying oxidative potential in this series of experiments. Therefore, this section consists of 7 *Figures* each with its own corresponding oxidative potential applied to the MEA during the oxidative phase of each cycle (i.e., 0, +0.5, +1.0, +1.5, +2.0, +2.5 and +3.0V vs. counter-side). This series of experiments contributed to the data shown in **Figure 4-A** of the main manuscript where it attempted to observe the effect of oxidation potential on propylene separation performance. A 50:50 molar ratio propylene-propane feed was introduced to the MEA's during the oxidative phase as well. Reductive potential was kept constant at -2.0V for all 7 MEA samples.

No separation performance or any propylene activity was observed at 0V and +0.5V (**Figures S4-A and S4-B**) most likely because the potential did not reach the thermodynamic minimum of +0.82V to oxidize the nickel dithiolene species. Separation performance was observed initially at +1.0V (**Figure S4-C**), followed by a local increase at +1.5V (**Figure S4-D**), and then a general decrease in separation performance at higher potentials until +3.0V (**Figures S4-E thru S4-G**). This general decrease may have been caused by parasitic oxidation of carbon or other organic components in the ionogel inferring from the elevated oxidative FE's of carbon monoxide and carbon dioxide at higher potentials of +2.5V and +3.0V (**Figures S4-F and S4-G**).

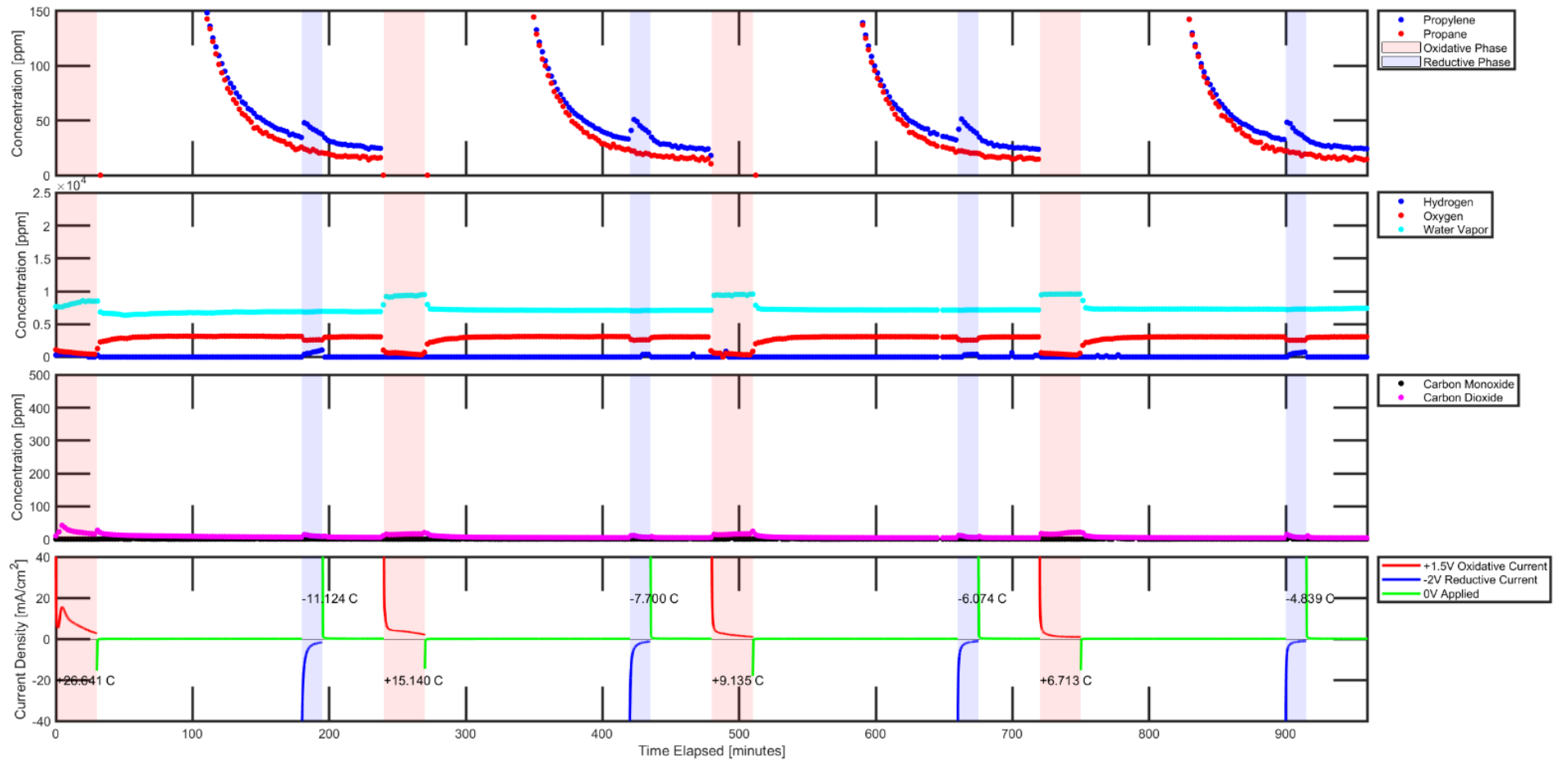
S4-A

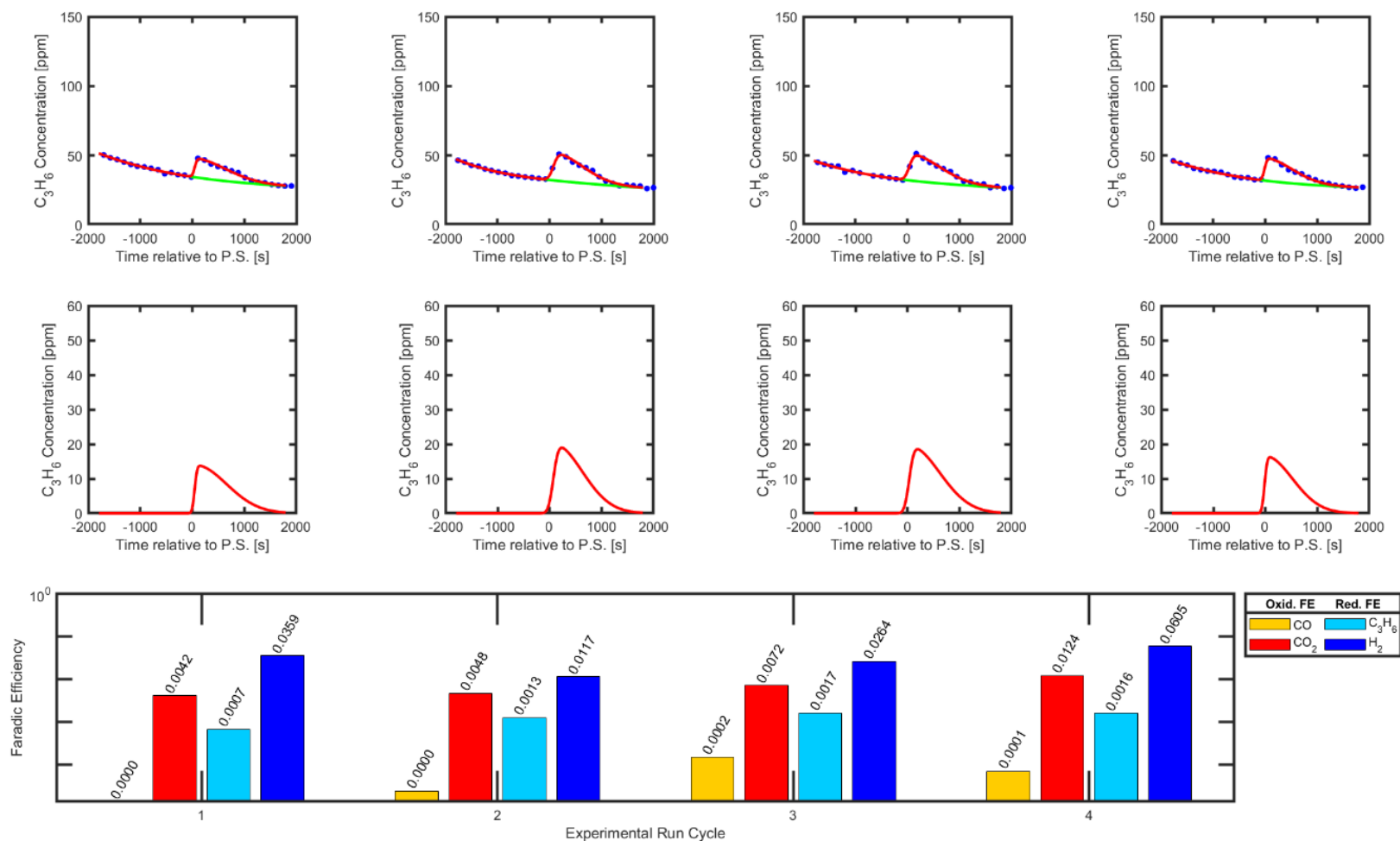


**Figure S4-A: 0V Oxidative Potential.** Gas concentration measurements via Agilent Micro GC 990 and Chronoamperometry via Potentiostat, Spray-deposited layer consisted of 5 mg/cm<sup>2</sup> Carbon Nanoparticles, 4 mg/cm<sup>2</sup> Nafion ionomer, 4 mg/cm<sup>2</sup> [BMIM][PF<sub>6</sub>] ionic liquid, and 8 mg/cm<sup>2</sup> [N(Et)<sub>4</sub>]<sub>2</sub>[Ni(mnt)<sub>2</sub>] salt onto Sigracet 39 BB Carbon GDL. Feed composition of propane/propylene mixture was 50% by volume at 20 sccm total flow rate. Oxidative Potential of 0V was applied.

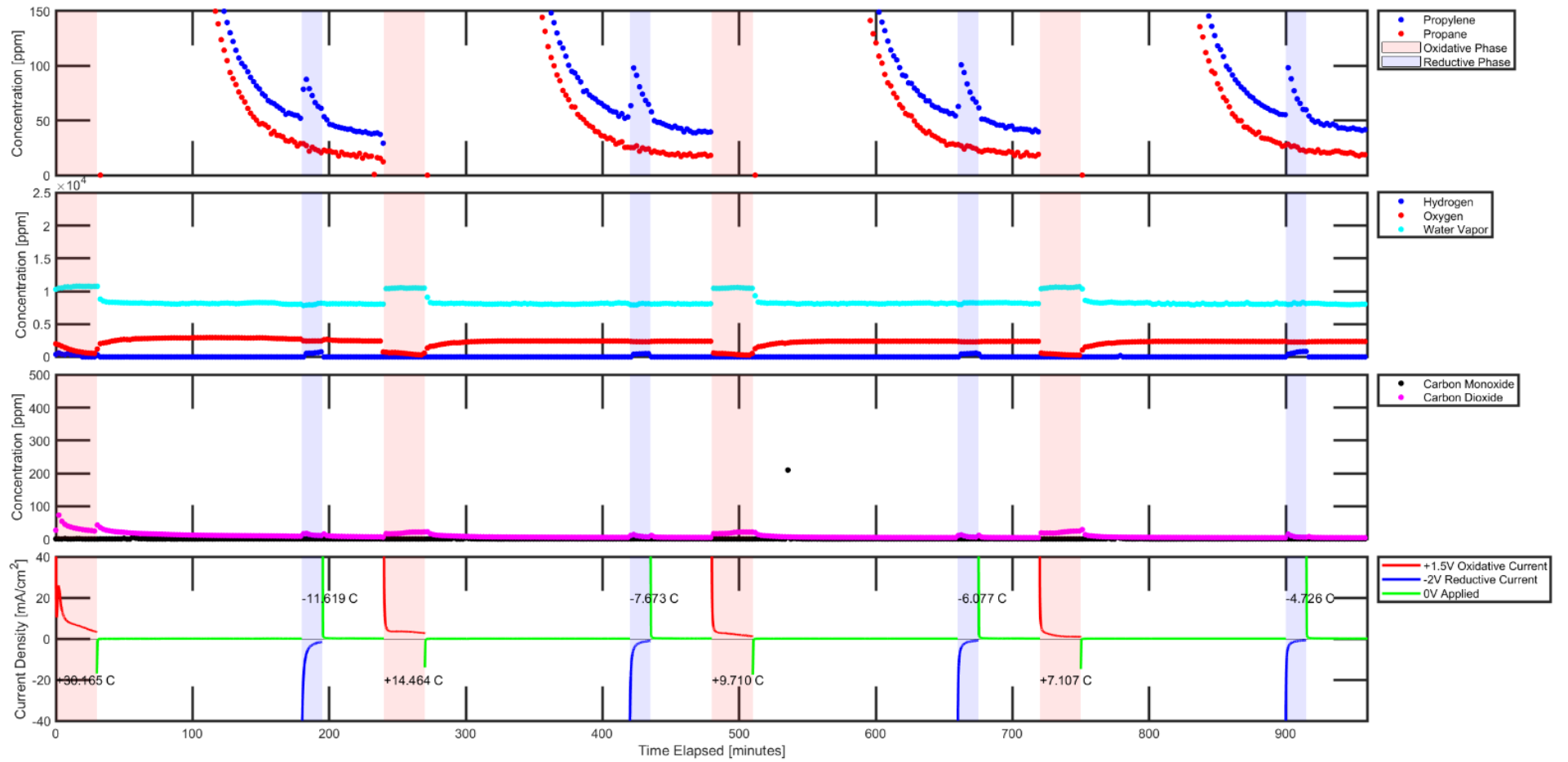


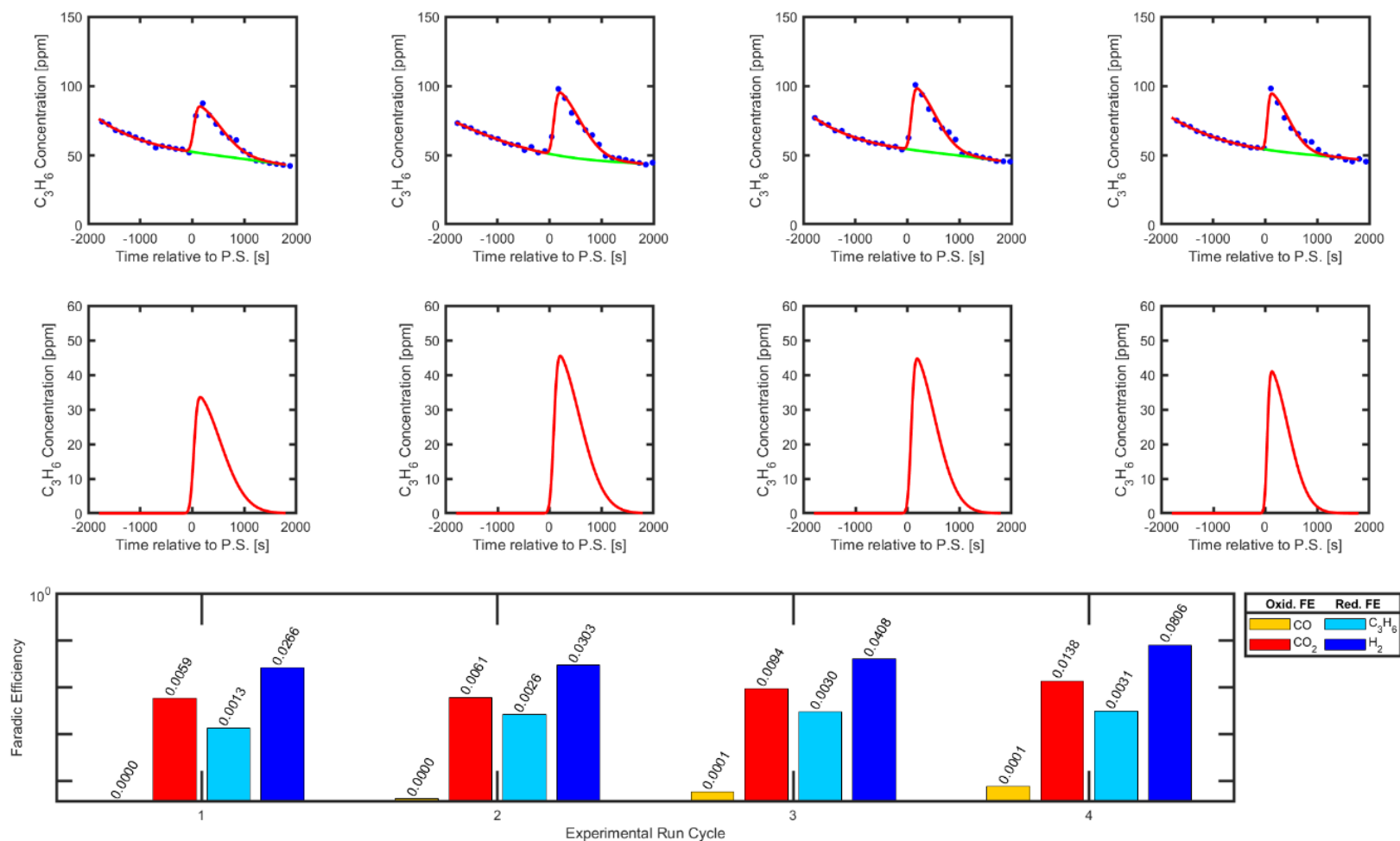
**Figure S4-B: +0.5V Oxidative Potential.** Gas concentration measurements via Agilent Micro GC 990 and Chronoamperometry via Potentiostat. Spray-deposited layer consisted of 5 mg/cm<sup>2</sup> Carbon Nanoparticles, 4 mg/cm<sup>2</sup> Nafion ionomer, 4 mg/cm<sup>2</sup> [BMIM][PF<sub>6</sub>] ionic liquid, and 8 mg/cm<sup>2</sup> [N(Et)<sub>4</sub>]<sub>2</sub>[Ni(mnt)<sub>2</sub>] salt onto Sigracet 39 BB Carbon GDL. Feed composition of propane/propylene mixture was 50% by volume at 20 sccm total flow rate. Oxidative Potential of +0.5V was applied.



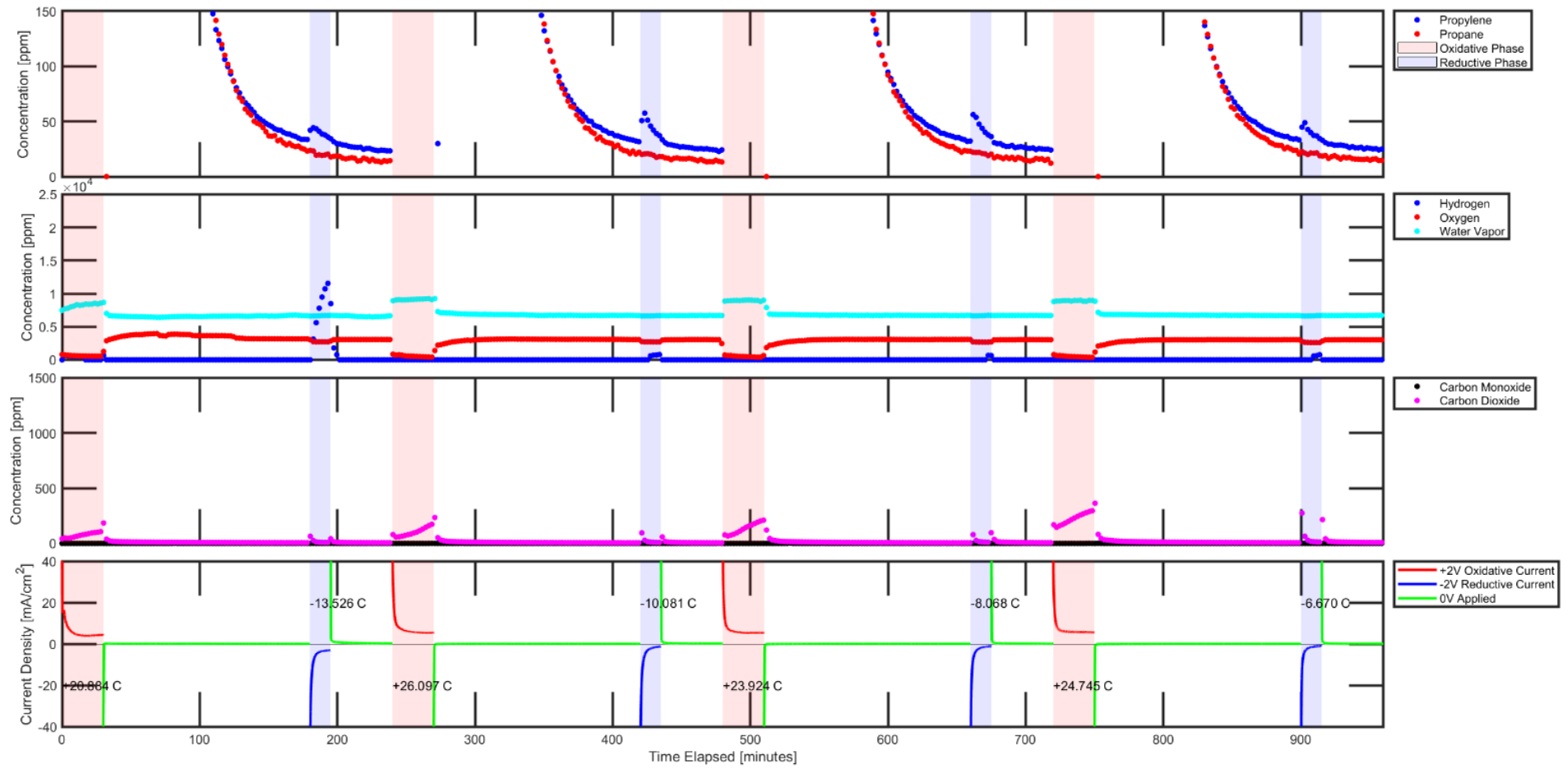


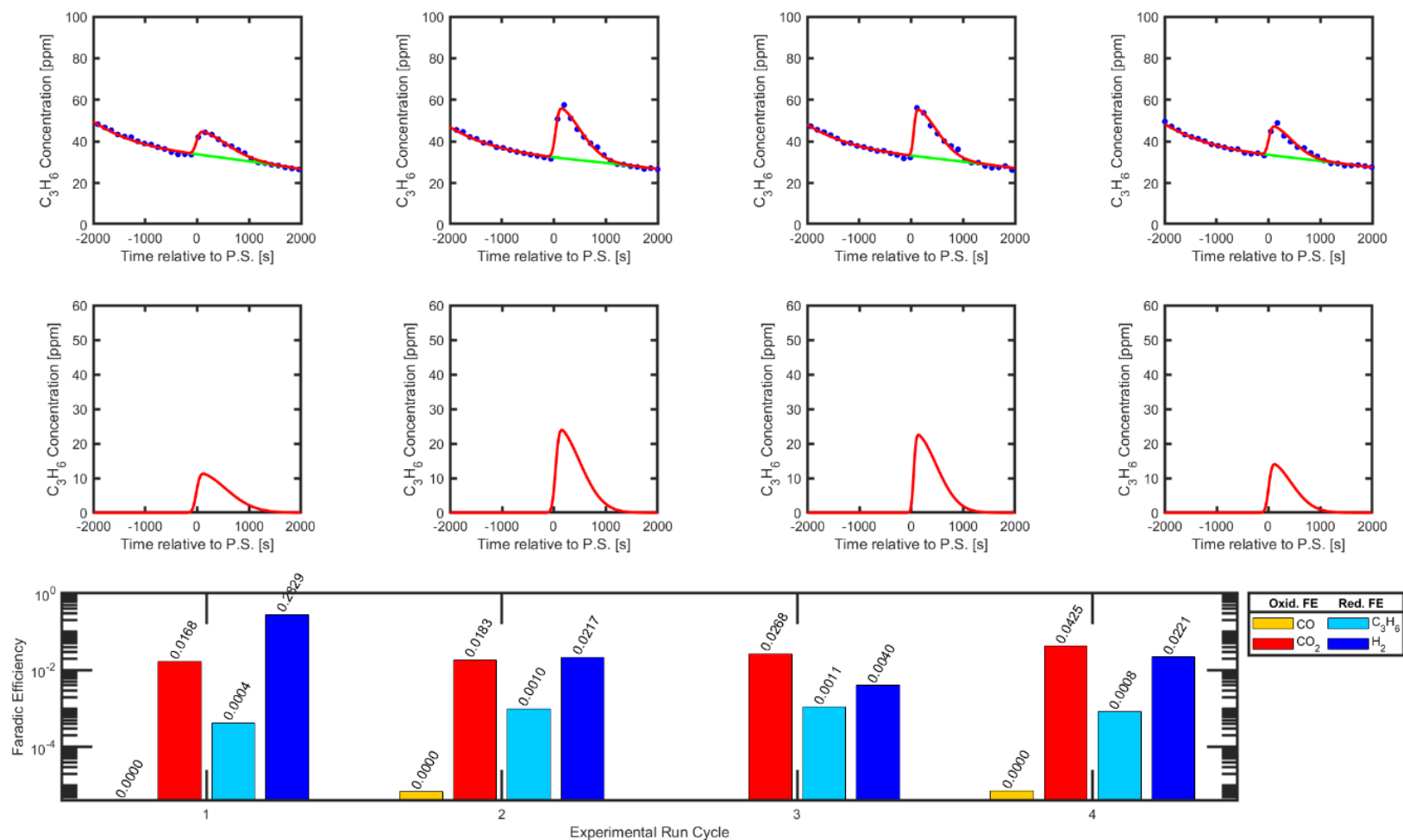
**Figure S4-C: +1.0V Oxidative Potential.** Gas concentration measurements via Agilent Micro GC 990, Chronoamperometry via Potentiostat, and graphical analysis of propylene captured and released via Electrochemical Modulation. Second row of graphical analysis depicts deconvoluted graphs of propylene concentration separated by electrochemical modulated complexation mechanism. Spray-deposited layer consisted of 5 mg/cm<sup>2</sup> Carbon Nanoparticles, 4 mg/cm<sup>2</sup> Nafion ionomer, 4 mg/cm<sup>2</sup> [BMIM][PF<sub>6</sub>] ionic liquid, and 8 mg/cm<sup>2</sup> [N(Et)<sub>4</sub>]<sub>2</sub>[Ni(mnt)<sub>2</sub>] salt onto Sigracet 39 BB Carbon GDL. Feed composition of propane/propylene mixture was 50% by volume at 20 sccm total flow rate. Oxidative Potential of +1.0V was applied.



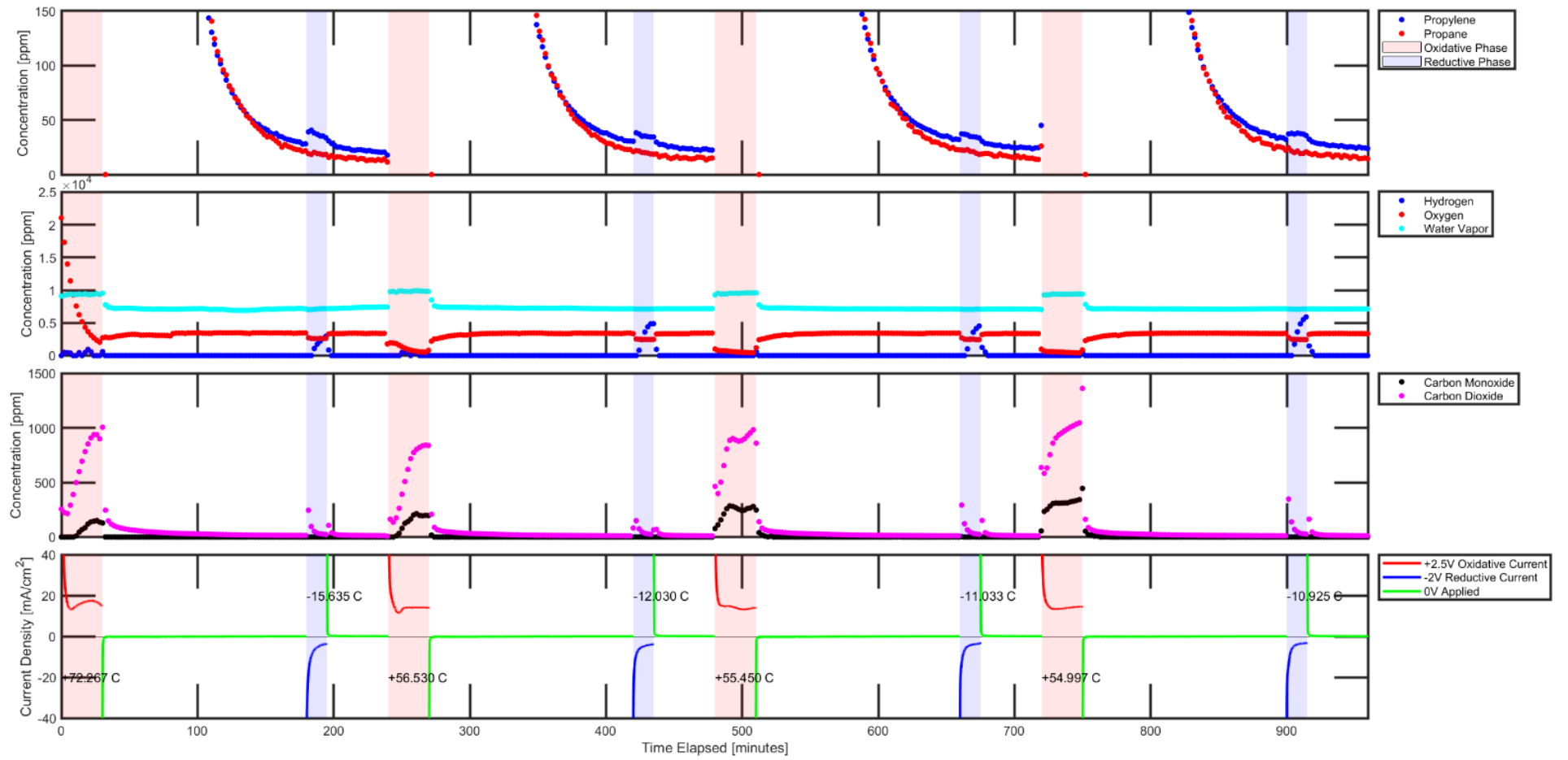


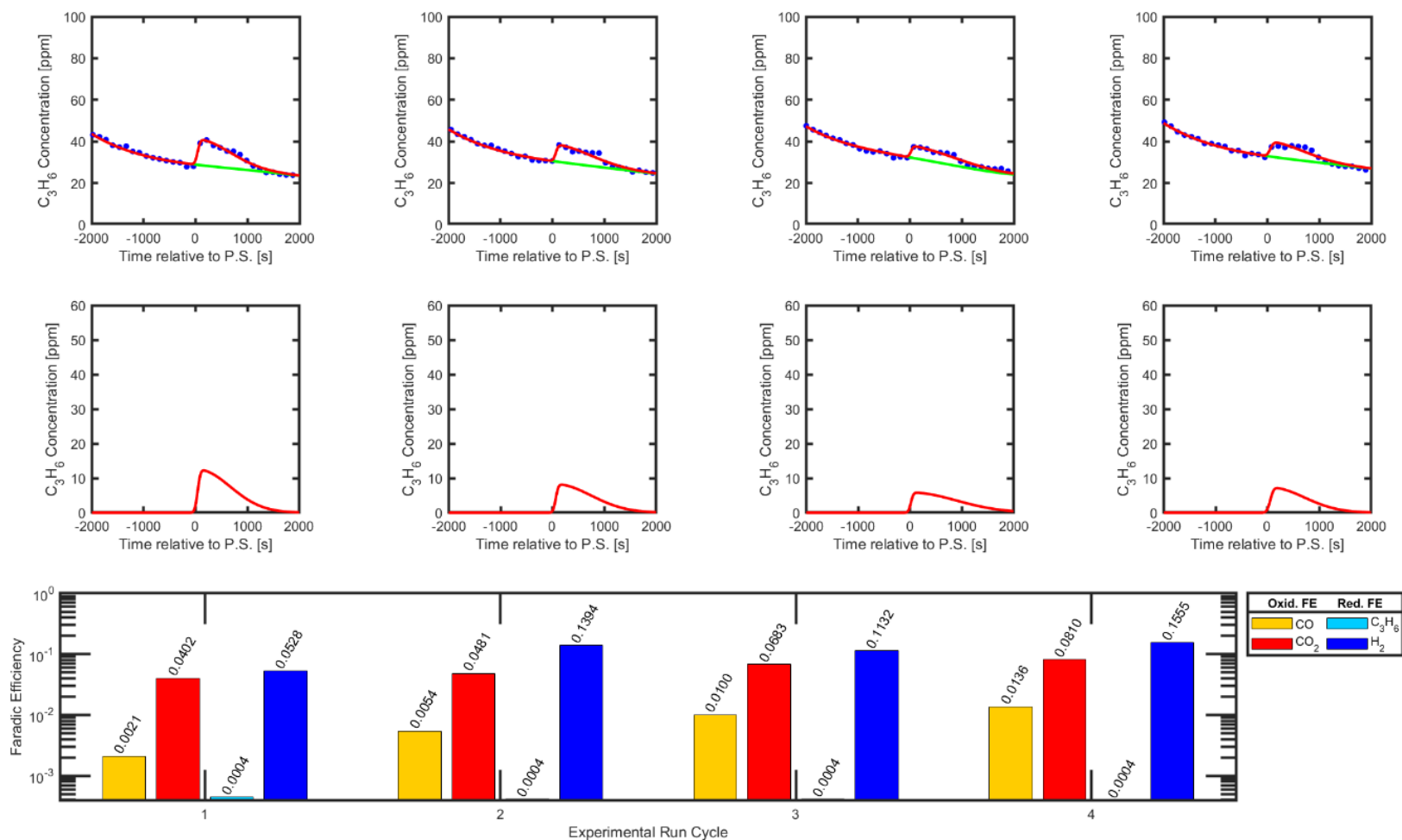
**Figure S4-D: +1.5V Oxidative Potential.** Gas concentration measurements via Agilent Micro GC 990, Chronoamperometry via Potentiostat, and graphical analysis of propylene captured and released via Electrochemical Modulation. Second row of graphical analysis depicts deconvoluted graphs of propylene concentration separated by electrochemically modulated complexation mechanism. Spray-deposited layer consisted of 5 mg/cm<sup>2</sup> Carbon Nanoparticles, 4 mg/cm<sup>2</sup> Nafion ionomer, 4 mg/cm<sup>2</sup> [BMIM][PF<sub>6</sub>] ionic liquid, and 8 mg/cm<sup>2</sup> [N(Et)<sub>4</sub>]<sub>2</sub>[Ni(mnt)<sub>2</sub>] salt onto Sigracet 39 BB Carbon GDL. Feed composition of propane/propylene mixture was 50% by volume at 20 sccm total flow rate. Oxidative Potential of +1.5V was applied.



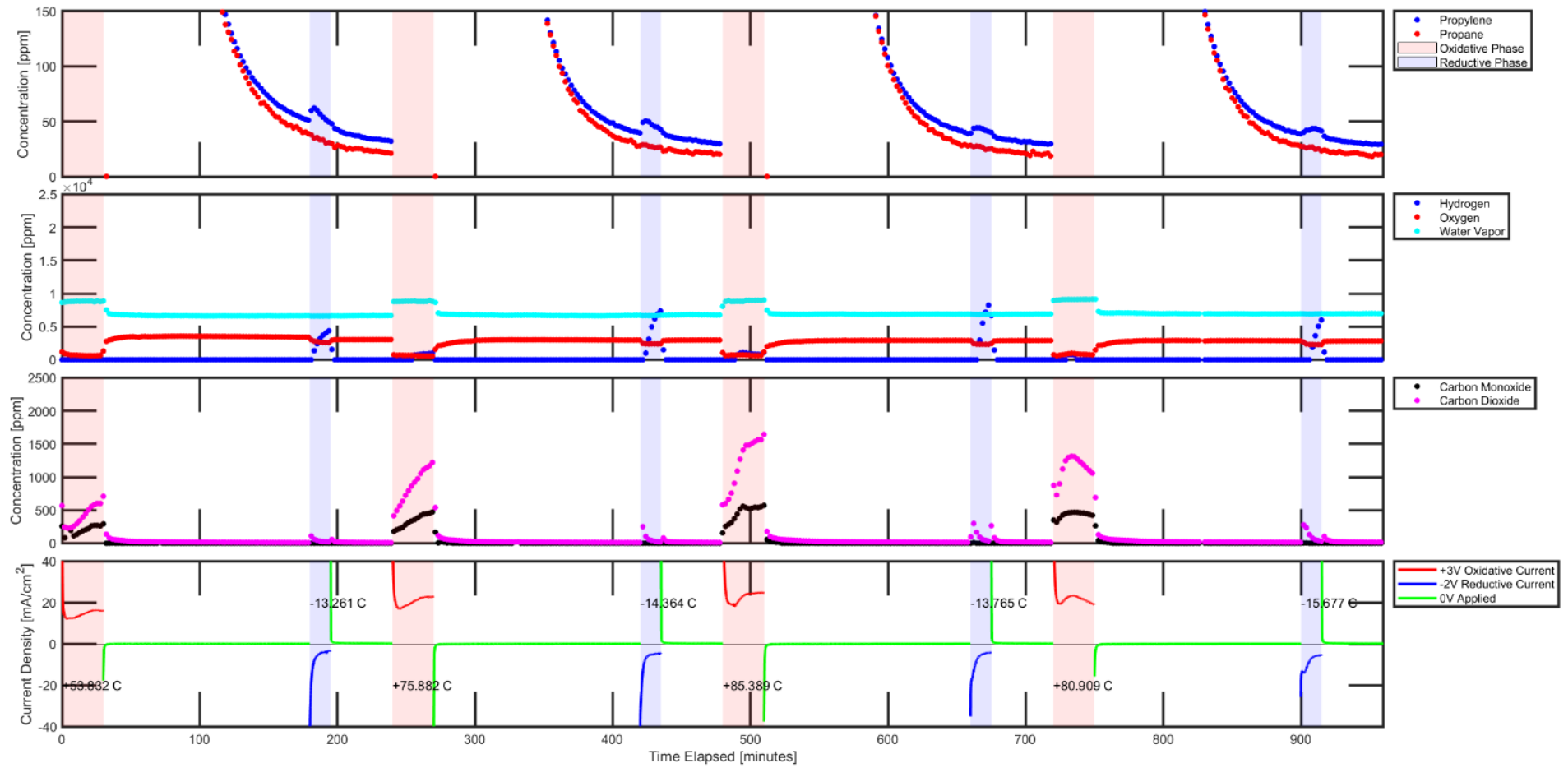


**Figure S4-E: +2.0V Oxidative Potential.** Gas concentration measurements via Agilent Micro GC 990, Chronoamperometry via Potentiostat, and graphical analysis of propylene captured and released via Electrochemical Modulation. Second row of graphical analysis depicts deconvoluted graphs of propylene concentration separated by electrochemically modulated complexation mechanism. Spray-deposited layer consisted of 5 mg/cm<sup>2</sup> Carbon Nanoparticles, 4 mg/cm<sup>2</sup> Nafion ionomer, 4 mg/cm<sup>2</sup> [BMIM][PF<sub>6</sub>] ionic liquid, and 8 mg/cm<sup>2</sup> [N(Et)<sub>4</sub>]<sub>2</sub>[Ni(mnt)<sub>2</sub>] salt onto Sigracet 39 BB Carbon GDL. Feed composition of propane/propylene mixture was 50% by volume at 20 sccm total flow rate. Oxidative Potential of +2.0V was applied.





**Figure S4-F: +2.5V Oxidative Potential.** Gas concentration measurements via Agilent Micro GC 990, Chronoamperometry via Potentiostat, and graphical analysis of propylene captured and released via Electrochemical Modulation. Second row of graphical analysis depicts deconvoluted graphs of propylene concentration separated by electrochemically modulated complexation mechanism. Spray-deposited layer consisted of 5 mg/cm<sup>2</sup> Carbon Nanoparticles, 4 mg/cm<sup>2</sup> Nafion ionomer, 4 mg/cm<sup>2</sup> [BMIM][PF<sub>6</sub>] ionic liquid, and 8 mg/cm<sup>2</sup> [N(Et)<sub>4</sub>]<sub>2</sub>[Ni(mnt)<sub>2</sub>] salt onto Sigracet 39 BB Carbon GDL. Feed composition of propane/propylene mixture was 50% by volume at 20 sccm total flow rate. Oxidative Potential of +2.5V was applied.



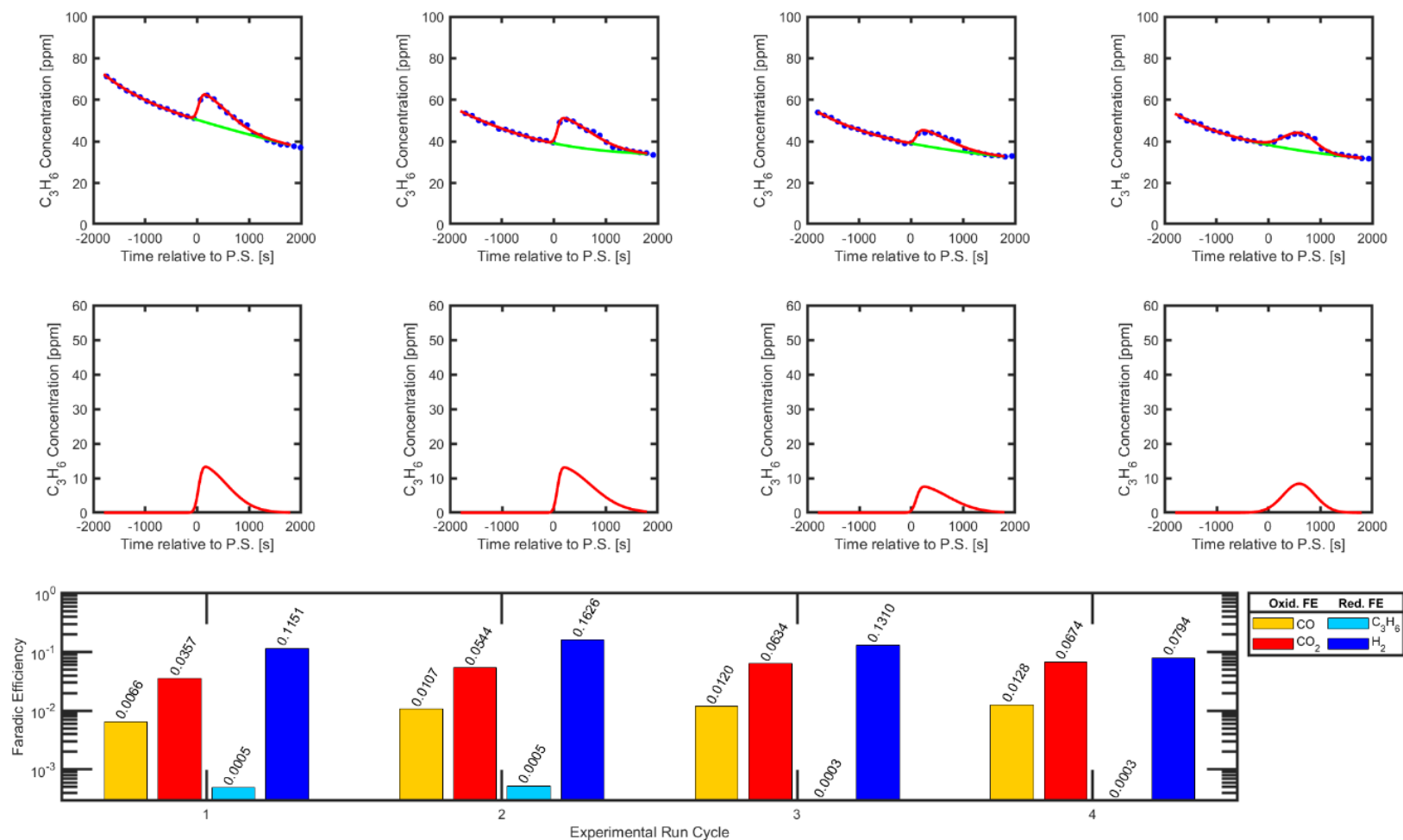


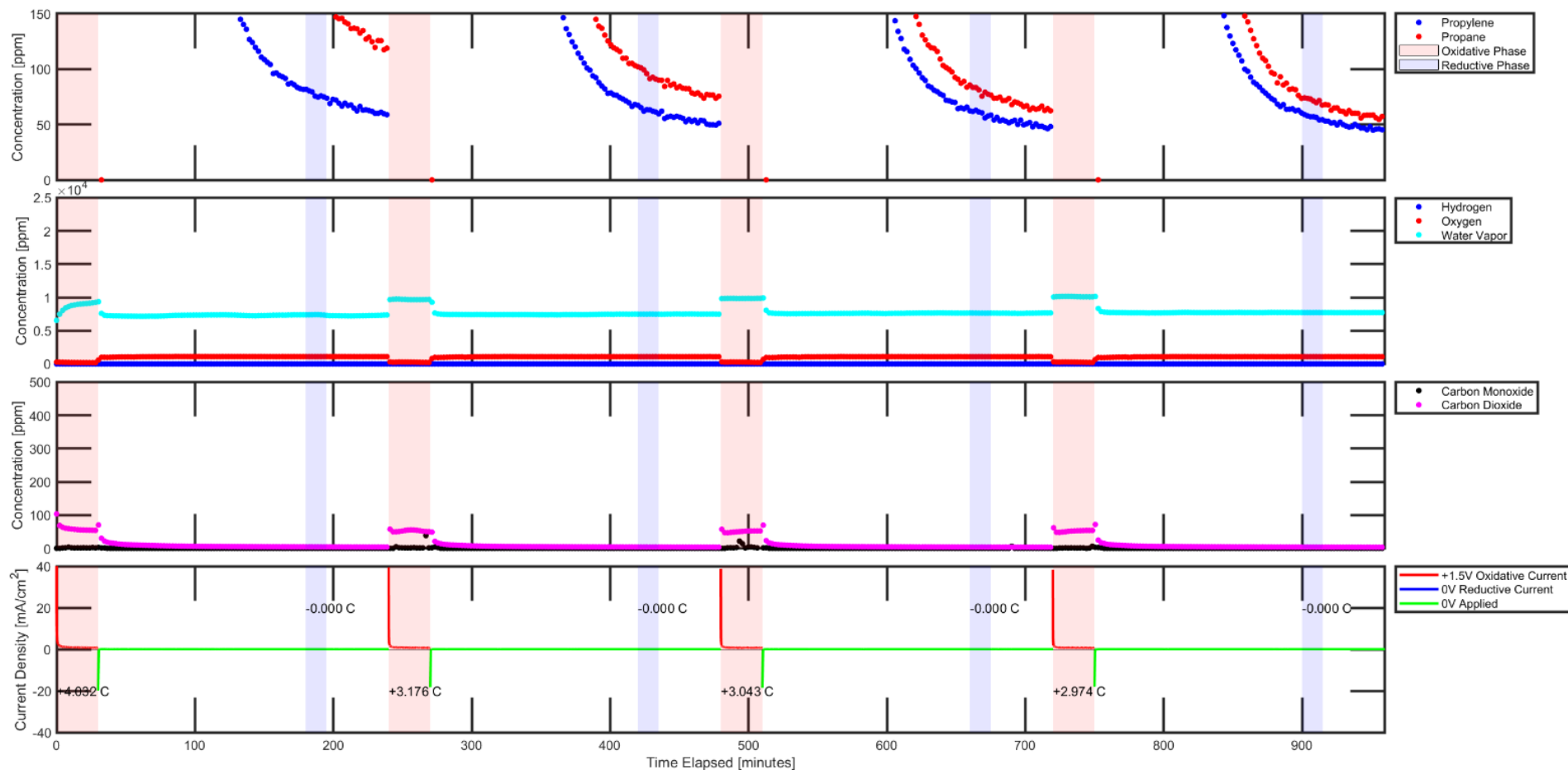
**Figure S4-G: +3.0V Oxidative Potential.** Gas concentration measurements via Agilent Micro GC 990, Chronoamperometry via Potentiostat, and graphical analysis of propylene captured and released via Electrochemical Modulation. Second row of graphical analysis depicts deconvoluted graphs of propylene concentration separated by electrochemically modulated complexation mechanism. Spray-deposited layer consisted of 5 mg/cm<sup>2</sup> Carbon Nanoparticles, 4 mg/cm<sup>2</sup> Nafion ionomer, 4 mg/cm<sup>2</sup> [BMIM][PF<sub>6</sub>] ionic liquid, and 8 mg/cm<sup>2</sup> [N(Et)<sub>4</sub>]<sub>2</sub>[Ni(mnt)<sub>2</sub>] salt onto Sigracet 39 BB Carbon GDL. Feed composition of propane/propylene mixture was 50% by volume at 20 sccm total flow rate. Oxidative Potential of +3.0V was applied.

**Section Summary:**

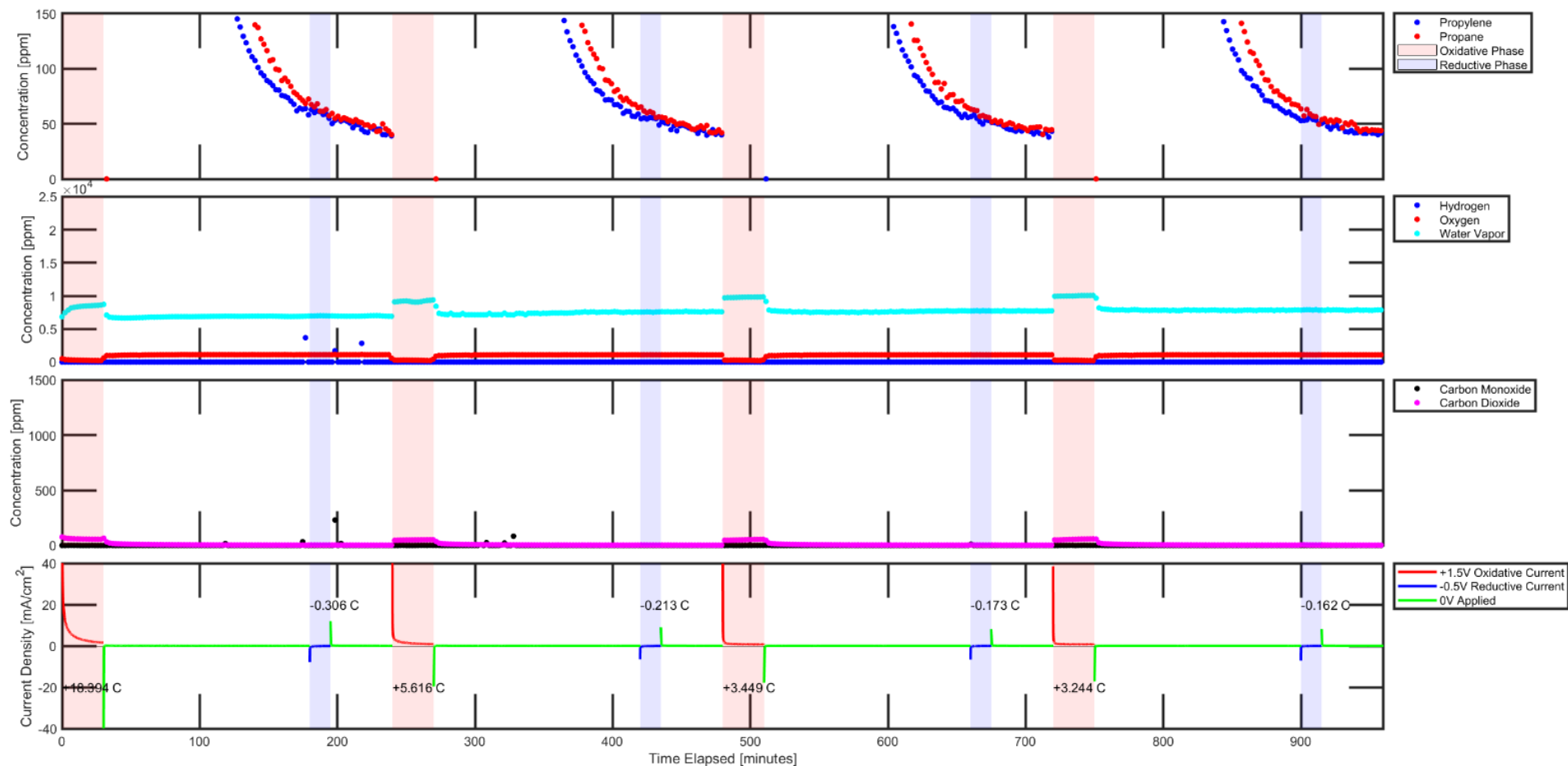
5 MEA samples of identical loading compositions were tested at varying reductive potential in this series of experiments. Therefore, this section consists of 5 *Figures* each with its own corresponding reductive potential applied to the MEA during the reductive phase of each cycle (i.e., 0, -0.5, -1.0, -2.0, and -3.0V vs. counter-side). This series of experiments contributed to the data shown in **Figures 4-B** and **4-C** of the main manuscript where it attempted to observe the effect of reductive potential on propylene separation performance. A 50:50 molar ratio propylene-propane feed was introduced to the MEA's during the oxidative phase as well. Oxidative potential was kept constant at +1.5V for all 5 MEA samples.

No separation performance or any propylene activity was observed at 0V, -0.5V, and -1.0V (**Figures S5-A** thru **S5-C**) most likely because the potential did not reach the thermodynamic minimum of to reduce the complexed nickel dithiolene species to release the captured propylene. Separation performance was observed initially at -2.0V reductive potential (**Figure S5-D**). However, applying a higher reductive potential of -3.0V resulted in the release of both propylene and propane upon applying that reductive potential (**Figure S5-E**), leading to the failure of the device in elevating propylene composition versus propane compared to that of the original feed. Therefore, excessive reductive potential can defeat the targeted goal of olefin purification due to parasitic propylene hydrogenation. It is not unexpected to see propane production at -3V especially because hydrogen gas was commonly observed as a side product even at a less powerful reductive potential of -2V. At least 10-20% of reductive charge contributed to hydrogen gas production in nearly all experiments running -2V potential during the reductive phase (refer to **Section S1**, **S2**, and **S3's** reductive FE bar graphs).

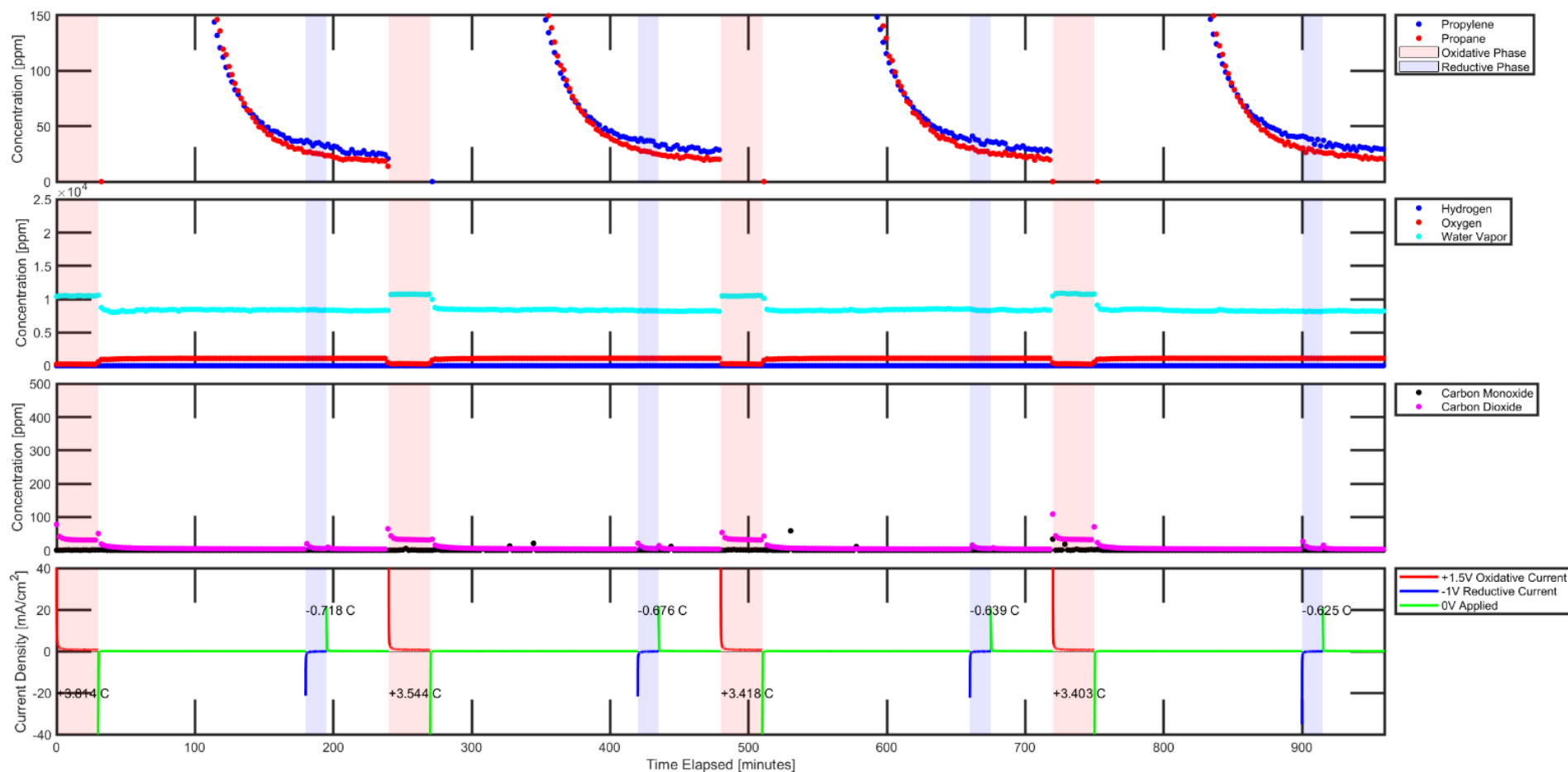
S5-A



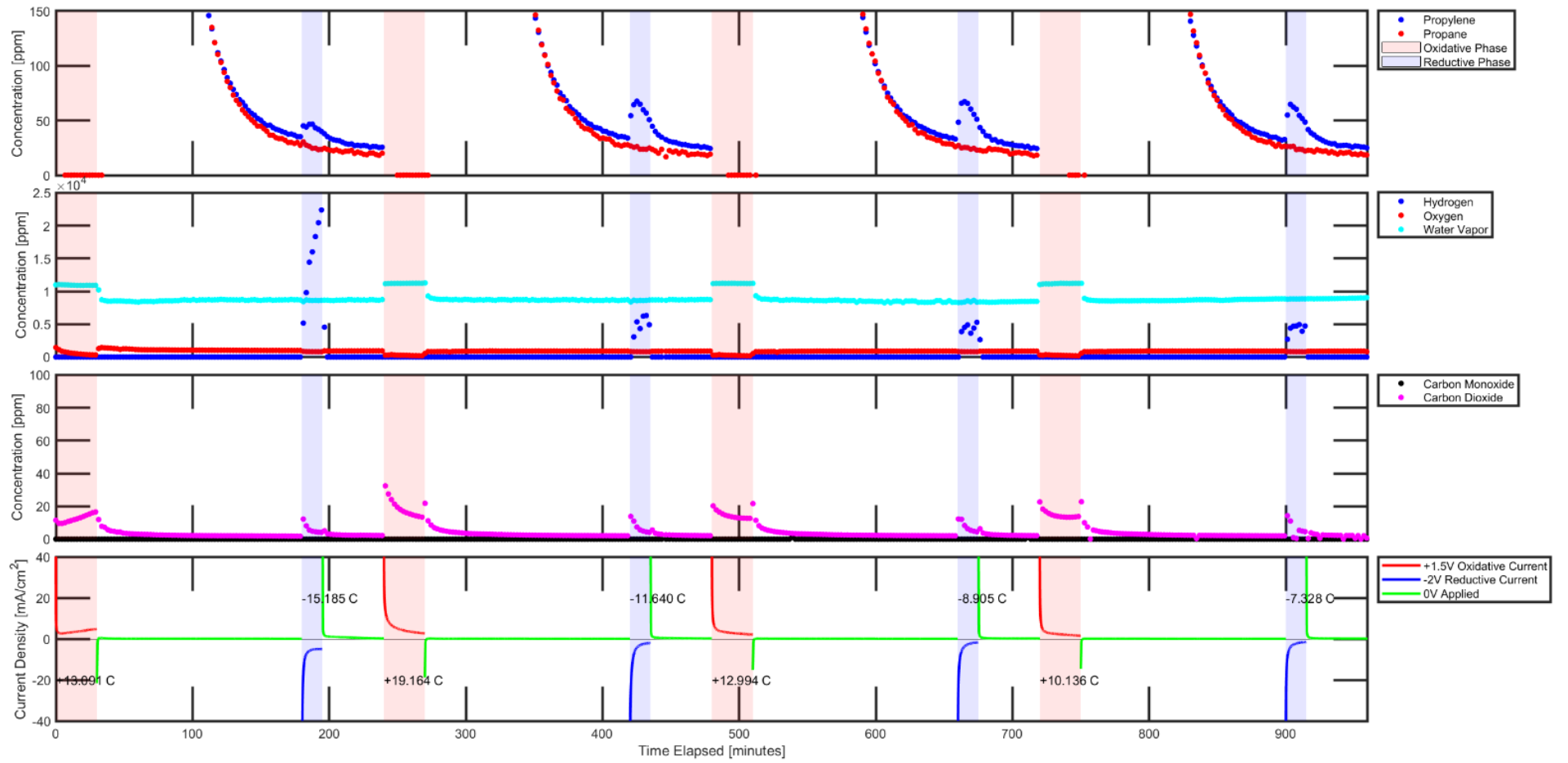
**Figure S5-A: 0V Reductive Potential.** Gas concentration measurements via Agilent Micro GC 990 and Chronoamperometry via Potentiostat. Spray-deposited layer consisted of 5 mg/cm<sup>2</sup> Carbon Nanoparticles, 4 mg/cm<sup>2</sup> Nafion ionomer, 4 mg/cm<sup>2</sup> [BMIM][PF<sub>6</sub>] ionic liquid, and 8 mg/cm<sup>2</sup> [N(Et)<sub>4</sub>]<sub>2</sub>[Ni(mnt)<sub>2</sub>] salt onto Sigracet 39 BB Carbon GDL. Feed composition of propane/propylene mixture was 50% by volume at 20 sccm total flow rate. Reductive Potential of 0V was applied.



**Figure S5-B: -0.5V Reductive Potential.** Gas concentration measurements via Agilent Micro GC 990 and Chronoamperometry via Potentiostat. Spray-deposited layer consisted of 5 mg/cm<sup>2</sup> Carbon Nanoparticles, 4 mg/cm<sup>2</sup> Nafion ionomer, 4 mg/cm<sup>2</sup> [BMIM][PF<sub>6</sub>] ionic liquid, and 8 mg/cm<sup>2</sup> [N(Et)<sub>4</sub>]<sub>2</sub>[Ni(mnt)<sub>2</sub>] salt onto Sigracet 39 BB Carbon GDL. Feed composition of propane/propylene mixture was 50% by volume at 20 sccm total flow rate. Reductive Potential of -0.5V was applied. (Note: Duplicate of **Figure S1-E**)



**Figure S5-C: -1.0V Reductive Potential.** Gas concentration measurements via Agilent Micro GC 990 and Chronoamperometry via Potentiostat. Spray-deposited layer consisted of 5 mg/cm<sup>2</sup> Carbon Nanoparticles, 4 mg/cm<sup>2</sup> Nafion ionomer, 4 mg/cm<sup>2</sup> [BMIM][PF<sub>6</sub>] ionic liquid, and 8 mg/cm<sup>2</sup> [N(Et)<sub>4</sub>]<sub>2</sub>[Ni(mnt)<sub>2</sub>] salt onto Sigracet 39 BB Carbon GDL. Feed composition of propane/propylene mixture was 50% by volume at 20 sccm total flow rate. Reductive Potential of -1.0 V was applied.



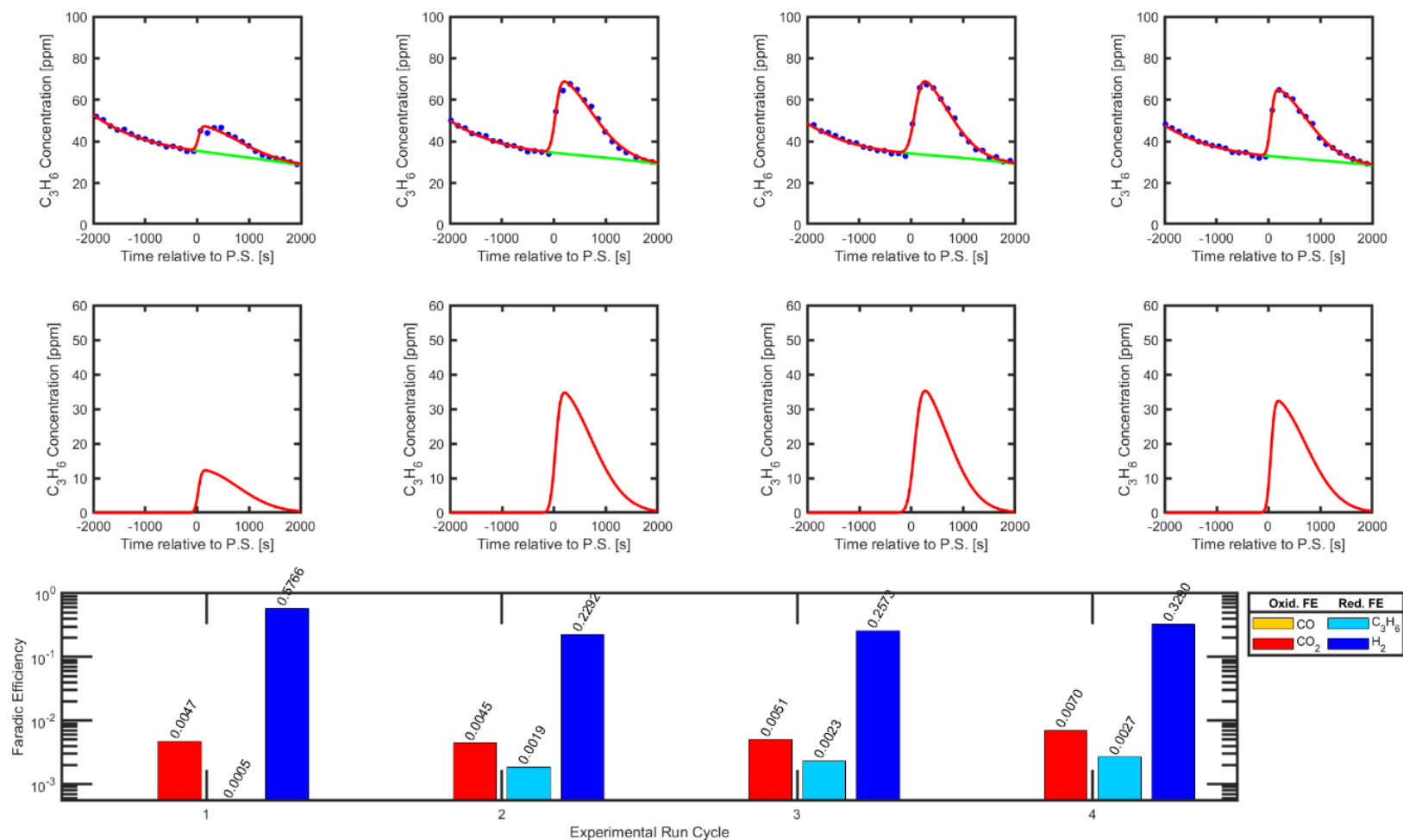


**Figure S5-D: -2.0V Reductive Potential.** Gas concentration measurements via Agilent Micro GC 990, Chronoamperometry via Potentiostat, and graphical analysis of propylene captured and released via Electrochemical Modulation. Second row of graphical analysis depicts deconvoluted graphs of propylene concentration separated by electrochemically modulated complexation mechanism. Spray-deposited layer consisted of 5 mg/cm<sup>2</sup> Carbon Nanoparticles, 4 mg/cm<sup>2</sup> Nafion ionomer, 4 mg/cm<sup>2</sup> [BMIM][PF<sub>6</sub>] ionic liquid, and 8 mg/cm<sup>2</sup> [N(Et)<sub>4</sub>]<sub>2</sub>[Ni(mt)<sub>2</sub>] salt onto Sigracet 39 BB Carbon GDL. Feed composition of propane/propylene mixture was 50% by volume at 20 sccm total flow rate. Reductive Potential of -2.0 V was applied

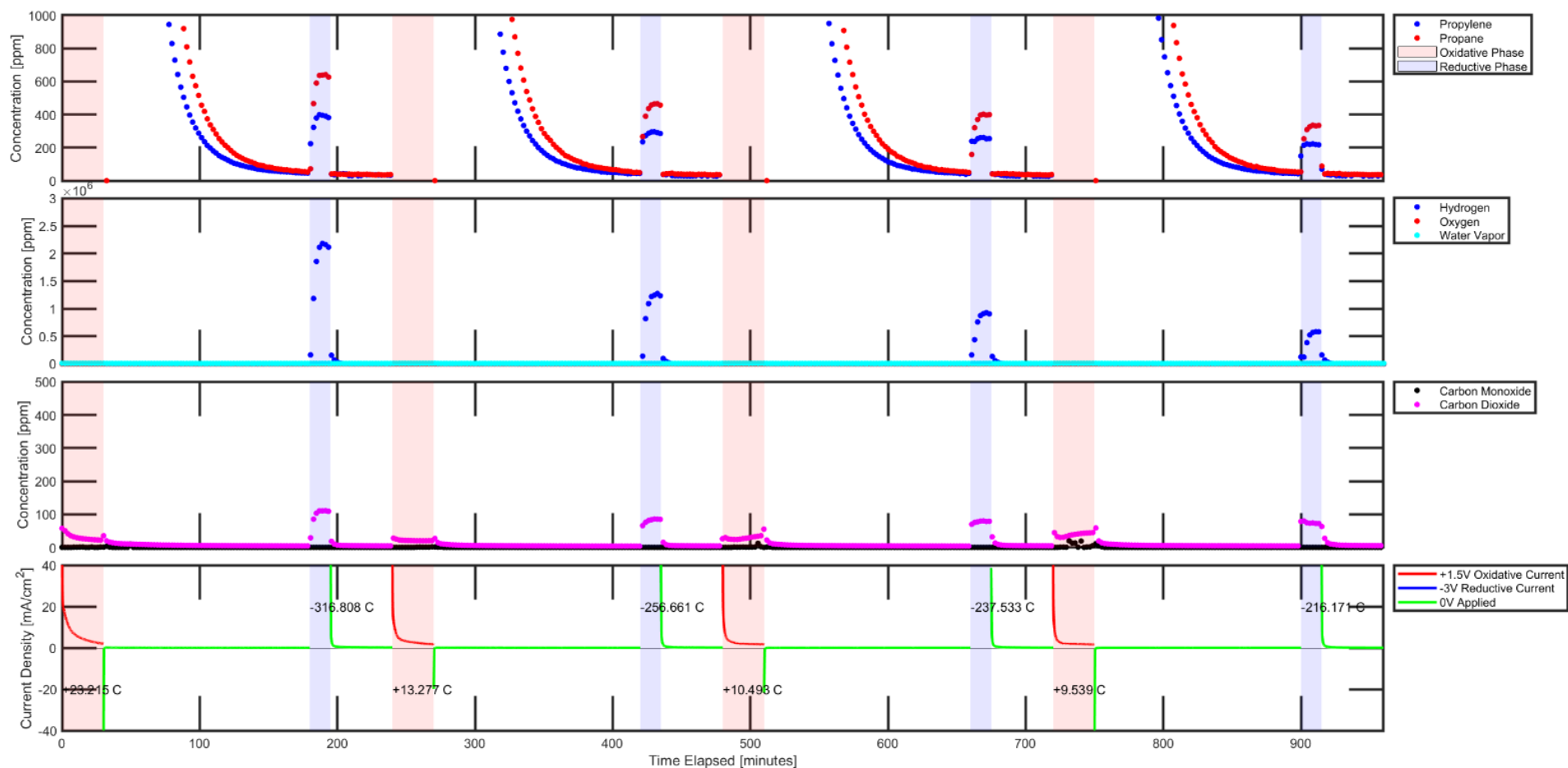
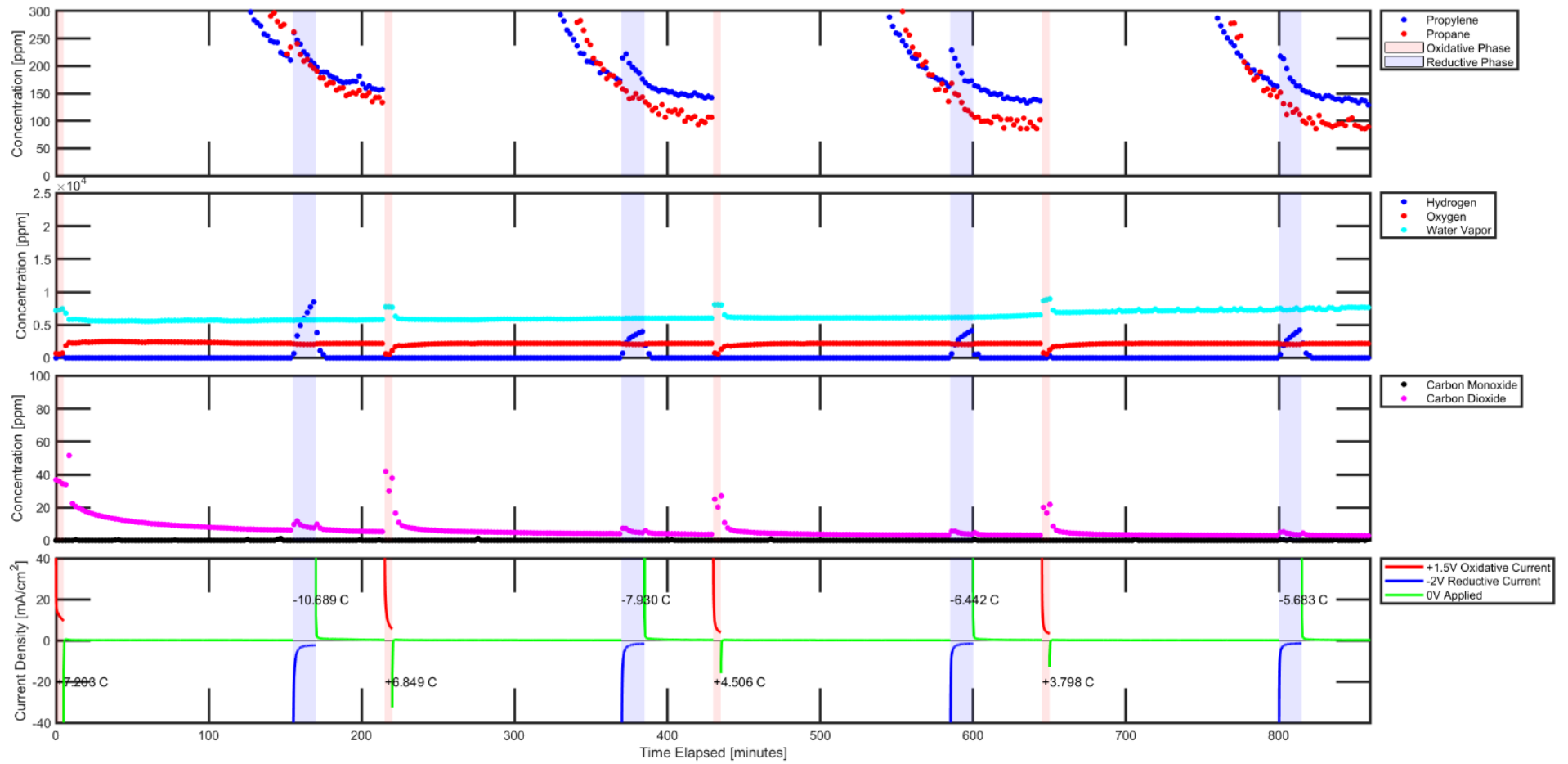


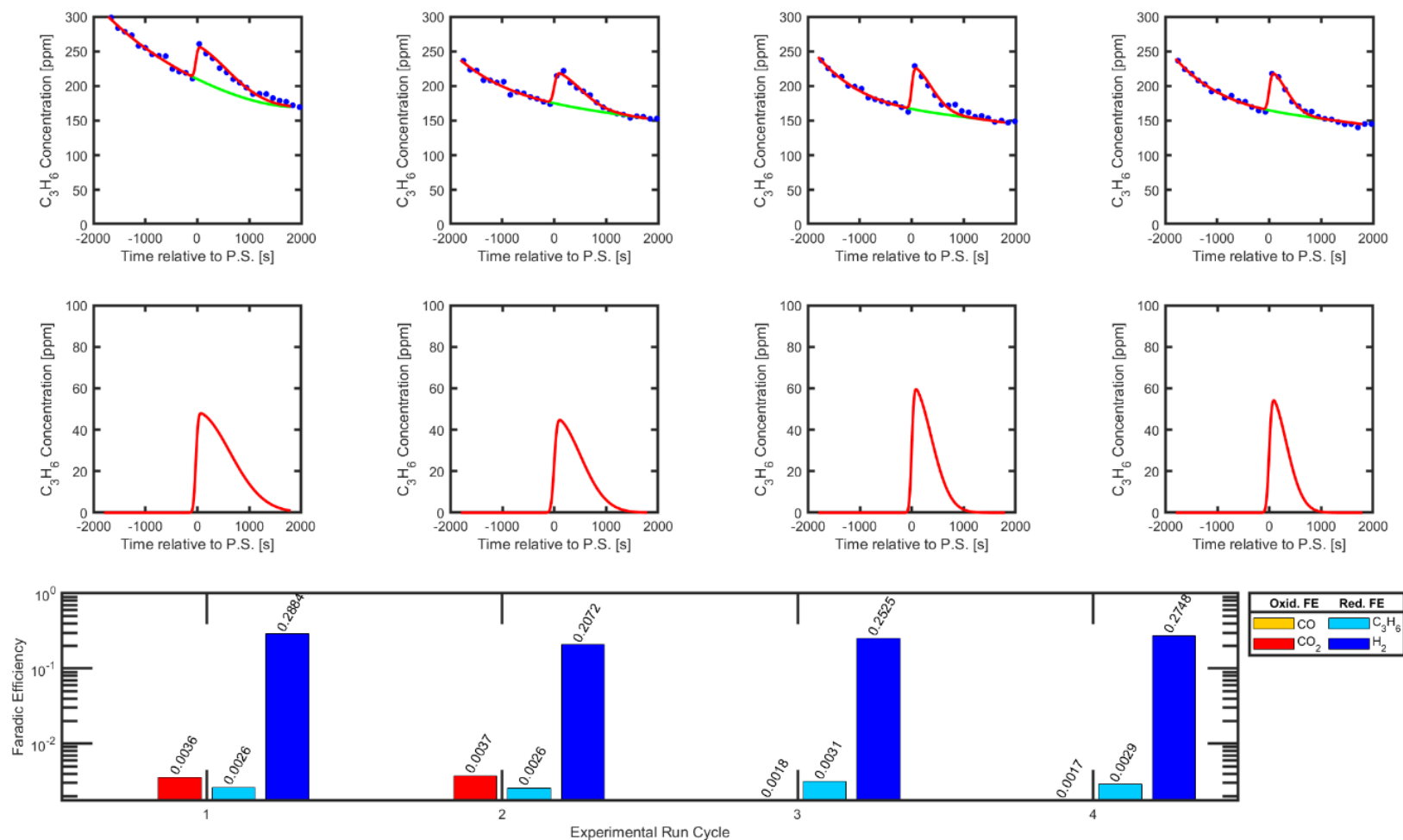
**Figure S5-E: -3.0V Reductive Potential.** Gas concentration measurements via Agilent Micro GC 990 and Chronoamperometry via Potentiostat. Spray-deposited layer consisted of 5 mg/cm<sup>2</sup> Carbon Nanoparticles, 4 mg/cm<sup>2</sup> Nafion ionomer, 4 mg/cm<sup>2</sup> [BMIM][PF<sub>6</sub>] ionic liquid, and 8 mg/cm<sup>2</sup> [N(Et)<sub>4</sub>]<sub>2</sub>[Ni(mnt)<sub>2</sub>] salt onto Sigracet 39 BB Carbon GDL. Feed composition of propane/propylene mixture was 50% by volume at 20 sccm total flow rate. Reductive Potential of -3.0 V was applied. Because excessive propane was detected, it was observed that propylene separation did not happen at this this reductive potential due to parasitic hydrogenation of propylene. The subsequent propylene quantifications and FE calculations were neglected for this case because the true amount of propylene released from the nickel dithiolene complex during the reductive phase cannot be quantified due to the competing parasitic reaction consuming the propylene that was released.

**Section Summary:**

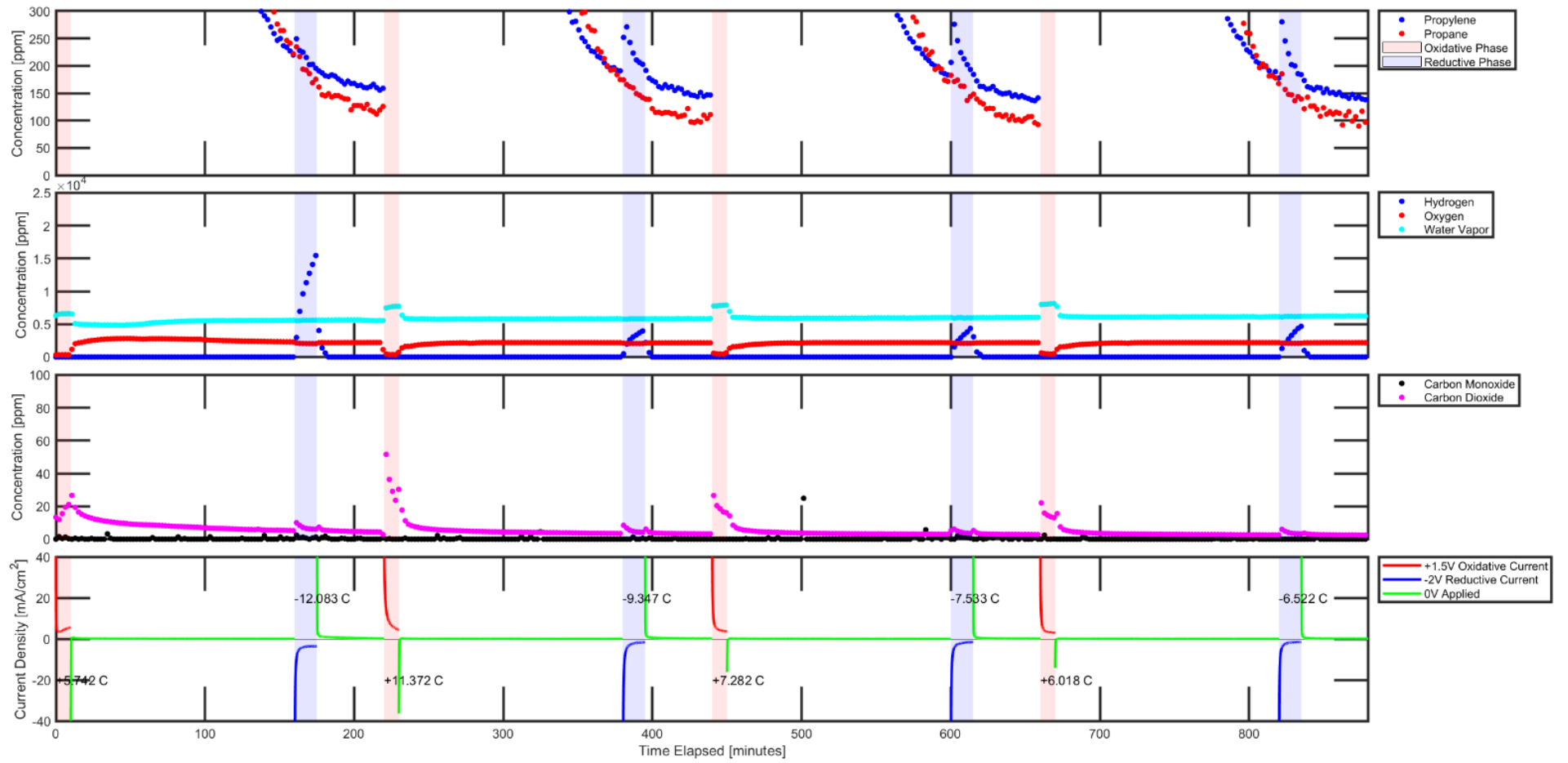
MEA samples of identical loading compositions to that of the MEA's used in **Section S4** and **S5** were tested at varying propylene-propane feed exposure time (and oxidative phase duration). Because 6 different exposure times were tested, this *Section* consists of 6 *Figures* each with its own corresponding feed exposure time (i.e., 5, 10, 20, 30, 45 and 60 minutes). This series of experiments contributed to the data shown in **Figure 3-D** of the main manuscript where it attempted to observe the effect of varying feed exposure time on propylene separation performance. A 50:50 molar ratio propylene-propane feed was introduced to the MEA's during the oxidative phase as well. All 6 MEA experiments utilized the same oxidative and reductive potentials of +1.5V and -2V, respectively.

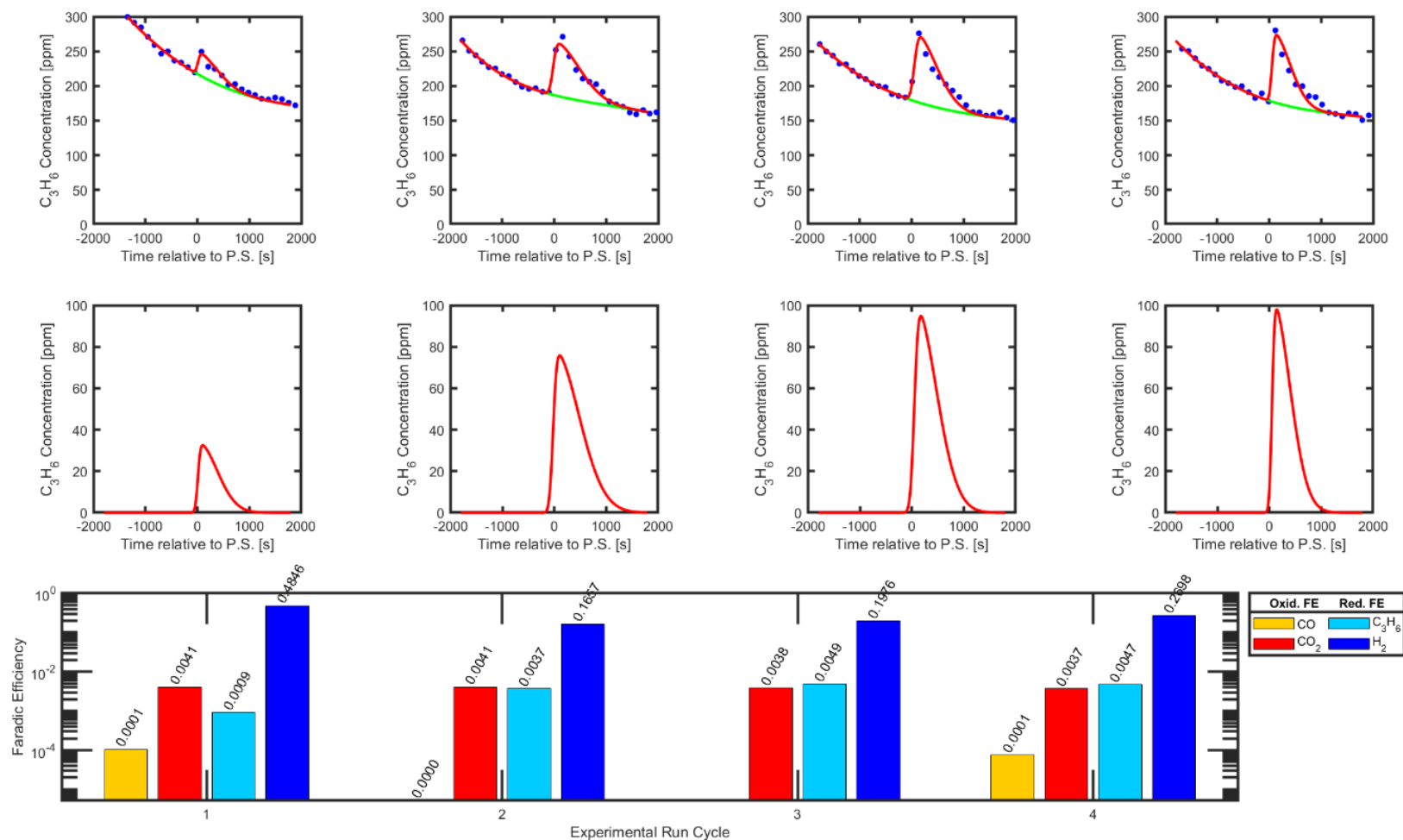
There was approximately 30% increase in the separation performance from 5-minute to 10-minute feed exposure time with a local slope of approximately 0.004  $\mu\text{mol}$  per minute of exposure (**Figure S6-A** and **S6-B**). At higher exposure times however, the separation performance did not increase as rapidly, stabilizing to a linear slope of approximately 0.002  $\mu\text{mol}$  per minute of exposure (**Figure S6-B** thru **S6-F**), half the slope of between 5-minute and 10-minute exposure. Furthermore, approximately 70-80% of the total charge was applied in the first 10 minutes of oxidative phase, indicating that most of the oxidative processes occurred in this window of time for a typical 30-minute phase, including the oxidation of  $[\text{Ni}(\text{mnt})_2]^{-2}$  to  $[\text{Ni}(\text{mnt})_2]^0$ . The 10-minute exposure's separation performance covered >70% of the 30-minute exposure's performance as well.



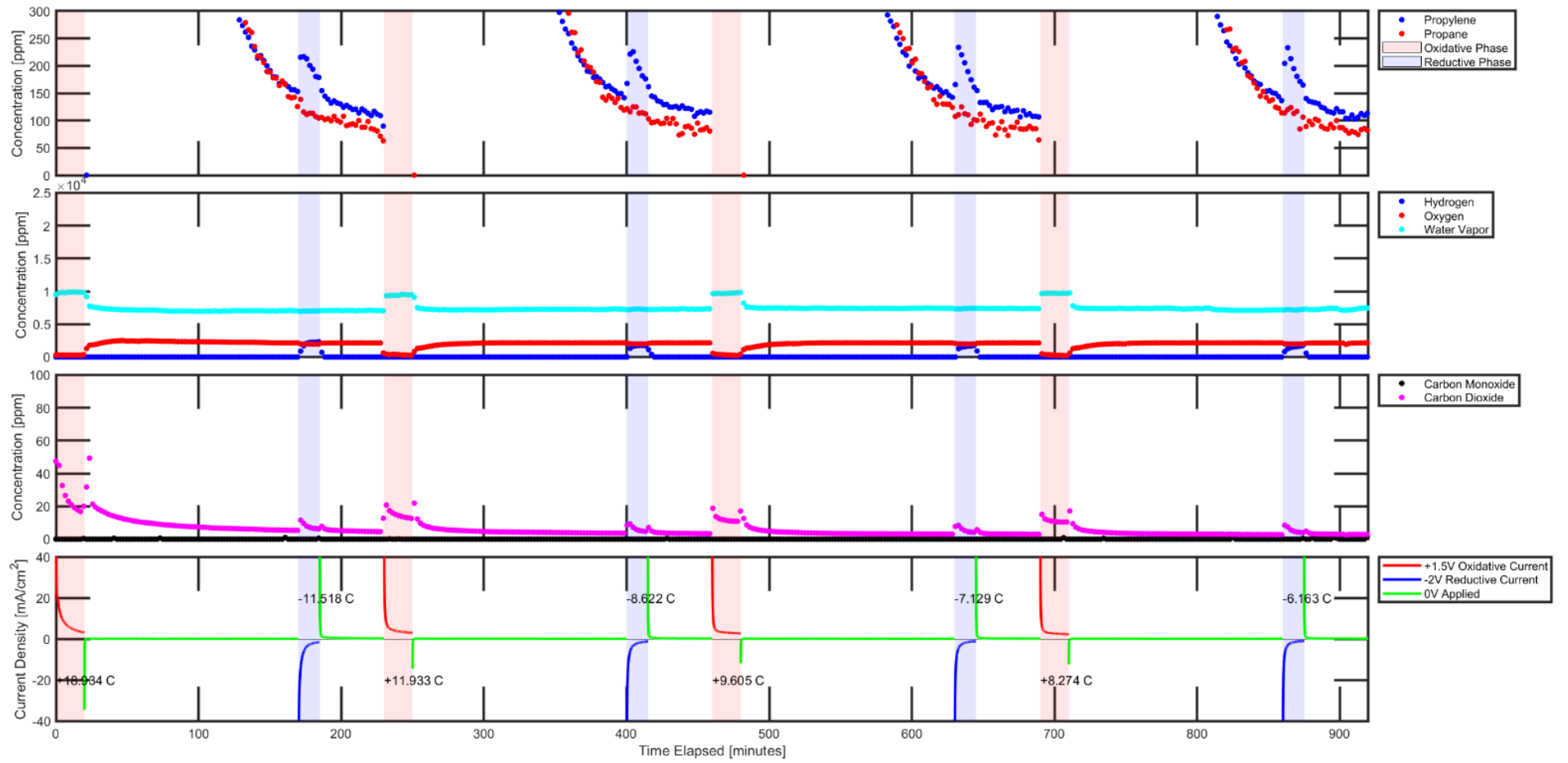


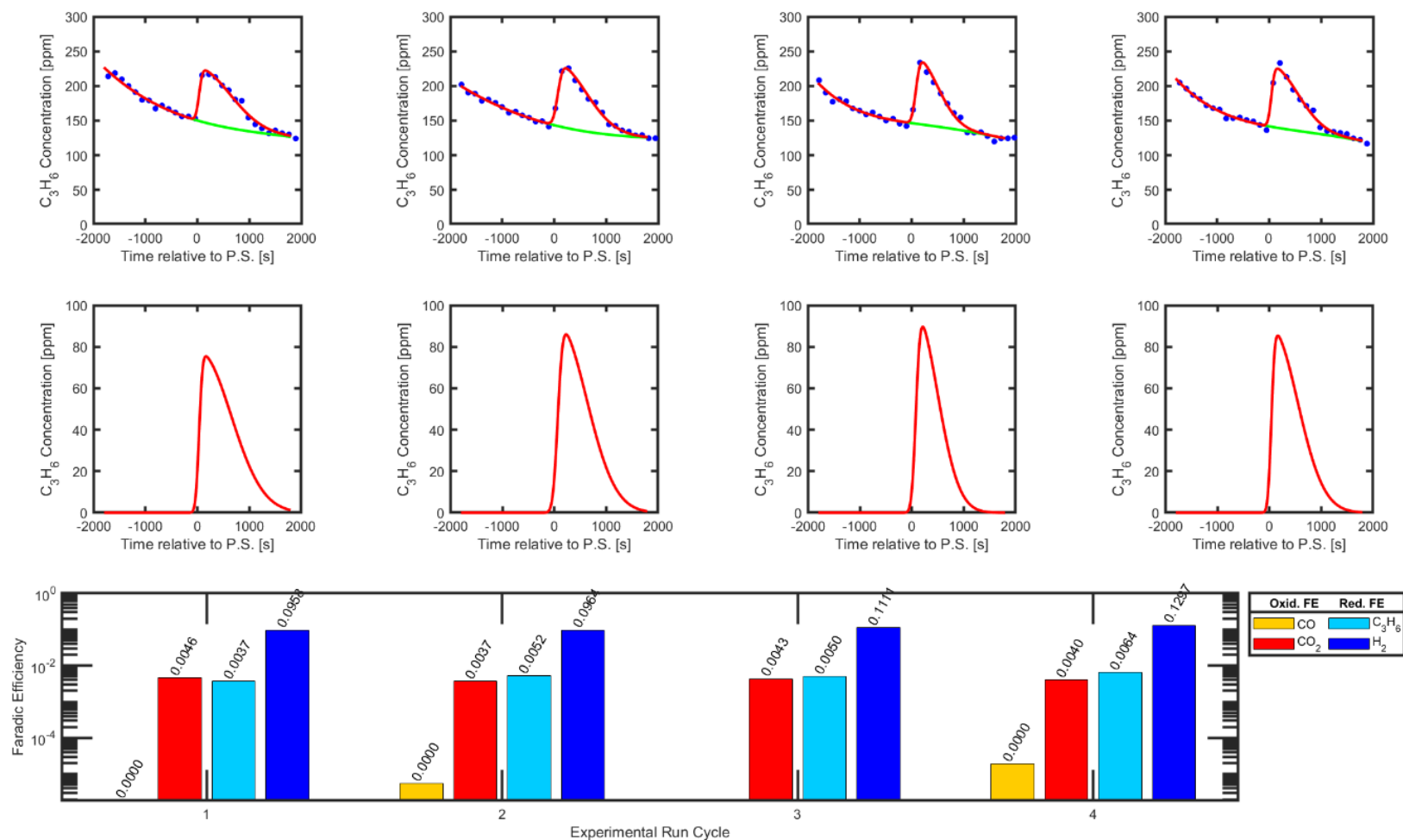
**Figure S6-A: 5-minute Feed Exposure.** Gas concentration measurements via Agilent Micro GC 990, Chronoamperometry via Potentiostat, and graphical analysis of propylene captured and released via Electrochemical Modulation. Second row of graphical analysis depicts deconvoluted graphs of propylene concentration separated by electrochemically modulated complexation mechanism. Spray-deposited layer consisted of 5 mg/cm<sup>2</sup> Carbon Nanoparticles, 4 mg/cm<sup>2</sup> Nafion ionomer, 4 mg/cm<sup>2</sup> [BMIM][PF<sub>6</sub>] ionic liquid, and 8 mg/cm<sup>2</sup> [N(Et)<sub>4</sub>]<sub>2</sub>[Ni(mnt)<sub>2</sub>] salt onto Sigracet 39 BB Carbon GDL. Feed composition of propane/propylene mixture was 50% by volume at 20 sccm total flow rate. Feed Exposure Time was 5 minutes.



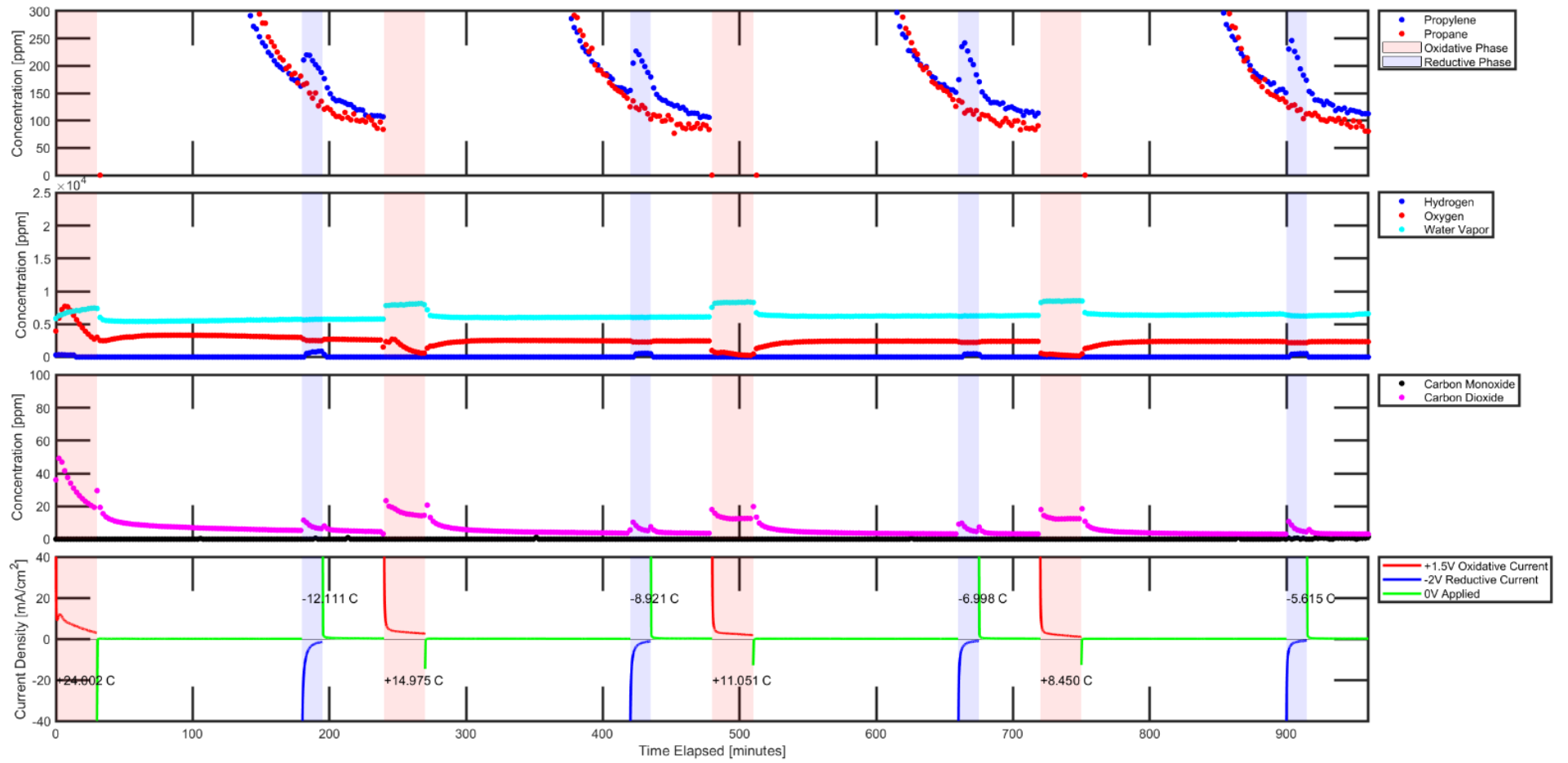


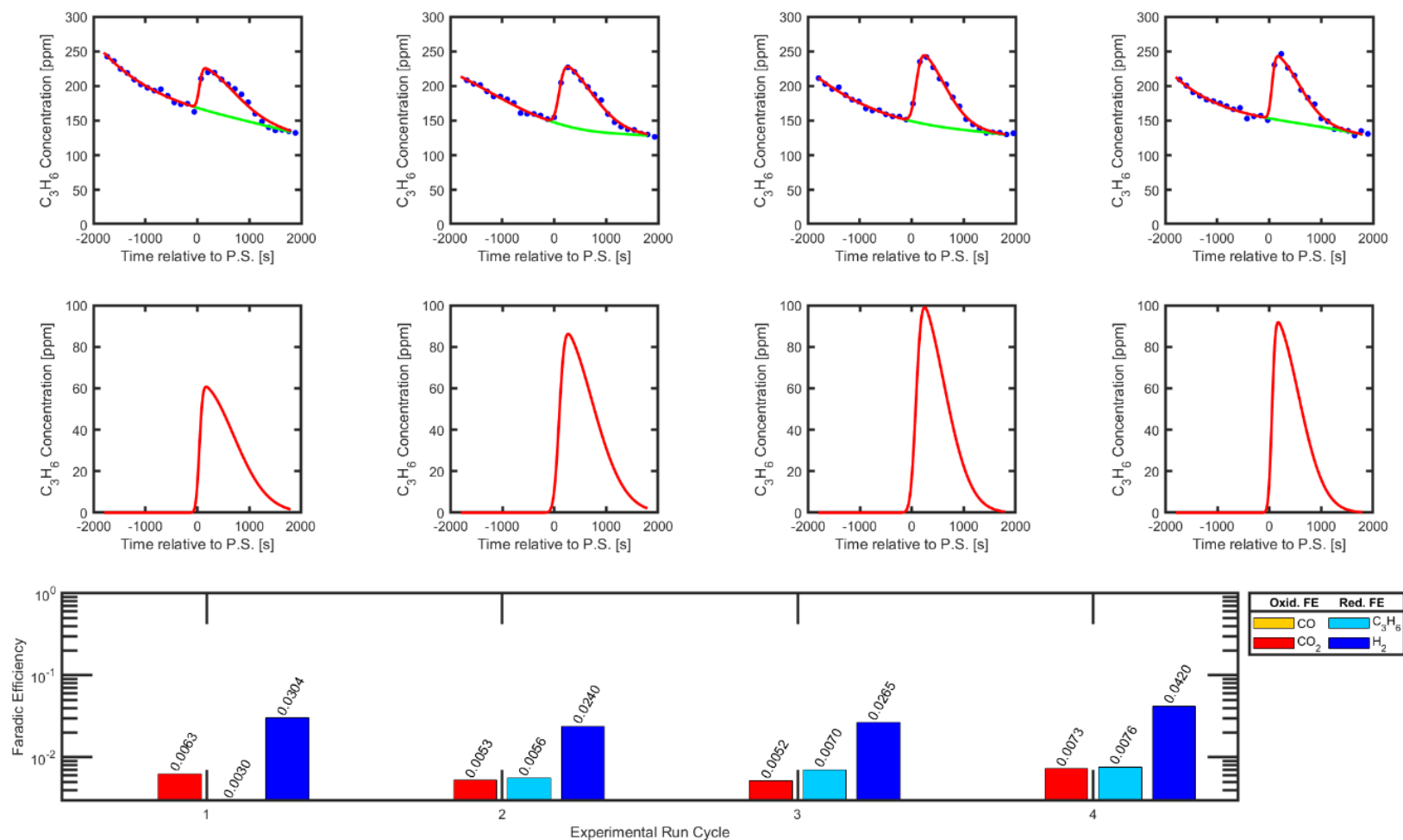
**Figure S6-B: 10-minute Feed Exposure.** Gas concentration measurements via Agilent Micro GC 990, Chronoamperometry via Potentiostat, and graphical analysis of propylene captured and released via Electrochemical Modulation. Second row of graphical analysis depicts deconvoluted graphs of propylene concentration separated by electrochemically modulated complexation mechanism. Spray-deposited layer consisted of 5 mg/cm<sup>2</sup> Carbon Nanoparticles, 4 mg/cm<sup>2</sup> Nafion ionomer, 4 mg/cm<sup>2</sup> [BMIM][PF<sub>6</sub>] ionic liquid, and 8 mg/cm<sup>2</sup> [N(Et)<sub>4</sub>]<sub>2</sub>[Ni(mnt)<sub>2</sub>] salt onto Sigracet 39 BB Carbon GDL. Feed composition of propane/propylene mixture was 50% by volume at 20 sccm total flow rate. Feed Exposure Time was 10 minutes.



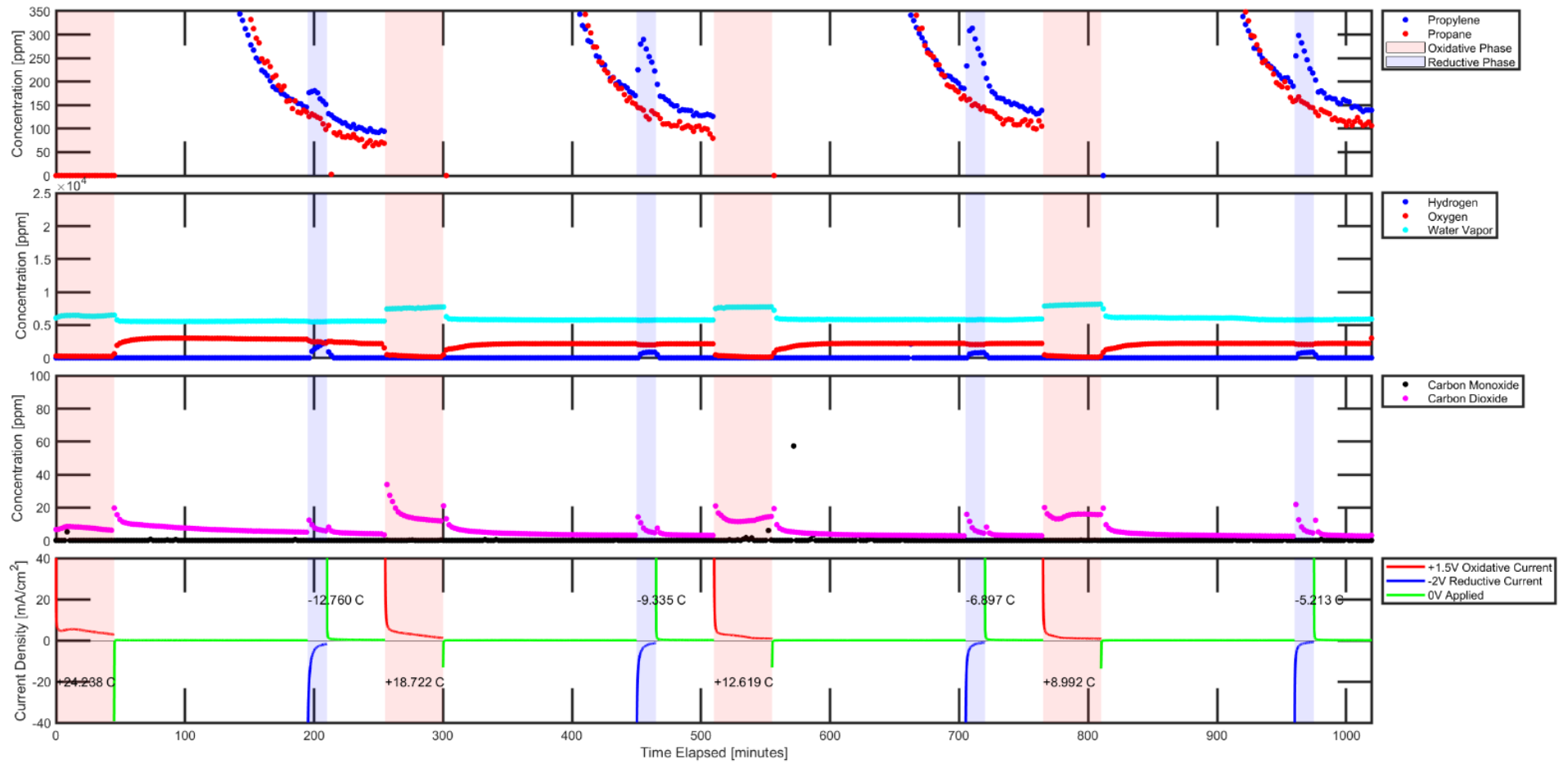


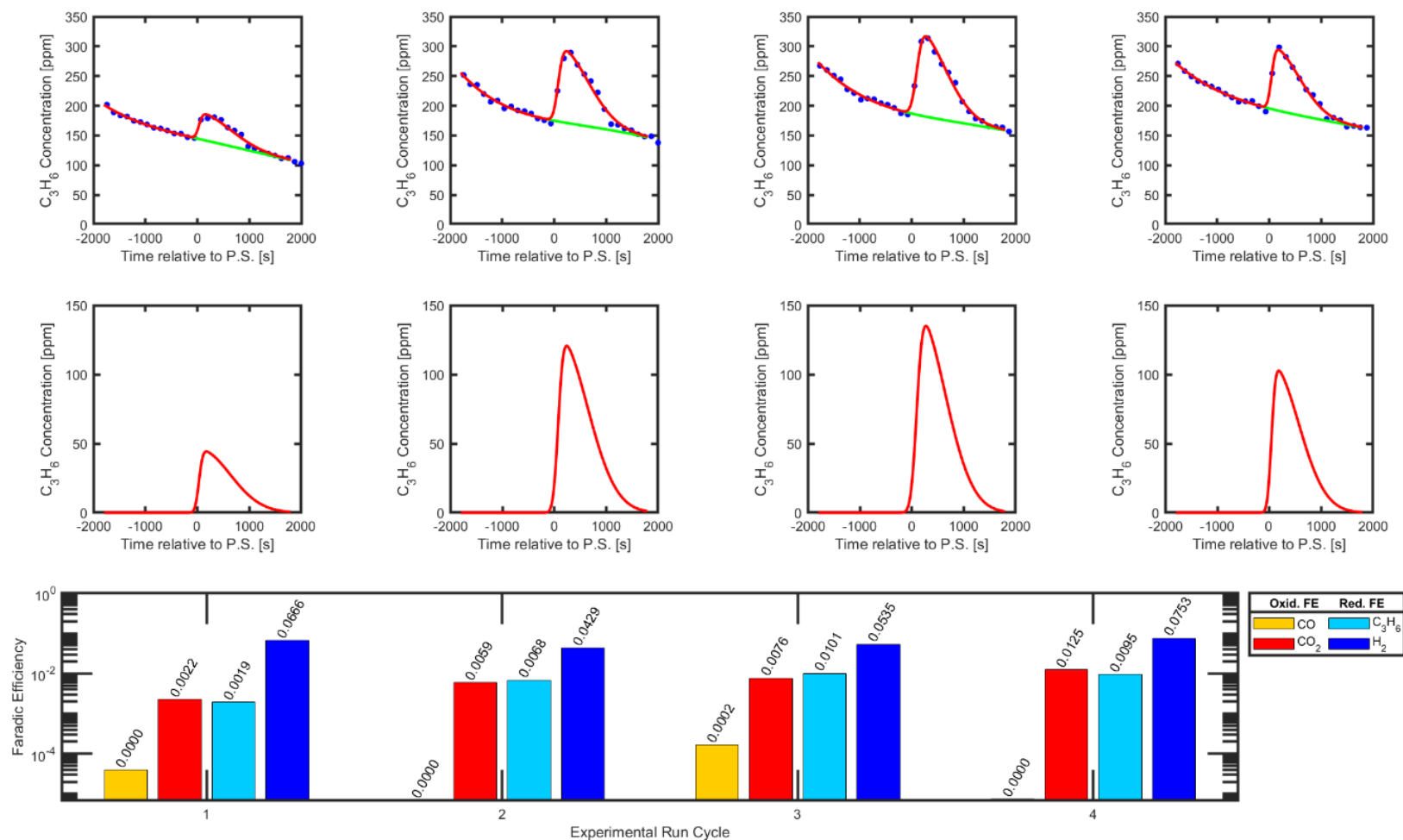
**Figure S6-C: 20-minute Feed Exposure.** Gas concentration measurements via Agilent Micro GC 990, Chronoamperometry via Potentiostat, and graphical analysis of propylene captured and released via Electrochemical Modulation. Second row of graphical analysis depicts deconvoluted graphs of propylene concentration separated by electrochemically modulated complexation mechanism. Spray-deposited layer consisted of 5 mg/cm<sup>2</sup> Carbon Nanoparticles, 4 mg/cm<sup>2</sup> Nafion ionomer, 4 mg/cm<sup>2</sup> [BMIM][PF<sub>6</sub>] ionic liquid, and 8 mg/cm<sup>2</sup> [N(Et)<sub>4</sub>]<sub>2</sub>[Ni(mnt)<sub>2</sub>] salt onto Sigracet 39 BB Carbon GDL. Feed composition of propane/propylene mixture was 50% by volume at 20 sccm total flow rate. Feed Exposure Time was 20 minutes.



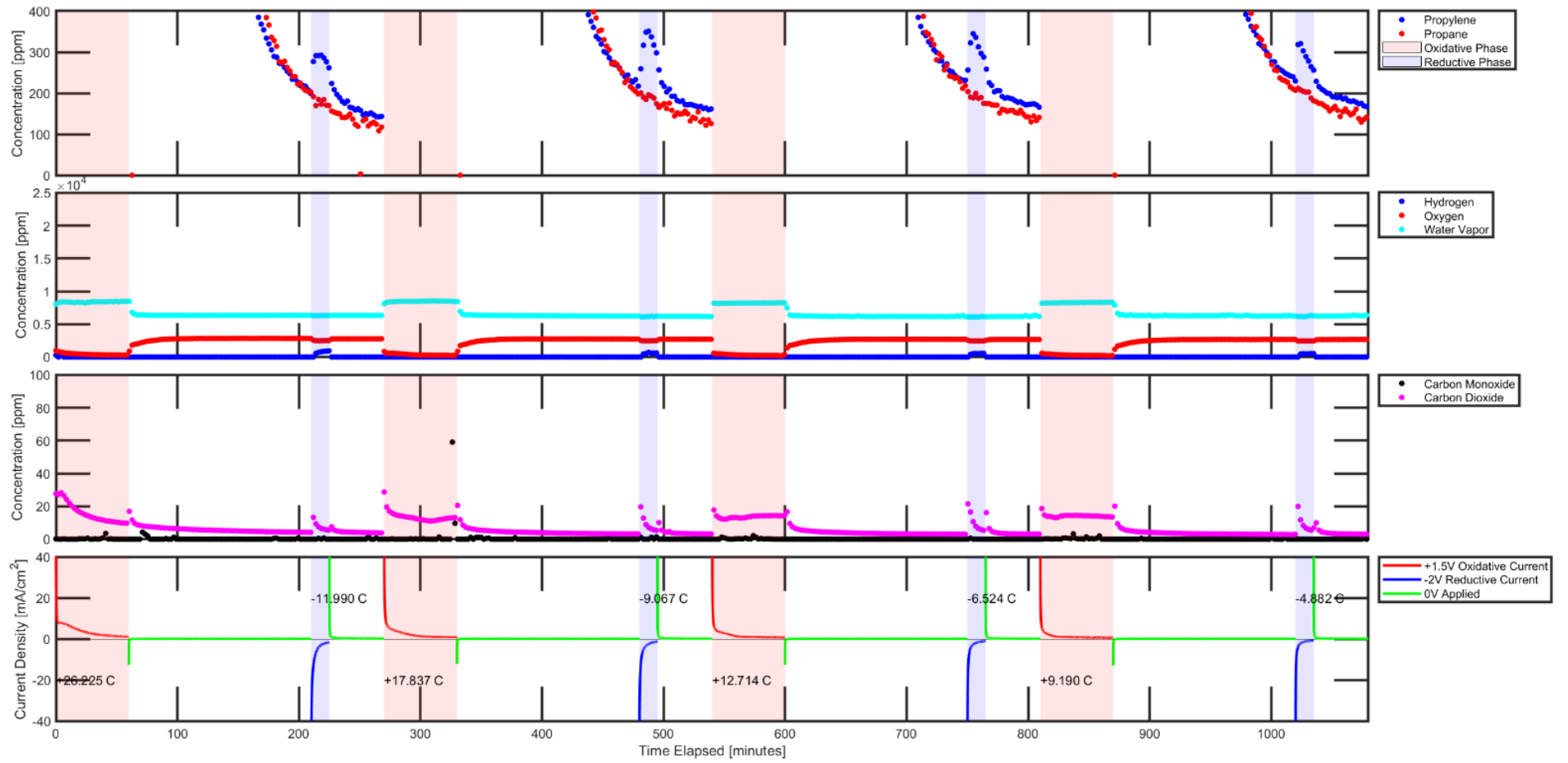


**Figure S6-D: 30-minute Feed Exposure.** Gas concentration measurements via Agilent Micro GC 990, Chronoamperometry via Potentiostat, and graphical analysis of propylene captured and released via Electrochemical Modulation. Second row of graphical analysis depicts deconvoluted graphs of propylene concentration separated by electrochemically modulated complexation mechanism. Spray-deposited layer consisted of 5 mg/cm<sup>2</sup> Carbon Nanoparticles, 4 mg/cm<sup>2</sup> Nafion ionomer, 4 mg/cm<sup>2</sup> [BMIM][PF<sub>6</sub>] ionic liquid, and 8 mg/cm<sup>2</sup> [N(Et)<sub>4</sub>]<sub>2</sub>[Ni(mnt)<sub>2</sub>] salt onto Sigracet 39 BB Carbon GDL. Feed composition of propane/propylene mixture was 50% by volume at 20 sccm total flow rate. Feed Exposure Time was 30 minutes.





**Figure S6-E: 45-minute Feed Exposure.** Gas concentration measurements via Agilent Micro GC 990, Chronoamperometry via Potentiostat, and graphical analysis of propylene captured and released via Electrochemical Modulation. Second row of graphical analysis depicts deconvoluted graphs of propylene concentration separated by electrochemically modulated complexation mechanism. Spray-deposited layer consisted of 5 mg/cm<sup>2</sup> Carbon Nanoparticles, 4 mg/cm<sup>2</sup> Nafion ionomer, 4 mg/cm<sup>2</sup> [BMIM][PF<sub>6</sub>] ionic liquid, and 8 mg/cm<sup>2</sup> [N(Et)<sub>4</sub>]<sub>2</sub>[Ni(mnt)<sub>2</sub>] salt onto Sigracet 39 BB Carbon GDL. Feed composition of propane/propylene mixture was 50% by volume at 20 sccm total flow rate. Feed Exposure Time was 45 minutes.



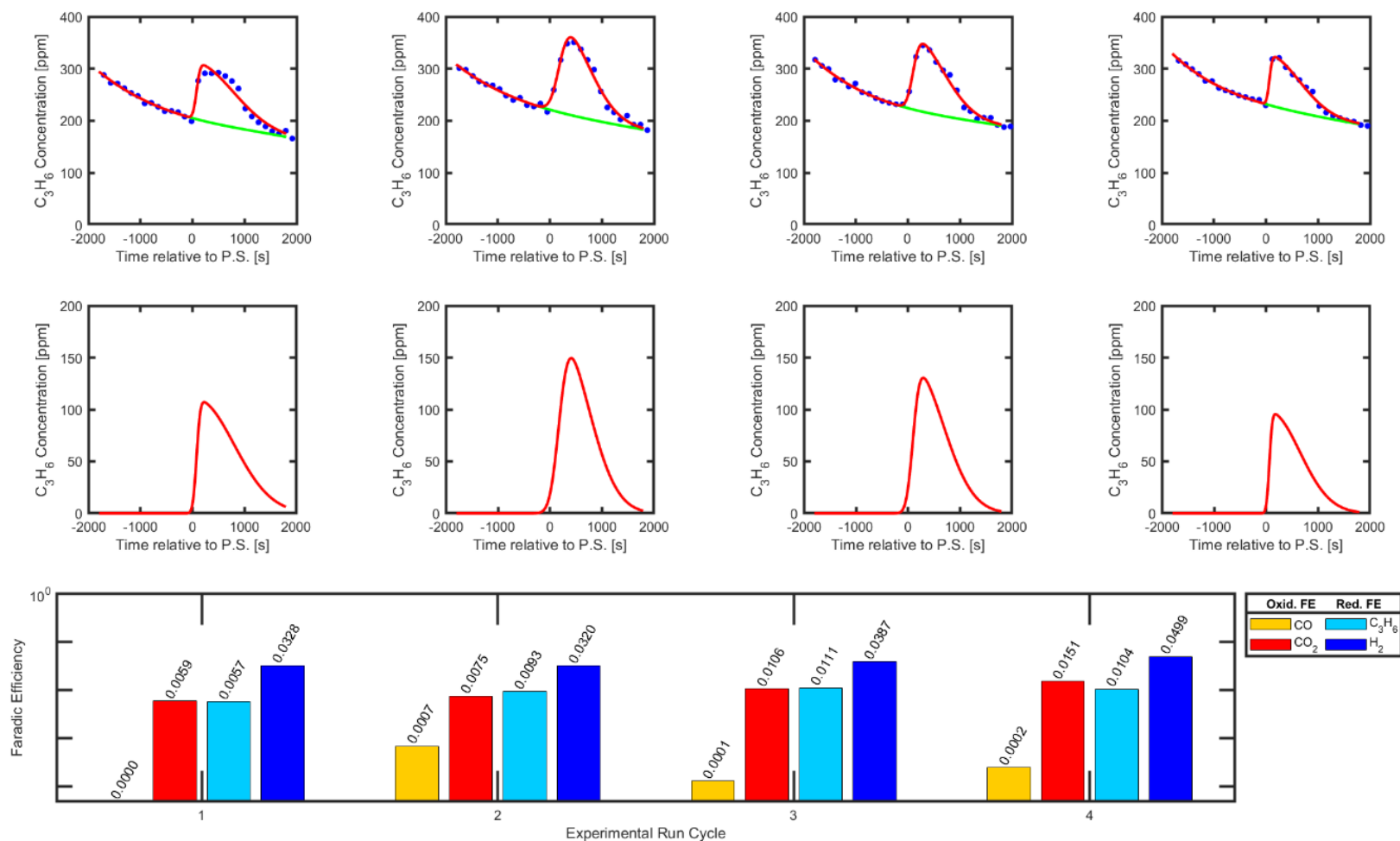


**Figure S6-F: 60-minute Feed Exposure.** Gas concentration measurements via Agilent Micro GC 990, Chronoamperometry via Potentiostat, and graphical analysis of propylene captured and released via Electrochemical Modulation. Second row of graphical analysis depicts deconvoluted graphs of propylene concentration separated by electrochemically modulated complexation mechanism. Spray-deposited layer consisted of 5 mg/cm<sup>2</sup> Carbon Nanoparticles, 4 mg/cm<sup>2</sup> Nafion ionomer, 4 mg/cm<sup>2</sup> [BMIM][PF<sub>6</sub>] ionic liquid, and 8 mg/cm<sup>2</sup> [N(Et)<sub>4</sub>]<sub>2</sub>[Ni(mnt)<sub>2</sub>] salt onto Sigracet 39 BB Carbon GDL. Feed composition of propane/propylene mixture was 50% by volume at 20 sccm total flow rate. Feed Exposure Time was 60 minutes.

Section Summary:

To better understand the plateauing separation performance at high  $[N(Et)_4]_2[Ni(mnt)_2]$  loadings shown in **Figure 3-A** of the main manuscript, ionogel film containing  $[N(Et)_4]_2[Ni(mnt)_2]$  were spin-casted on silicon wafers and observed under AM Microscope under 50x magnification. Phase separation can be visually observed starting at a ratio of 0.8. Plateauing behavior of separation performance occurred at an equivalent ratio of 1.0 according to **Figure 3-A** (at the data point representing  $8 \text{ mg/cm}^2$  loading of  $[N(Et)_4]_2[Ni(mnt)_2]$ ) which may likely correlate to the frequency of phase separation of  $[N(Et)_4]_2[Ni(mnt)_2]$  crystals. Therefore, the transport limitation sources can be attributed to possible phase separation of  $[N(Et)_4]_2[Ni(mnt)_2]$  crystals out of the ionogel medium due to oversaturation

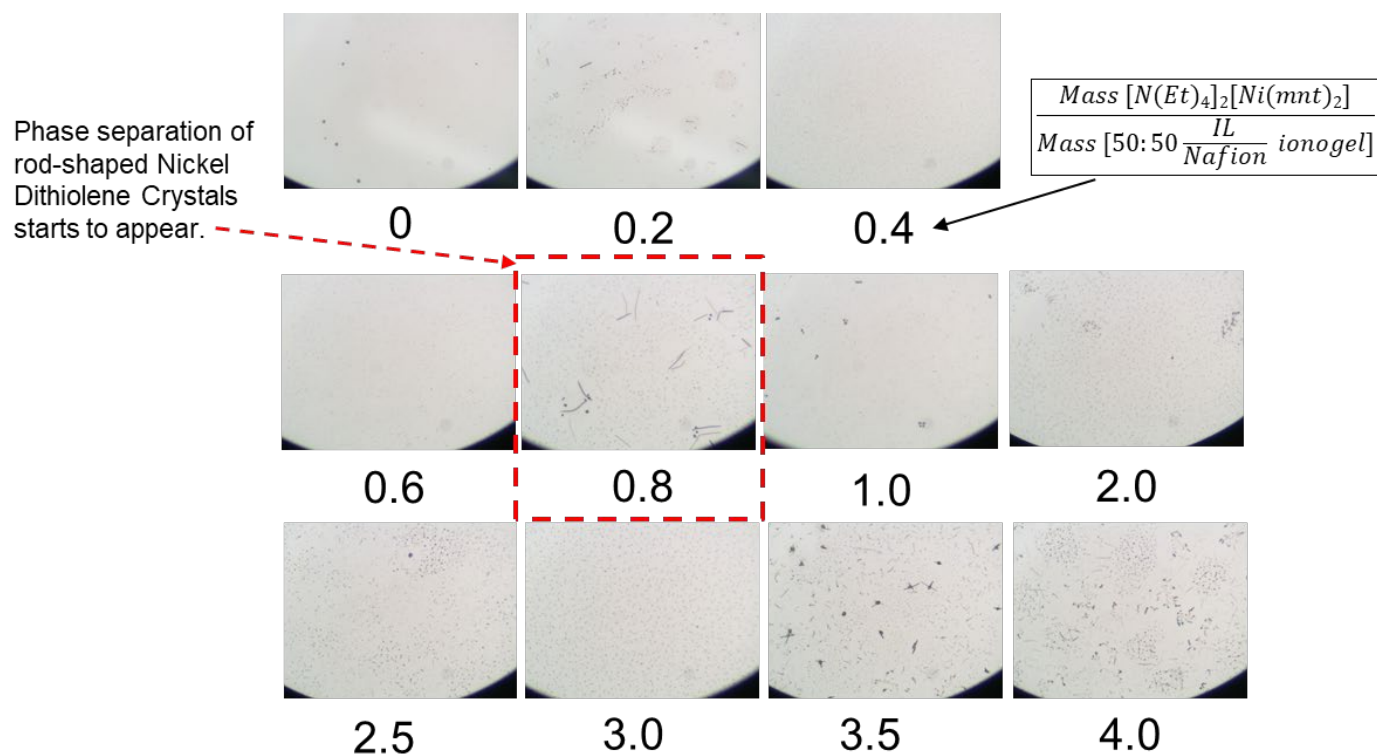


**Figure S7.** Solution mixtures of Nafion, IL, and  $[N(Et)_4]_2[Ni(mnt)_2]$  were prepared in isopropanol and spin-casted onto silicon substrate to simulate thin film coating of MEA's ionogel coating over carbon nanoparticles. Varying mass ratios of  $[N(Et)_4]_2[Ni(mnt)_2]$  vs. [IL and Nafion] were spin-casted to study the possible effect of this ratio on the homogeneity of the ionogel medium. Note that a 50:50 ratio of IL vs. Nafion was utilized in all spin-casted samples.

**Section Summary:**

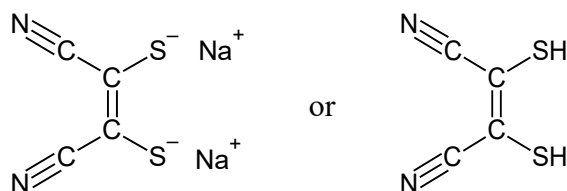
To supplement the methods section from the main manuscript, this section provides a detailed procedure used in synthesizing  $[N(Et)_4]_2[Ni(mnt)_2]$  salt for propylene/propane separating MEA system.

**Introduction:**

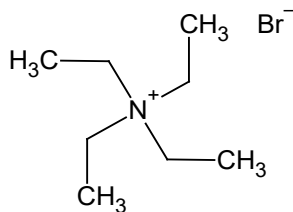
This procedure consists of laboratory instructions in how to prepare nickel (II) maleonitrile dithiolene complex ion. Since an ion cannot be isolated, it will be produced as a salt with tetraethylammonium. The product crystals should be bright red in color. This procedure is expected to produce about 6 grams of crystal after the filtration steps. If recrystallization process is utilized with ethanol and acetone, approximately 4.5 grams of crystal should remain with improved purity. The product composition can be characterized through the use of spectrophotometer at characteristic infrared band maxima shown in the research literature by Billig et. al.

**Required Materials:**

1. Sodium maleonitrile dithiolate salt ( $Na_2[C_4N_2S_2]$ ) or maleonitrile dithiol ( $C_4N_2S_2H_2$ )



2. Tetraethyl ammonium bromide ( $[N(C_2H_5)_4]Br$ )

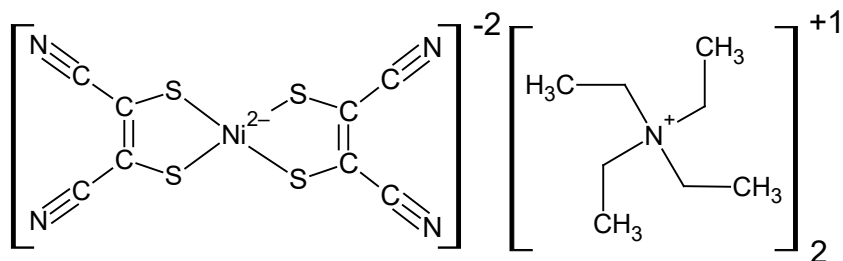


3. Nickel (II) Chloride ( $NiCl_2$ )
4. Methanol ( $CH_3OH$ )
5. Ethanol ( $C_2H_5OH$ )
6. Acetone ( $C_3H_6O$ )
7. Distilled Water

**Procedure:**

1. Prepare about 30 mL of methanol and water mixture with 1:1 mole ratio composition.
  - a. Mix 20.2 mL of methanol with 9 mL of distilled water in a 50-mL beaker
  - b. Use stirrer and mix well for about 3 minutes.
2. Prepare the Sodium Dithiolate solution
  - a. Pour 17 mL of the methanol/water mixture made in step 1 into a separate 50-mL beaker.
  - b. Carefully add 3.8 grams of Sodium maleonitrile dithiolate salt into the solution.
  - c. Return the bottle containing leftover Sodium maleonitrile dithiolate salt into the fridge room for preservation purpose as soon as possible.
  - d. Use stirrer and mix well for about 5 minutes.

3. Prepare the Nickel Chloride Solution
  - a. Pour 5 mL of the methanol/water mixture made in step 1 into a small 10-mL tube.
  - b. Carefully add 2.4 grams of Nickel Chloride powder into the solution.
  - c. Place an inert cap and shake and mix the solution well for about 1 minute.
4. Prepare Tetraethylammonium bromide solution (type I)
  - a. Pour 5 mL of the methanol/water mixture made in step 1 into a small 10-mL tube.
  - b. Carefully add 2.6 grams of Tetraethylammonium bromide powder into the solution.
  - c. Place an inert cap and shake and mix the solution well for about 1 minute.
5. Prepare Tetraethylammonium bromide solution (type II)
  - a. Pour 5 mL of distilled water into a small 10-mL tube.
  - b. Carefully add 1.2 grams of Tetraethylammonium bromide powder into the solution.
  - c. Place an inert cap and shake and mix the solution well for about 1 minute.
6. Produce nickel dithiolene complex
  - a. Add all nickel chloride solution made in step 3 to the beaker containing the sodium dithiolate solution from step 2.
  - b. Heat solution to approximately 50 degrees Celsius and stir well for about 10 minutes.
  - c. Filtrate the solution with vacuum and collect the filtrate.
  - d. Heat the filtrate in a new beaker and add all tetraethylammonium bromide solution (type I) from step 4 to the filtrate mixture.
  - e. Continue to heat and stir the solution for another 10 minutes.
  - f. Take beaker off hot plate and rapidly cool the mixture with an ice bath. Once enough crystals form, proceed to collecting the crystals through another filtration process.
  - g. Save the crystals formed in the filtration onto a petri dish and pour the filtrate into a beaker to salvage additional products. Add all tetraethylammonium bromide solution (type II) from step 5 to the filtrate mixture.
  - h. Continue to heat and stir the solution for another 10 minutes.
  - i. Take beaker off hot plate and rapidly cool the mixture with an ice bath. Once enough crystals form, proceed to collecting the crystals through another filtration process.
  - j. Save the crystals formed in this filtration and add it to the petri dish containing crystals from the previous filtration.
  - k. Recrystallize the red crystals in acetone/ethanol mixture to acquire purer crystals.



**Reference:**

E. Billig, Raymond Williams, I. Bernal, James H Waters, and Harry B. Gray. "The Electronic Structures of Square-Planar Metal Complexes. The Complexes of Maleonitriledithiolate with Copper(II), Nickel(II), Palladium(II), and Platinum(II)." *Inorganic Chemistry*. Vol. 3, Issue No. 5, pp. 663-666. May, 1964.

**Section Summary:**

To supplement the methods section of the main manuscript, this section provides purity evidence of the  $[\text{N}(\text{Et})_4]_2[\text{Ni}(\text{mnt})_2]$  salt used in the MEA system. After  $[\text{N}(\text{Et})_4]_2[\text{Ni}(\text{mnt})_2]$  salt was synthesized using the procedure outline in **Section S8**, the purity of the compound was tested using XRD and elemental analysis. The prominent XRD peaks representing the interplanar spacing of the salt crystal matched with the literature values while the elemental analysis result showed that the experimental weights of individual element were all within 2% of the theoretical value, confirming that we have synthesized a relatively pure  $[\text{N}(\text{Et})_4]_2[\text{Ni}(\text{mnt})_2]$  salt.

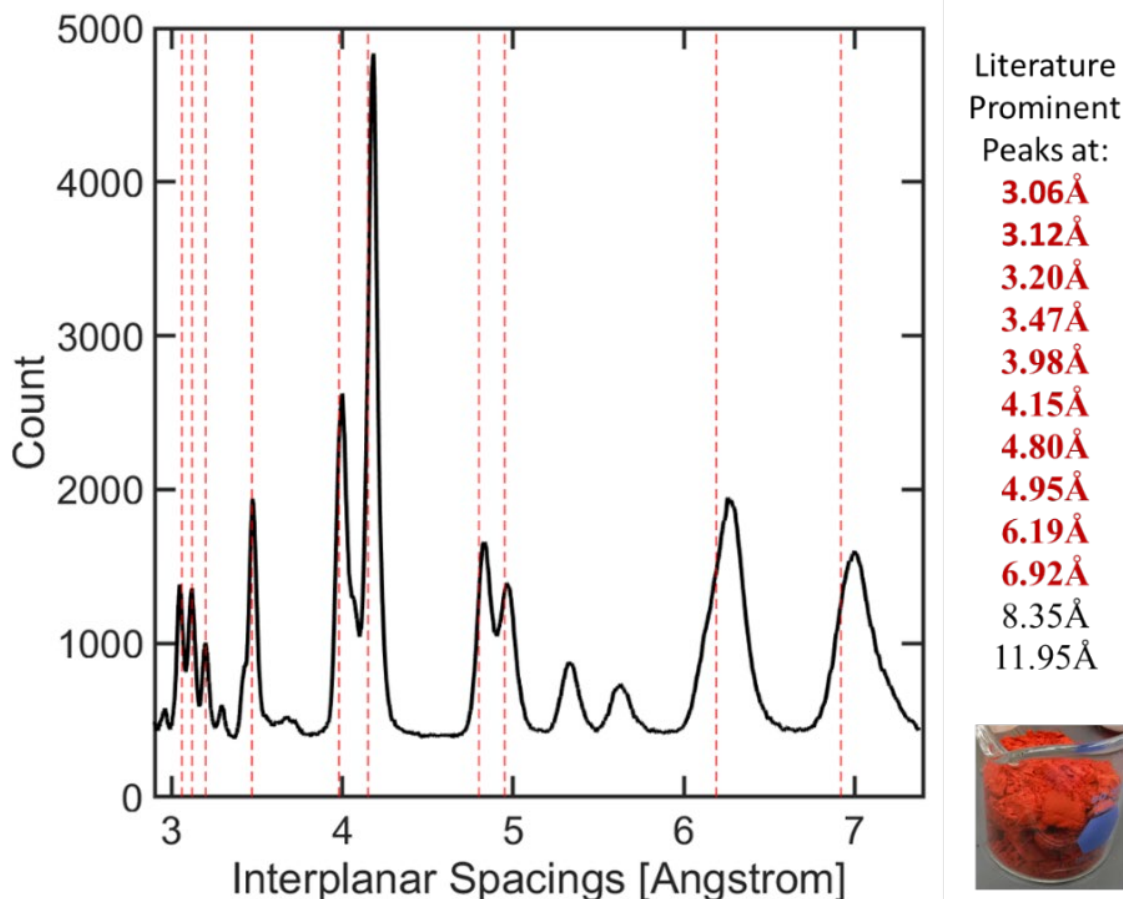


**Figure S9-A:** Tetraethylammonium salt powder of  $[\text{Ni}(\text{CN}_2\text{C}_2\text{S}_2)_2]^n$  was analyzed with XRD. The 2-theta angles were converted to interplanar spacings using Bragg's Law into units of Angstroms and matched with the literature listing of spacings that had the most prominent peaks (as bolded in red and marked with red-dotted reference line on the graph).

**Reference:**

A. Davidson, N. Edelstein, R.H. Holm, & A.H. Maki. "The Preparation and Characterization of Four-Coordinate Complexes Related by Electron-Transfer Reactions." *Inorganic Chemistry*. Vol 2, no 6, December 1963, pp 1227-1232.

**Table S9:** *Elemental Analysis of Synthesized Tetraethylammonium salt of  $[Ni(CN_2C_2S_2)_2]^n$* 

<b>Organic Element</b>	<b>Theoretical Mass Percent [%]</b>	<b>Experimentally Determined Mass Percent [%]</b>	<b>Percent Deviation [%]</b>
Carbon	48.08	48.31	0.48
Hydrogen	6.73	6.63	1.34
Nitrogen	14.02	13.88	1.00
Sulfur	21.39	21.43	0.19

\*Analysis was conducted by third-party specialist, Atlantic Microlab Inc.

## Section Summary:

To supplement the methods section of the main manuscript, this section provides electrochemical characterization evidence of synthesized  $[\text{N}(\text{Et})_4]_2[\text{Ni}(\text{mnt})_2]$  salt that was to be eventually used in the MEA system. The synthesized  $[\text{N}(\text{Et})_4]_2[\text{Ni}(\text{mnt})_2]$  salt was tested in a liquid electrochemical cell before being used in a pseudo-solid-state MEA system so that its cyclic voltammetry (CV) behavior can be compared to literature works. **Figure S10** compares the CV conducted under propane environment vs. CV conducted under propylene environment. Both CV's have been corrected with  $iR$  compensation to account for voltage loss incurred by the resistance property of the electrolyte solution. Notable peaks are labeled with transition equations of appropriate charge of  $[\text{Ni}(\text{mnt})_2]^n$ . The red arrows indicate oxidative transition while blue arrows indicate reductive transition between different charges of  $[\text{Ni}(\text{mnt})_2]^n$ . It should be noted that the peak amplitude at the oxidative transition from  $[\text{Ni}(\text{mnt})_2]^{-1}$  to  $[\text{Ni}(\text{mnt})_2]^0$  (at approximately  $+0.35\text{V}$  vs.  $\text{Ag}/\text{AgCl}$ ) decreased more readily over consecutive cycles when the solution is under propylene environment than when the solution is under propane environment. This is most likely due to cumulative consumption of  $[\text{Ni}(\text{mnt})_2]^n$  species in the vicinity of the carbon graphite electrode by turning into  $[\text{Ni}(\text{mnt})_2]^0 \cdot \text{C}_3\text{H}_6$  complex and then diffusing away from the electrode surface. As additional  $[\text{Ni}(\text{mnt})_2]^n$  species gets complexed to propylene with every cycle, less  $[\text{Ni}(\text{mnt})_2]^n$  species become available to complex with the propylene, decreasing the magnitude of the peak until enough cycles have passed at which a stabilizing equilibrium (that is concentration driven) occurs between the  $[\text{Ni}(\text{mnt})_2]^0 \cdot \text{C}_3\text{H}_6$  and  $[\text{Ni}(\text{mnt})_2]^n$  inside the electrochemical batch reaction solution. Electrochemically reversible couples of  $[\text{Ni}(\text{mnt})_2]^{2/-1}$  and  $[\text{Ni}(\text{mnt})_2]^{-1/0}$  have been observed at  $0.05\text{V}$  and  $0.37\text{V}$  vs.  $\text{Ag}/\text{AgCl}$  reference, respectively.

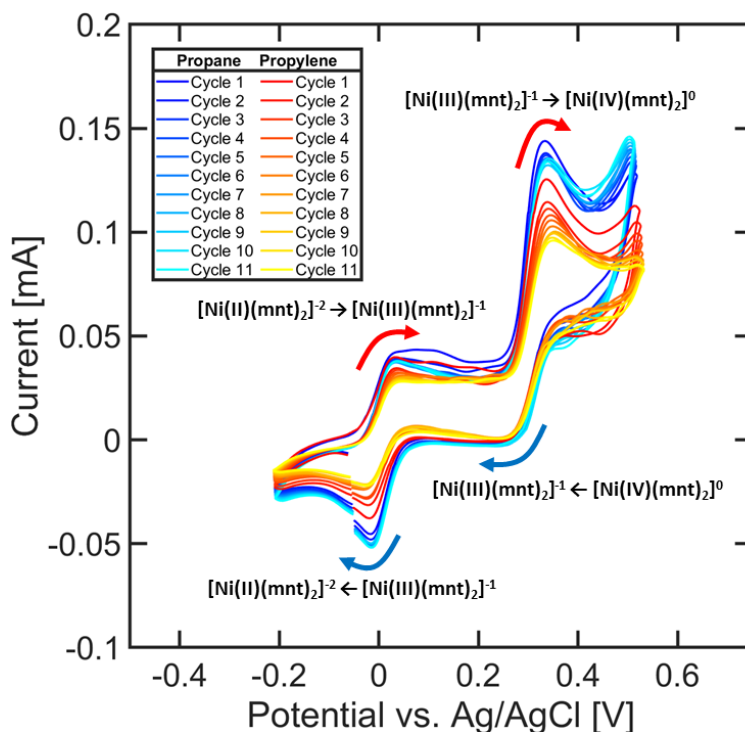


**Figure S10: Liquid Solution CV with Propane/Propylene.** Cyclic Voltammogram of 1 mM Tetraethylammonium Nickel Dimercaptomaleonitrile salt and 0.1 M tetrabutylammonium hexafluorophosphate supporting electrolyte in dichloromethane solvent at a scan rate of  $50\text{ mV/s}$  in a single-chamber cell. The blue-shaded plots were from runs in presence of continuous gas bubbling feed of propane gas at  $10\text{ sccm}$ . The red/yellow-shaded plots were from runs in presence of continuous gas bubbling feed of propylene at  $10\text{ sccm}$  with carbon working electrode, platinum counter electrode and  $\text{Ag}/\text{AgCl}$  reference electrode.

## Section Summary:

To supplement the methods section in the main manuscript, this section shows electrochemical characterization to help identify workable potentials for the olefin capture-and-release mechanism. Minimum thermodynamic oxidative and reductive potentials of +0.82V and -1.46V, respectively, were required to induce the propylene complexation and decoupling to the  $[\text{Ni}(\text{mnt})_2]^n$  species. CV's were taken in the range encompassing these two potentials.

The synthesized  $[\text{N}(\text{Et})_4]_2[\text{Ni}(\text{mnt})_2]$  salt was embedded into the MEA ionogel system. The two CV's shown in **Figure S11** are taken under gaseous environment of pure propane (left) and of pure propylene (right). On the pure propylene CV plot, a peak at approximately +1V (outlined in dotted yellow line) seems to be missing when compared to the pure propane CV plot. The cause of this anomaly may possibly be similar in nature to the peak decrease identified in the liquid solution CV from the previous *Section*, except it is located at the portion of the CV where there is most likely reductive transition from  $[\text{Ni}(\text{mnt})_2]^0$  to  $[\text{Ni}(\text{mnt})_2]^{-1}$ . If most of the “available”  $[\text{Ni}(\text{mnt})_2]^0$  complexed with the propylene gas during the oxidative transition, then it is possible that the “accessible”  $[\text{Ni}(\text{mnt})_2]^n$  species became scarce very quickly within the ionogel medium, especially considering that possibly large fraction of  $[\text{Ni}(\text{mnt})_2]^n$  species may not have sufficient access to interfacial surface of the gas phase to begin with. The decrease in peak amplitude would make sense if not enough  $[\text{Ni}(\text{mnt})_2]^n$  are available to be reduced again. Furthermore, the CV below only barely reaches the thermodynamic minimum potential of decoupling the propylene from the complex so regeneration of free  $[\text{Ni}(\text{mnt})_2]^n$  was more restricted, resulting in depletion of available  $[\text{Ni}(\text{mnt})_2]^n$  species.

Based on observing the CV's and from calculating the thermodynamic minimum potentials, +1.5V was chosen for the oxidative potential to be used in the standard MEA testing procedure since the peak anomaly manifested when +1.5V was utilized on the positive potential limit during CV measurements. -2V was chosen for the reductive potential even though -1.5V still showed a peak on both CV's because of concern of its close proximity to the minimum thermodynamic potential.

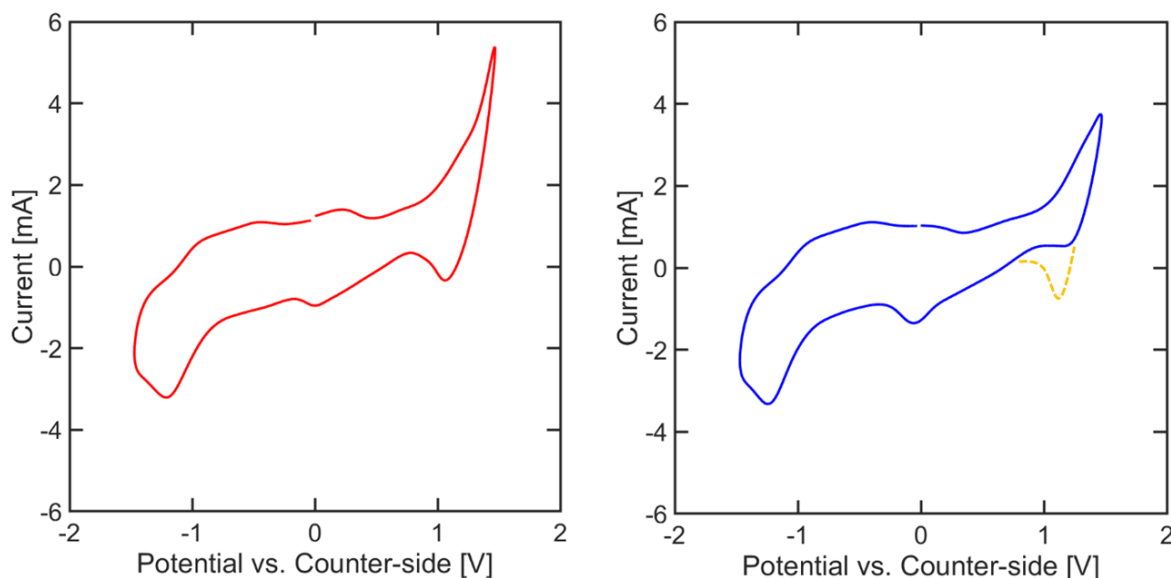


**Figure S11.** Cyclic Voltammogram of MEA sample with Spray-deposited layer consisting of 5 mg/cm<sup>2</sup> Carbon Nanoparticles, 4 mg/cm<sup>2</sup> Nafion ionomer, 4 mg/cm<sup>2</sup> [BMIM][PF<sub>6</sub>] ionic liquid, and 4 mg/cm<sup>2</sup>  $[\text{N}(\text{C}_2\text{H}_5)_4]_2[\text{Ni}(\text{CN}_2\text{C}_2\text{S}_2)_2]$  salt on Sigracet 39 BB Carbon GDL. Left-hand graph in red is from runs in presence of pure propane. Right-hand graph in blue is from runs in presence of pure propylene. Note the absence of peak highlighted in yellow outline on the propylene run. Scan rate was 50 mV/s for all runs.

**Section Summary:**

To supplement the methods section in the main manuscript, additional information regarding the spray deposition system used in preparing the MEA samples is provided in this section. The spray deposition system used in preparing the MEA samples onto GDL layers is shown in Figure S12 shown below. A nozzle was fixed to a central position supported by metal beams. The nozzle was connected to both a source of pressurized air (usually set to approximately 15 psig) and a source of the ink solution. The ink was fed through a chemical-resistant tube from a syringe. The flow rate of the ink was carefully controlled with a syringe pump. All MEA's prepared for this work was sprayed at a rate of 0.1 ml/min ink solution because this setting exhibited the most consistent and homogenous deposition of porous layers onto the GDL. The GDL substrate was secured onto a motorized stage that can move in 2 dimensions. The motorized stage was programmed by LabView software to move in a constant repeatable serpentine pattern. Furthermore, a mini-stir bar was placed inside the syringe so that a nearby magnetic stirrer can keep the colloidal ink solution in good suspension during extended periods of spray deposition.

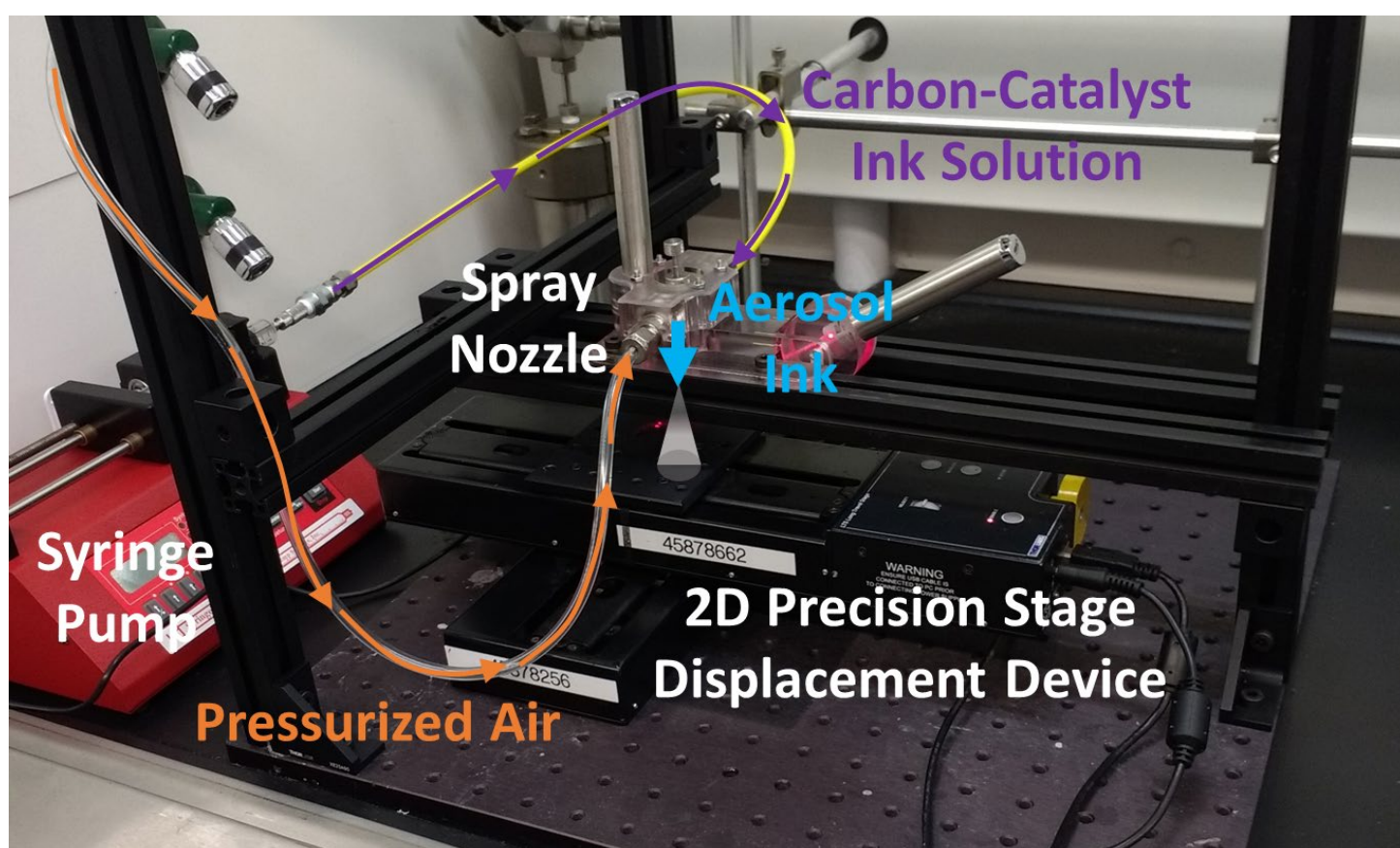


**Figure S12.** Spray Deposition system of catalyst layer using automated moving stage and nozzle sprayer.

## Section Summary:

The following section shows the mole fraction of the propylene gas released via either physisorption or chemisorption related phenomenon during the reductive phase of the separation experiment. The fractions were calculated from the last 3 cycles of individual experiments observed in Sections S1 and S2. The amount of propylene released by the effect of electrochemical modulation is due to chemisorption effect. The amount of propylene released due to gradual desorption from contact surfaces (helped by nitrogen flush) within the flow cell system is due to physisorption effect. All chemisorption/physorption fractions are calculated based on the assumption that the propylene gases were collected for 2000 seconds since the start of the reductive phase. Since the longest chemisorption-related propylene release lasted approximately 2000 seconds, this time interval was chosen as the integration range for the purpose of calculation consistency in all observed propylene “peaks” from the concentration profile data. Therefore, when determining the chemisorption/physorption fractions, the integral area of the propylene concentration profile was calculated only within the time interval of  $0 < t < 2000$  seconds with respect to the start of the reductive phase.

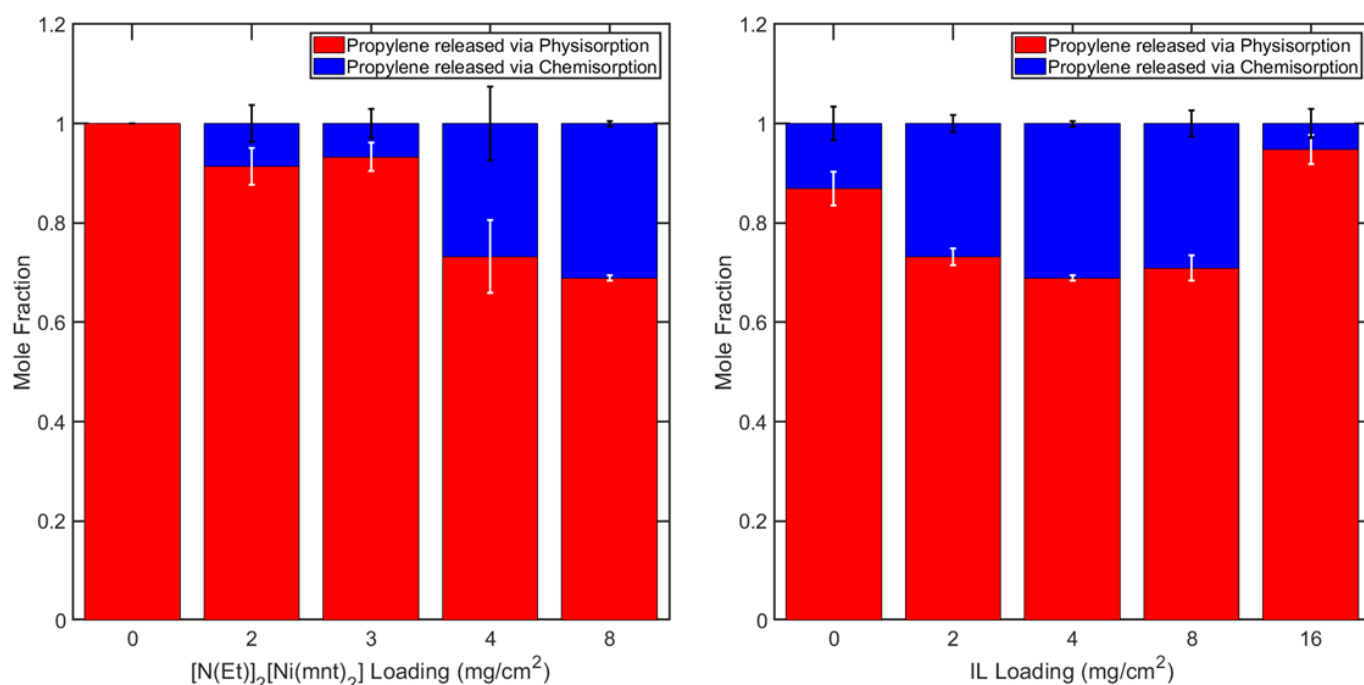


**Figure S13.** The graphs above depict mole fraction between propylene gases released via physisorption effect (in red) and via chemisorption effect (in blue). The graph on the left shows the physisorption/chemisorption fraction of the released propylene gas at varying  $[N(Et)_2][Ni(mnt)_2]$  loading while the graph on the right shows the physisorption/chemisorption fraction at varying ionic liquid (IL) loading.

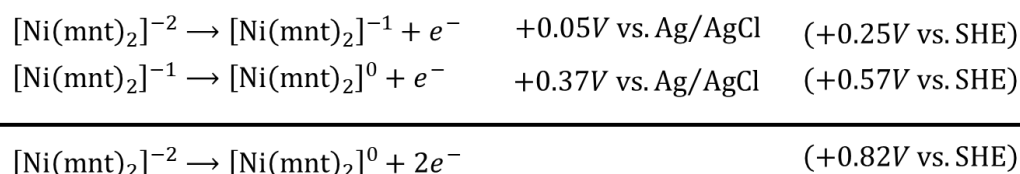
**Section Summary:**

The following section demonstrates the calculation of the thermodynamic minimum potentials needed to electrochemically modulate the oxidation state of the  $[\text{Ni}(\text{mnt})_2]^n$  species to facilitate the selective propylene capture-and-release mechanism. Note that during the oxidative phase (olefin capture), hydrogen gas is being produced on the counter-side electrode, while oxygen evolution reaction is taking place on the counter-side electrode during the reductive phase (olefin release). Refer to Section S10 for the specific half-reaction potentials of the  $[\text{Ni}(\text{mnt})_2]^n$  species.

**General Equation:**

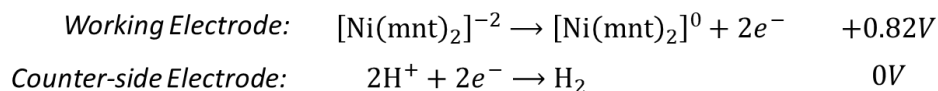
$$E_{\text{cell}} = E_{\text{cell}}^0 + \eta_{\text{ohmic}} + \eta_{\text{concentration}} + \eta_{\text{resistance}}$$

**Half-Reaction Potentials:**



**Thermodynamic Minimum Potentials:**

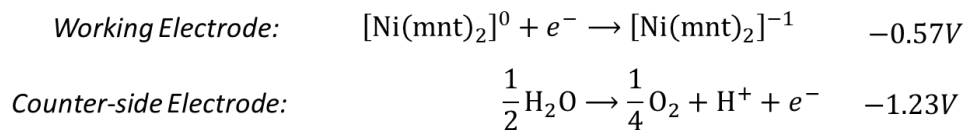
**Oxidative Phase**



$$E_{\text{cell}}^0 = E_{\text{working}} + E_{\text{counter-side}} = \boxed{+0.82V}$$

$$E_{\text{cell}} > 0.82V$$

**Reductive Phase**



$$E_{\text{cell}}^0 = E_{\text{working}} + E_{\text{counter-side}} = \boxed{-1.8V}$$

$$E_{\text{cell}} < -1.8V$$